LBNL-42881

ERNEST ORLANDO LAWRENCE
BERKELEY NATIONAL LABORATORY

Overlap Domain Decomposition Technique for Modeling Wave Propagation

Jianli Fan

Earth Sciences Division

December 1998

Ph.D. Thesis

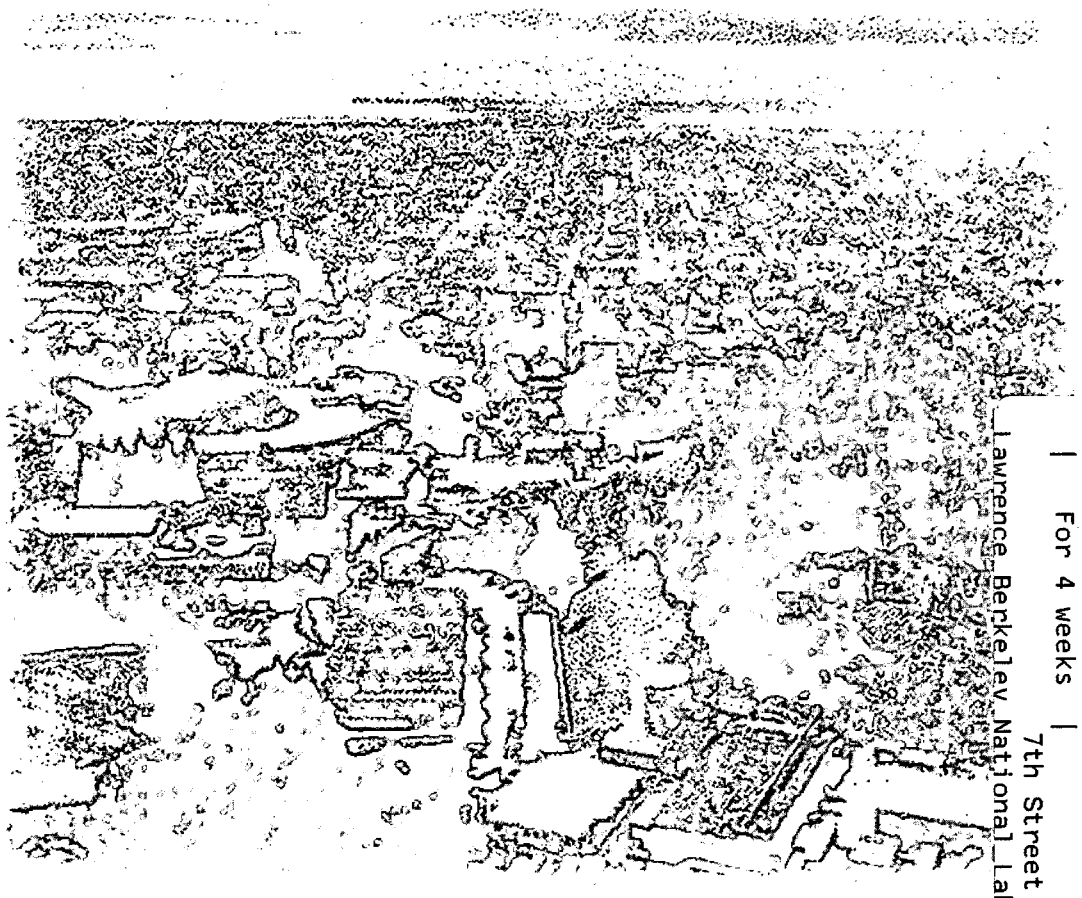

DISCLAIMER

LBNL-42881

Overlap Domain Decomposition Technique for Modeling Wave Propagation

Jianli Fan
Ph.D. Thesis

Department of Materials Science and Mineral Engineering
University of California, Berkeley

and

Earth Sciences Division
Ernest Orlando Lawrence Berkeley National Laboratory
University of California
Berkeley, CA 94720

December 1998

This work was supported in part by the Director, Office of Science, Office of Basic Energy Sciences, of the U.S. Department of Energy under Contract No. DE-AC03-76SF00098, and the Gas Research Institute under Contract No. 5093-260-2663 to Larry Myer and Kurt Nihei.

Overlap Domain Decomposition Technique for Modeling Wave Propagation

by

Jianli Fan

B.S. (Peking University) 1984
M.S. (Peking University) 1987

A dissertation submitted in partial satisfaction of the

requirements for the degree of

Doctor of Philosophy

in

Engineering-Materials Science
and Mineral Engineering

in the

GRADUATE DIVISION

of the

UNIVERSITY OF CALIFORNIA, BERKELEY

Committee in charge:

Professor James W. Rector III, Chair
Professor Alex Becker
Professor Steven D. Glaser
Dr. Kurt T. Nihei

1998

Overlap Domain Decomposition Technique for Modeling Wave Propagation

by

Jianli Fan

ABSTRACT

Overlap Domain Decomposition Technique for Modeling Wave Propagation

by

Jianli Fan

Doctor of Philosophy in Engineering

University of California, Berkeley

Professor James W. Rector III, Chair

This dissertation presents the results of research on the development of a general computationally efficient overlap domain decomposition (ODD) technique based on Huygens' Principle for modeling wave propagation. The ODD technique divides a large domain into several smaller overlapping subdomains, and allows the exchange of waves between the subdomains through the overlapping regions without the need for any internal interface connecting conditions. Calculations are performed independently in each subdomain, and the wavefield in the whole domain is then obtained from the local solutions in the subdomains. The ODD technique itself is not restricted to a specific numerical method. Different numerical methods for solving the wave equation can be incorporated into the ODD framework without any boundary conditions at the interfaces between subdomains. This flexibility is particularly advantageous because it enables highly accurate but computationally expensive methods to be used in subdomains with strong gradients in the wavefield and faster less accurate methods in the remaining subdomains to achieve a desired level of accuracy and computing speed.

The ODD technique is described in detail for 1-D cases and extended to 2-D and 3-D cases. The finite difference (FD) method and Fourier pseudospectral (PS) method for solving the wave equation are incorporated into the ODD framework and the resulting algorithms are given. The lengths of the overlap areas for different methods in 1-D, 2-D, and 3-D are presented. By using the ODD technique, calculations can be "turned-off" in subdomains that do not have appreciable wave activity, resulting in savings of computing time and memory use.

An example of guided wave propagation in a low velocity layer demonstrates the flexibility and efficiency of the ODD technique. The accurate but computationally intensive PS method is used in the subdomains containing the source and the low velocity layer where the wavelength is shorter, and the FD method is applied to surrounding high velocity media which have longer wavelengths. The results are compared to experimental results from physical modeling. Both the physical and numerical models show a concentration of wave energy along the low velocity layer.

Approved by: James W. Rector III, Committee Chairman

TABLE OF CONTENTS

Acknowledgments vii

Chapter 1 Introduction and Overview

1.1 Introduction 1
1.2 Review of Numerical Modeling of Wave Propagation in Geologic Media 2
1.3 Domain Decomposition Technique 6
1.4 Objectives and Overview 8

Chapter 2 Overlap Domain Decomposition Technique for Wave Propagation

2.1 Introduction 11
2.2 Overlap Domain Decomposition (ODD) Technique 11
2.3 Application of ODD to the Finite Difference (FD) Method 14
2.3.1 1-D Finite Difference Method 14
2.3.2 ODD for 1-D Finite Difference Method 16
2.4 Application of ODD to the Fourier Pseudospectral (PS) Method 19
2.4.1 1-D Fourier Pseudospectral Method 19
2.4.2 ODD for 1-D Fourier Pseudospectral Method 21
2.5 Application of ODD to the Mixed FD and PS Method 25
2.6 Stability Condition 27
2.6.1 Stability Condition for the 2nd Order FD Method 29
2.6.2 Stability Condition for the 4th Order FD method 30
2.6.3 Stability Condition for the Fourier PS Method 32
2.7 Dispersion Condition 33
2.7.1 Temporal Dispersion 33
2.7.2 Spatial Dispersion 38
2.7.3 Coupled Temporal and Spatial Dispersion 44

2.8 Turning On & Off Subdomain Computations 48
2.9 Examples 49
2.10 Summary 51

Chapter 3 Overlap Domain Decomposition For 2-D Problems

3.1 Introduction 52
3.2 2-D Overlap Domain Decomposition 52
3.3 Turning on and off Computations in Inactive Subdomains 53
3.4 Application of ODD to 2-D Acoustic Problems 55
3.4.1 ODD for the 2-D Acoustic FD Method 55
3.4.2 ODD for the 2-D Acoustic Fourier PS Method 58
3.4.3 Acoustic Example 61
3.5 Application of ODD to 2-D Elastic Problems 65
3.5.1 ODD for the 2-D Elastic FD Method 66
3.5.2 ODD for the 2-D Elastic Fourier PS Method 70
3.5.3 Elastic Example 70
3.6 Stability and Dispersion Condition 77
3.6.1 Stability Condition for 2-D Acoustic Problems 77
3.6.2 Stability Condition for 2-D Elastic Problems 79
3.6.3 Dispersion for 2-D Acoustic Problems 82
3.6.4 Dispersion for 2-D Elastic Problems 83
3.7 Summary 86

Chapter 4 Simulation of Guided Waves with the ODD Technique

4.1 Introduction 87
4.2 Numerical Simulations and Experimental Measurements of Channel Waves 88
4.2.1 Experimental Model Setup 88
4.2.2 Numerical Model Setup for the ODD Technique 90

4.2.3 Comparison of Results from Experiments and Numerical Simulations 93
4.3 Summary 104

Chapter 5 Overlap Domain Decomposition Technique For 3-D Problems

5.1 Introduction 105
5.2 3-D Acoustic Finite Difference Method 105
5.3 Application of ODD to 3-D Acoustic FD Method 108
5.4 Summary 111

Chapter 6 Conclusions and Future Work

6.1 Conclusions 112
6.2 Future Work 113

BIBLIOGRAPHY 115
APPENDIX A 122
APPENDIX B 125
APPENDIX C 134
APPENDIX D 137
APPENDIX E 139

Acknowledgments

First, I would like to thank my advisors, Professor Neville G. W. Cook and Dr. Larry Myer, who gave me the opportunity of studying and working at the University of California at Berkeley and the Lawrence Berkeley National Lab, and provided consistent academic guidance and financial support for me. They taught me to see the importance and the difference. Their standards of excellence will always give me inspiration for my life. Professor Cook was a great man who thought about himself little and helped us a lot. I also thank his wife, Jennifer, for her fully support for Professor Cook and "Cook rock mechanics group".

I am grateful to my advisor, Professor James Rector, for guiding and helping me for my research and career. He taught me to deeply understand the applied geophysics and the signal processing.

Special thanks to my research supervisor, Dr. Kurt Nihei. Without him, I never could have gotten started on the overlap domain decomposition (ODD) technique. He has been both a friend and a constant source of help in everything from giving daily advises to providing new ideas. He spent so much time for helping me to organize and write my dissertation.

Professor Alex Becker and Steven Glaser also deserve my great appreciation for their time, kindness, comments and suggestions while reviewing my dissertation and being my qualifying exam committee, which give me the great help for finishing my dissertation. Also thanks Professor George Cooper and Fiona Doyle for being my qualifying and preliminary exam committee, and teaching me.

I have learned so much by taking the courses by Professor Richard Goodman, Robert Taylor, Jonathan Bray, Raymond Seed, Yuram Rubin, Gregory Fenves, Sanjay Govindjee, Francisco Armero, Lane Johnson, Ken Goldberg, and Sharon Jones. Professor Taylor also provided his FEAP program for my early research. I express my sincere thanks for Professor Chi-yuen Wang for his kindness of giving me the opportunity of working in his lab.

I have been a privilege to work with a team of brilliant and enthusiastic colleagues sharing similar aspirations at Berkeley. Dr. Galen Hesler not only helped me for reviewing my dissertation, but also gave me tremendous advises for my studying and living in the United States. Dr. Seiji Nakagawa reviewed my dissertation and having so many helpful discussions for my research, and we had a lot of good time for taking classes and doing research. Dr. Boliang Gu, Gemei Yang and Zhong Liu, gave me many good suggestions for my study. Brad Bessinger helped me a lot for my English class reports. I enjoyed sharing the office with Weidong Yi and Pingan Huang. Thanks Valeri Korneev and Henk Keers for reviewing my papers. Thanks all your helps from Pascual Benito, Steve Blair, Fang Fang, Brun Hilbert, Taylor Hwong, Roberto Suarez-Rivera, Mike Kowalsky, Ziqiong Zheng, Deb Hopkins, Stacey Ita, John Kemeny, Ken Lee, Sanjit Roy, Laura Pyrak-Nolte, Grace Su, Jil Geller, Qicheng Dong, Joongmoo Byun, Paul Milligan, Erika Schlueter, Clark Scott, Bing Wang, Tao Zhen, and Zhuping Liu.

I wish to thank Dr. Gen-hua Shi for teaching me his DDA and manifold method. He told me the beauty of combination of mathematics and engineering. Special thanks to Professor Yongen Cai for his constant helps for my life and research. A lot of thanks to Professor Lei Li for his helpful discussions, reviewing of my thesis, and sharing of our

life. Thanks Guoping Liang for teaching me his LDDA. I also thank Dr. Jiangheng He for providing helps for my studying and having good time together at Berkeley. Thanks my old classmates and friends, Gutuan Zheng, Tanzhuo Liu and Jie Zhang, for their fully supports for my studying and sharing their life experiences with me.

I also need to thank people from YWCA, Sharon Bettinelli, Margaret Dury, Jane Abraham, Barbara Helm, and Dorothy Duncan for helping us at Berkeley, giving us friendship, and improving our English.

Finally, I should thanks my family for their unconditional support and inspiration for me. Especially, my parents, Qingwen Fan and Xiu Zhang, and my wife, Jin.

CHAPTER ONE

INTRODUCTION AND OVERVIEW

1.1 Introduction

Geophysical wave propagation modeling commonly deals with problems of large scale and complex structures characterized by irregular interfaces separating lithologic units such as low velocity layers and salt domes. Because these large-scale problems often can be extremely computationally intensive, it is desirable to develop efficient techniques that can reduce computation time and memory requirements. Domain decomposition techniques have recently emerged as an efficient approach for modeling large problems. These techniques provide a computational framework for dividing a large geometric domain into several smaller subdomains, enabling the use of parallel computing techniques, and different numerical methods for solving the wave equation in each subdomain.

The focus of this research is the development of a general overlap domain decomposition (ODD) technique based on Huygens' Principle that couples different numerical methods and reduces computation time and memory for wave propagation problems. The ODD technique splits a large domain into several smaller overlapping subdomains. Wavefields are independently calculated in each subdomain using a numerical method for solving the wave equation, and waves are passed from one subdomain to adjacent subdomains through the overlap regions. The wavefield in the whole domain is then obtained from the local solutions in the subdomains.

The ODD technique has several prominent features for wave propagation. First, it can be applied to different numerical methods for solving the wave equation (e.g. finite different, pseudospectral, finite element, and staggered grid methods, etc.). In addition, each subdomain can use a different numerical method. Second, the computing time and memory can be reduced by decreasing the computational domain size and by "turning-off" the calculations in the subdomains which do not have wave activity. Third, the boundary conditions between subdomains need not be specified since the boundary values of each subdomain can be obtained from the interior solution of the adjacent subdomain. Fourth, parallel computing techniques can be easily applied because each subdomain solution is computed independently at each time step from its neighbors.

1.2 Review of Numerical Modeling of Wave Propagation in Geologic Media

There are a variety of methods for modeling wave propagation in elastic media that can be classified as follows: analytical methods (*e.g.* Green function and Cagniard-de Hoop methods), semi-analytical methods (*e.g.* integral equation method), ray-geometric methods (ray tracing) and direct numerical methods (finite difference methods, pseudospectral methods and finite element methods). All these methods are based on a solution of the governing equation of motion, but differ in the formulation of the governing equations or in the means of finding the solution.

Analytical methods (*e.g.* Lamb, 1904 and Love, 1944) can yield exact results of high accuracy which can serve as reference solutions for other modeling methods. However, as they are based on closed form solutions of the governing equations, analytical solutions exist only for problems with simple geometries.

The integral equation method (Cruse and Rizzo, 1968; and Cruse, 1968; 1987) can be applied to 2-D or 3-D structures, in principle. However, the computational effort and storage requirements are too high for most practical applications with complex geometries.

Ray-tracing methods (Cerveny, Molotkov and Psencik 1977) yield a high-frequency approximation of the solution of the wave equation. Amplitudes and spectral characteristics determined with these methods are not always accurate, particularly when the medium contains wavelength-scale heterogeneity and strong velocity gradient. However, ray tracing methods are very efficient for computing the arrival times of waves.

Direct methods such as finite difference, pseudospectral and finite element methods are based on the numerical solution of the equation of motion on a discrete grid. Wave propagation in complex geological structures can be modeled by these methods. The solution at all grid points is computed at each time step, allowing snapshots of the wavefield at a given time to be produced. Also, high accuracy solutions can be achieved by using a fine grid. However, the computational effort may increase with square of the number of grid points for 2-D problems and the cube for 3-D problems.

Finite difference (FD) methods have been used in seismology to solve wave propagation problems since the 1960s. Pioneering works in applying the finite difference method to seismological problems were conducted by Alterman and her co-workers (Alterman and Kornfeld, 1968; Alterman and Karal, 1968; Alterman and Rotenberg, 1969). They developed numerical discrete solutions to the second order elastic wave equations in homogeneous regions by the use of explicit time integration methods.

However, because practical problems usually involve complex structures, the heterogeneous finite difference algorithm solution for the second order system of equations was introduced by Boore (1972) and extended by Kelly et al. (1976).

Refinements such as higher order derivative operators for the wave equation permit the use of coarse grids and results in potentially more efficient algorithms. Shubin and Bell (1987) developed fourth-order schemes by adding correction terms to second-order schemes, and Dablain (1986) considered a suite of classical finite difference operators of high order accuracy.

An alternative way for modeling wave propagation can be achieved by replacing the second-order wave equation by two first order equations (motion equation and constitutive equation) on two staggered grids. Madariaga (1976) developed the first of the currently popular staggered grid finite difference algorithms based on the first order equations. Fornberg (1996) applied the staggered grid to Fourier pseudospectral methods, and Grave (1996) used the technique to model 3-D elastic wave propagation.

The computational costs and memory requirements of numerical modeling have always been a concern, especially for 3-D elastic models. Under certain conditions, substantial computational savings can be achieved by using coarse grid Fourier pseudospectral (PS) methods as opposed to finite difference methods. The method was originally proposed in Kreiss and Oliger (1972). Early exploration geophysical uses are found in Gazdag (1981) and Kosloff and Baysal (1982). Additional basic theory can be found in Orszag (1972) and Fornberg (1975, 1987 and 1996). Furumura (1998) applied the Fourier pseudospectral method to 3-D problems. As an alternative to the Fourier

transform, Kosloff et al. (1990) developed the Chebychev pseudospectral method to solve elastic problems, and Saatcilar et al. (1990 and 1991) proposed a Hartley transform pseudospectral method for solving the elastic wave equation. Tessmer et al. (1992) used the Chebychev spectral method for one spatial direction and the Fourier spectral method for the other direction. Carcione (1994) coupled Chebychev function with space mapping for the wave equation in generalized coordinates. Tessmer and Kosloff (1994) extended the Chebychev spectral method to 3-D elastic problems.

The finite element method (FEM) is well known for its great flexibility in solving problems with complex geometries and heterogeneous structures, such as irregular surface topography, curved, dipping and rough interfaces, intrusions, cusps and holes. In addition, boundary conditions such as a free surface can be easily taken into account. This method has been largely employed in mechanical engineering, soil foundation engineering, structural engineering, nondestructive testing, and earthquake engineering. But it has not gained wide acceptance among geophysicists because, in its classical formulation, it has fairly low accuracy and computational efficiency for wave propagation problems. Lysmer and Drake (1971) and Drake (1972) are among the first to apply finite element modeling to seismic wave propagation. They used an explicit frequency domain formulation. An early 3-D application of finite elements to seismic wave propagation can be found in Schlue (1979). Marfurt (1984) and Lewis (1984) noted that significant computational cost savings can be achieved by using nested dissection numerical solution techniques (Gerge and Liu, 1981; Duff et al., 1986) in simulating multiple shot rolls for seismology characterized by numerically sparse sources and receivers. For reaching a high accuracy, Priolo et al. (1994); Faccioli et al., 1996;

Komatitsch and Vilotte (1998) adopted high order orthogonal interpolating functions for elements, called spectral element method, for simulating wave propagation.

1.3 Domain Decomposition Technique

The main idea of the domain decomposition algorithm for solving partial differential equations is to divide a large domain into a number of subdomains and to solve a similar problem on each subdomain. Recently, domain decomposition has been widely developed (Keyes and Xu, 1995) because of its many advantages:

- Simplification of complex geometry. The decomposition can either be fixed in time or be changed dynamically as the geometry and/or the solution evolve.
- Allowing the use of different resolutions and/or numerical methods in different subdomains. In each subdomain, one can choose a discretization method particularly well suited to geologic structure, such as a local low velocity zone. Different time steps can be used in different subdomains.
- Utilizing the capacity of parallel computers by assigning different subdomains to different processors.
- Permitting economical use of methods whose cost increases faster than linearly with domain size, such as the finite element method and the pseudospectral method.

The domain decomposition can be categorized as the overlap and non-overlap domain decompositions as showed on Figure 1.1. For the overlap domain decomposition, the adjacent subdomains overlap each other near their boundaries and exchange the information through the overlap region. For the non-overlap domain decomposition,

adjacent subdomains connect through the artificial boundaries and artificial boundary conditions are needed for exchanging information.

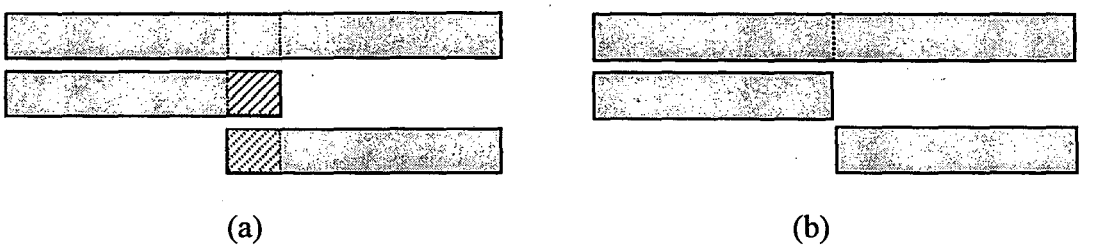

(a) (b)

Figure 1.1 (a) Overlap domain decomposition, (b) Non-overlap domain decomposition

Schwarz (1870) introduced the earliest overlap domain decomposition. By overlapping, the classic Schwarz alternating method essentially amounts to obtaining boundary values for each subdomain from the interior solution of another subdomain. A simple and commonly used demonstration problem is to solve Poisson's equation in an L-shape domain by applying fast Poisson solvers on two rectangular domains that overlap at the bend. Dryja and Widlund (1990) and Cai (1994) gave a general discussion about the Schwartz alternating method for solving PDE problems. Instead of iteration by the Schwartz method, Kuznetsov (1988) and Chen and Lazarov (1994) mathematically proposed a non-iterative overlap domain decomposition for solving parabolic partial differential equations such as heat transfer and diffusion problems. Liao and McMechan (1993) applied the non-iterative overlap domain decomposition to the Fourier pseudospectral method for modeling viscoacoustic wave propagation using a multi-processor computer to take advantage of the parallel computing. Xu and McMechan (1998) extended the technique to the 2nd order finite different method for viscoelastic media.

Quarteroni (1995) overviewed the non-overlap domain decomposition technique for wave propagation problems. Liang and He (1993) and Hilbert et al. (1994) used Lagrange multiplier to connect adjacent subdomains for dynamic discontinuous block systems. Tessmer, et al. (1992) coupled Fourier and Chebychev spectral methods by domain decomposition. Carcione (1991) decomposed the wave equation into incoming and outgoing wave modes at the boundaries of the subdomains.

1.4 Objectives and Overview

A potential limitation of non-overlapping techniques is the need for connectivity conditions at the (artificial) subdomain boundaries. The overlap domain decomposition technique does not need artificial interface conditions and exchanges the information through overlap areas. The technique naturally fits wave propagation problems since waves can be passed from one subdomain to other subdomains through the overlap areas. Thus, the ODD technique has only been applied to the Fourier pseudospectral method (Liao and McMechan, 1993) and finite difference method (Xu and McMechan, 1998) for wave propagation, but different methods have not been coupled together by the ODD technique. This dissertation addresses this problem of developing an ODD framework that can be used to couple different numerical methods.

This dissertation proposes a general overlap domain decomposition (ODD) technique based on Huygens' Principle for modeling wave propagation. This technique has the following advantages: it can easily couple different methods without connecting conditions at the interfaces, it can be directly implemented in uses parallel computation, it results in increases efficiency for methods whose operation count (i.e., "cost") increases

faster than linearly with domain size, and it can reduce computation time by "turning off" the calculations in subdomains which do not have wave activity.

In Chapter 2, the ODD technique is proposed for wave propagation in a 1-D medium. The ODD algorithm is applied to the 4th order accuracy FD method. The Fourier pseudospectral (PS) method for solving the wave equation is then briefly described, and the ODD algorithm for the PS method is introduced. Because of the periodic property of Fourier transform, a tapering technique for each subdomain is introduced to allow the ODD algorithm to be applied to the PS method. The ODD algorithm for mixed FD-PS methods for different subdomains is introduced and evaluated. The results show good agreement between the ODD FD, PS, mixed FD-PS methods and the conventional FD and PS methods. Also, the turning-off technique for inactive subdomains is introduced.

Similarly, the ODD technique for 2-D media and the implementations for acoustic and elastic media are described in Chapter 3. The results between the ODD FD, PS, mixed FD-PS methods and the conventional FD and PS methods are then discussed and compared.

Simulation of guided wave propagation in a low velocity layer is performed in Chapter 4. The composite ODD technique is employed, where the high accurate PS method is used in the subdomain encompassing the low velocity layer where the wavelength is shorter, and the FD method is applied to surrounding high velocity medium in which waves have longer wavelengths.

In Chapter 5, the 3-D ODD technique is described and the implementation for a 3-D acoustic medium is introduced. Finally, major conclusions and future applications of the

ODD technique are identified in Chapter 6. A general description of possible integration of other numerical methods such as FEM and BEM in to the ODD framework is discussed.

The algorithm of the ODD technique with the finite difference and Fourier pseudospectral methods is numerically implemented by C++ language, and the code can be run on IBM PC-Windows platform and any Unix platforms. The all results in this dissertation are run in a Pentium Pro 200 PC with 128 MB memory, and some of results are also tested on a SUN SPARC 10 Unix machine with 128 MB memory.

CHAPTER TWO

OVERLAP DOMAIN DECOMPOSITION TECHNIQUE FOR WAVE PROPAGATION

2.1 Introduction

Huygens' principle (Smith and Thomson, 1971; Dix, 1981) indicates that light wave propagates as a wavefront, and that at any instant every point on the wavefront is the origin source of a secondary wave which propagates outwards as a spherical wave. The secondary waves then combine to form a new wavefornt, so that successive positions of the wavefront may be calculated by a step-by-step process.

This chapter presents a general overlap domain decomposition (ODD) technique for wave propagation motivated by Huygens' Principle. The implementation of ODD algorithms for the fourth order finite difference (FD4) method, pseudospectral (PS) method and mixed FD4-PS method in a 1-D medium is introduced. A numerical example is presented to compare the results from the ODD methods with the results from conventional methods.

2.2 Overlap Domain Decomposition Technique

The overlap domain decomposition (ODD) technique is shown schematically in Figure 2.1 for 1-D wave propagation. The ODD algorithm can be described by the following steps as shown in Figure 2.1:

Step 1. A large domain Ω [a, e] containing a wavefield $f(x,n)$ is split into two subdomains Ω1 [a, d] with the wavefield $f1(x,n)$, and Ω2 [b, e] with the wavefield $f2(x,n)$ at a time step n.

$$f1(x,n) = f(x,n), \quad x \in [a, d] \text{ in } \Omega 1, \tag{2.2.1}$$

$$f2(x,n) = f(x,n), \quad x \in [b, e] \text{ in } \Omega 2. \tag{2.2.2}$$

Subdomains Ω1 and Ω2 have a common region Ωo [b, d] called the *overlapping region*. Note that both subdomains carry a common part of the wave in the overlapping region Ωo. The domain splitting introduces two artificial boundaries in the overlapping region Ωo [b, d] at point d for Ω1 and at point b for Ω2.

Step 2. Based on Huygens' Principle, the wavefields $f1(x,n)$ and $f2(x,n)$ at a time step n can be used as the sources for computing the wavefields $f1(x,n+1)$ and $f2(x,n+1)$ independently at a time step n+1 in Ω_1 and Ω_2. The overlapping region Ωo [b, d] belongs to both subdomains and the wavefield in Ωo is independently calculated twice. Although the artificial boundaries generate reflected waves, for a small time step dt the reflected waves from the boundaries should only affect a small region of the width $dx=vdt$, where v is the wave velocity, near the artificial boundaries. If the length of the overlapping region Ωo is chosen longer than $2dx$, then the reflected waves are present only within the half overlapping regions Ωo2 [c, d] in Ω1 and Ωo1 [b, c] in Ω2 near the boundaries. The wavefields within the half overlapping regions Ωo1 [b, c] in Ω1 and Ωo2 [c, d] in Ω2 are not affected by these artificial reflections.

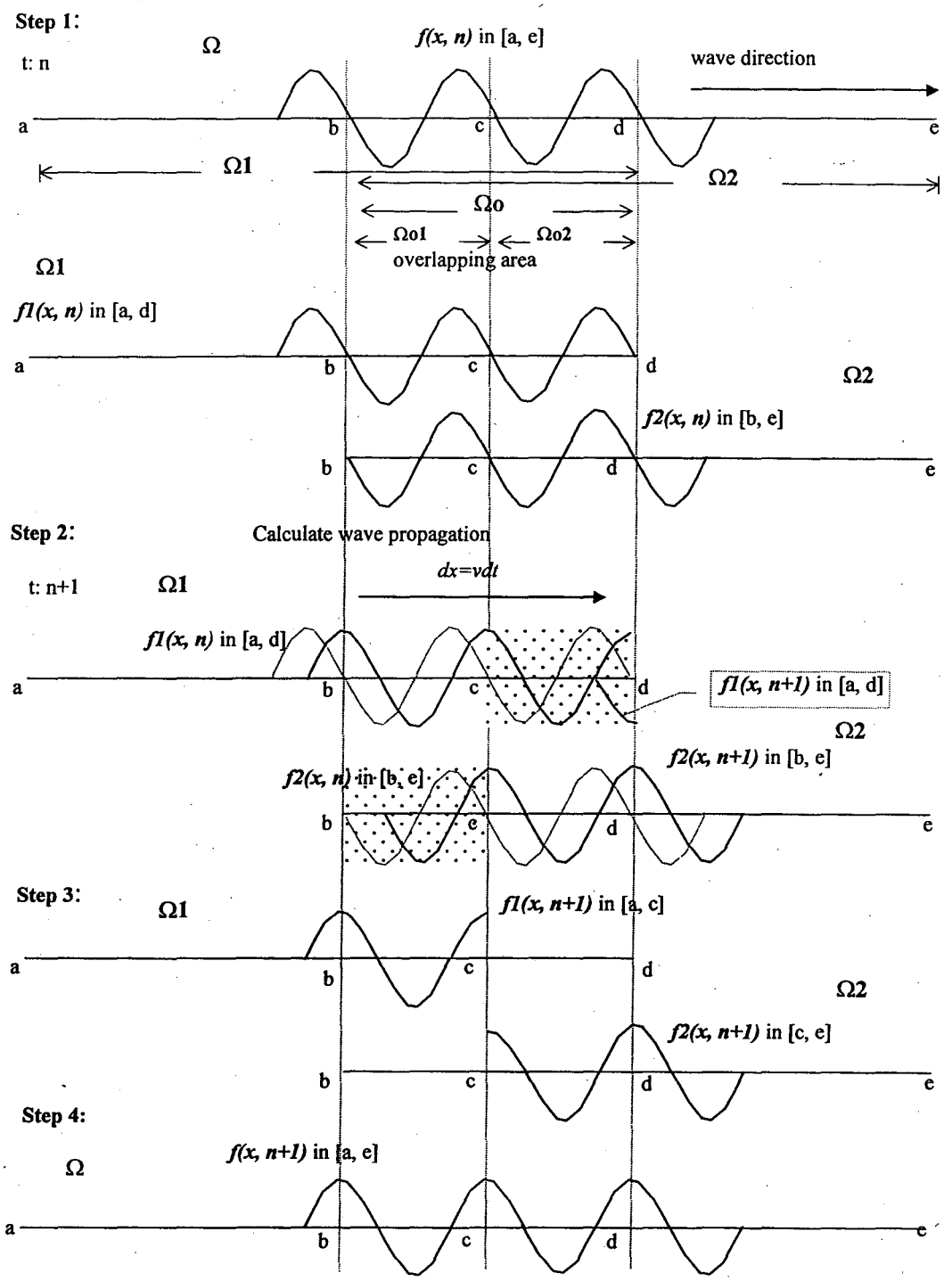

Figure 2.1. Schematic illustration of the 1-D overlap domain decomposition technique.

Step 3. Discard the "boundary contaminated" part of the wavefield from the region [c, d] in Ω1 and the region [b, c] in Ω2. Then, combine the wavefield from the region [a, c] in Ω1 and the region [c, e] in Ω2 to form the whole domain wavefield. Therefore, the new wavefield $f(x, n+1)$ is given by

$$f(x,n+1)=\begin{cases} f1(x,n+1) & x \in [a, c], \\ f2(x,n+1) & x \in [c, e]. \end{cases} \tag{2.2.3}$$

Thus, the reflected waves from the artificial boundaries are eliminated by taking the contributions from the respective solutions corresponding to the half of the overlapping region within each subdomain. The size of the overlapping region depends on the numerical method used for wave propagation.

2.3 Application of the ODD to the Finite Difference (FD) Method

The ODD technique can be directly implemented into the 1-D finite difference method. The key is how to determine the size of the overlapping area. In the following sections, the 1-D finite difference method is briefly reviewed and then the implementation of the ODD technique is discussed.

2.3.1 1-D Finite Difference Method

The 1-D wave equation for a medium with constant density ρ is

$$\frac{1}{c^2}\frac{\partial^2 u(x,t)}{\partial t^2}=\frac{\partial^2 u(x,t)}{\partial x^2}, \tag{2.3.1}$$

where u is the pressure, t is the time, and c is the wave velocity. For the FD method, the space and time domains are divided into finite grids with the spacings of dx and dt as shown in Figure 2.2. In this figure, $u(x_m, t_n)$ represents the pressure at the space point m and the time step n.

Centered FD approximations are made for both space and time derivatives of equation (2.3.1). For example, the fourth-order space FD and second-order time FD formulas are

$$\frac{\partial^2 u(x_m,t_n)}{\partial x^2} = \frac{1}{12\Delta x^2}\begin{bmatrix} -u(x_{m+2},t_n) + 16u(x_{m+1},t_n) - 30u(x_m,t_n) \\ +16u(x_{m-1},t_n) - u(x_{m-2},t_n) \end{bmatrix} + O([\Delta x]^4) \quad , (2.3.2)$$

and

$$\frac{\partial^2 u(x_m,t_n)}{\partial t^2} = \frac{1}{\Delta t^2}[u(x_m,t_{n+1}) - 2u(x_m,t_n) + u(x_m,t_{n-1})] + O([\Delta t]^2). \qquad (2.3.3)$$

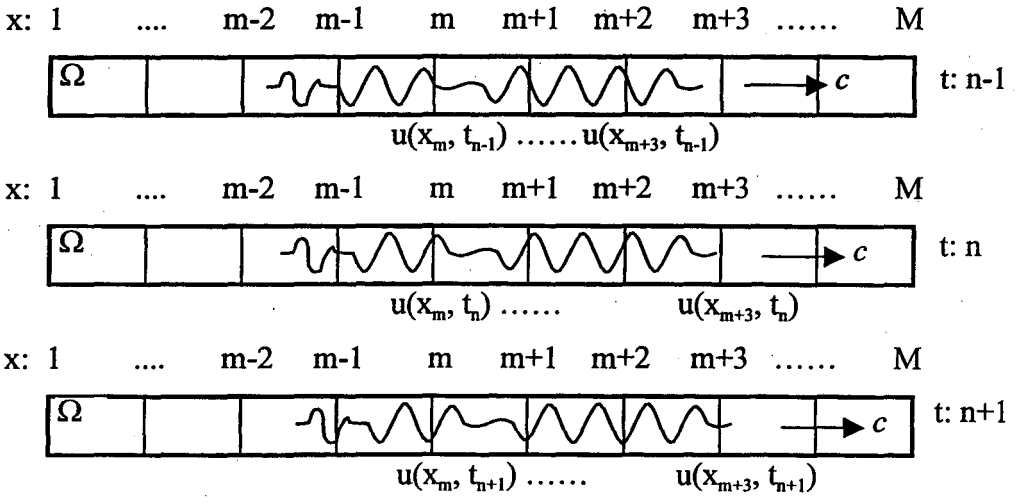

Figure 2.2. One dimensional grid for the finite difference method.

From equation (2.3.2) and (2.3.3) the explicit FD scheme for the wave equation (2.3.1) is

$$u(x_m,t_{n+1}) = 2u(x_m,t_n) - u(x_m,t_{n-1}) + \frac{c^2\Delta t^2}{12\Delta x^2}\begin{bmatrix} -u(x_{m+2},t_n)+16u(x_{m+1},t_n)-30u(x_m,t_n) \\ +16u(x_{m-1},t_n)-u(x_{m-2},t_n) \end{bmatrix} + O([\Delta x]^4,[\Delta t]^2). \quad (2.3.4)$$

The algorithm of the above equation is graphically shown in Figure 2.3. It is easy to see that u at time step n+1 only depends on u at the previous two time steps n and n-1. Furthermore, to determine $u(x_m, t_{n+1})$, only five values of u at adjacent grid points from m-2 to m+2 at time steps n and n-1 are required.

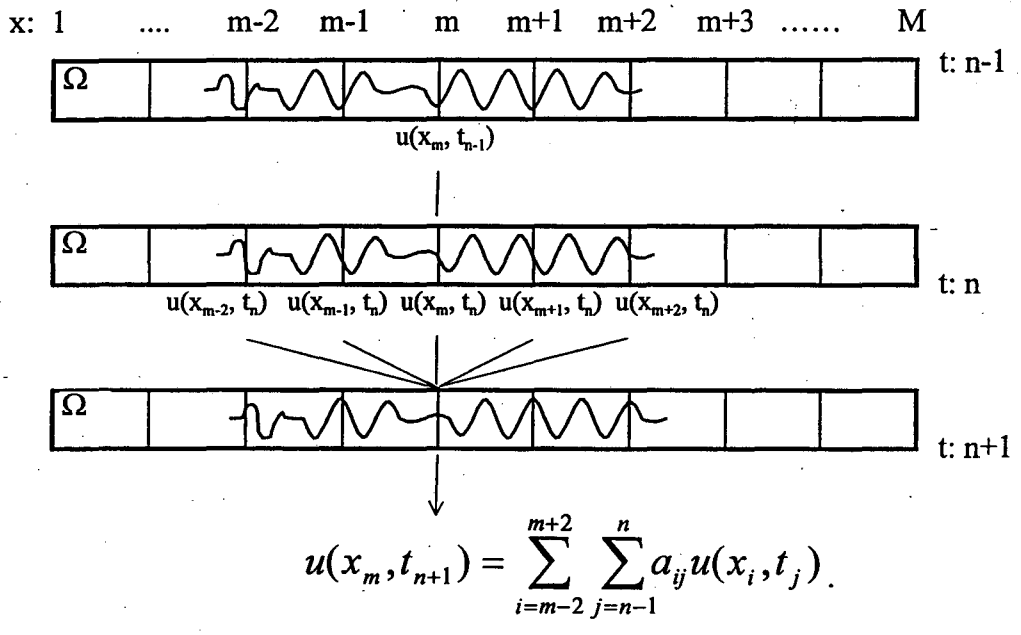

Figure 2.3. The finite different method with 4th order in space and 2nd order in time differencing, where a_{ij} are the coefficients in Equation (2.3.4).

2.3.2 ODD for the 1-D Finite Difference Method

To apply the ODD technique to equation (2.3.4), we divide the domain Ω into two subdomains Ω1 (dark shaded area) and Ω2 (light shaded area) as in Figure 2.4, where grid points 1, ... , m-2, m-1, m belong to Ω1 and grid points m+1, m+2, ... , M belong to Ω2. Grid point m is the last point in Ω1 where spatial derivative must be calculated; point m+1 is the first point in Ω2. The amount of overlap required between these two subdomains can be determined as follows. According to equation (2.3.4), in order to compute $u(x_m, t_{n+1})$ in Ω1, the values of two previous time steps are needed from the grid points m-2 through m+2. Assume that the pressures $u(x_i, t_n)$ and $u(x_i, t_{n-1})$ from the previous time steps n-1 and n are known values. If Ω1 is overlapped to cover the grid points m+1 and m+2, then $u(x_m, t_{n+1})$ can be solved within Ω1.

The grid points m+1 and m+2 which originally only belong to Ω2 now also belong to Ω1; therefore, these points form the overlapping region. $u(x_m, t_{n+1})$ can be calculated from Ω1 just as in the conventional FD. Similar to the grid point m+1 in Ω2, by adding two grid points m-1 and m to Ω2, $u(x_{m+1}, t_{n+1})$ can be calculated at the grid point m+1 in Ω2 using the values of u from grid points m-1 and m+3. The total overlapping region now spans the grid points from m-1 through m+2. As can be seen from this analysis, the overlapping region only needs four grid points for 4th order space differencing (Figure 2.4) to get the same results as the conventional FD method applied to the total domain Ω. More grid points in the overlapping region do not affect results.

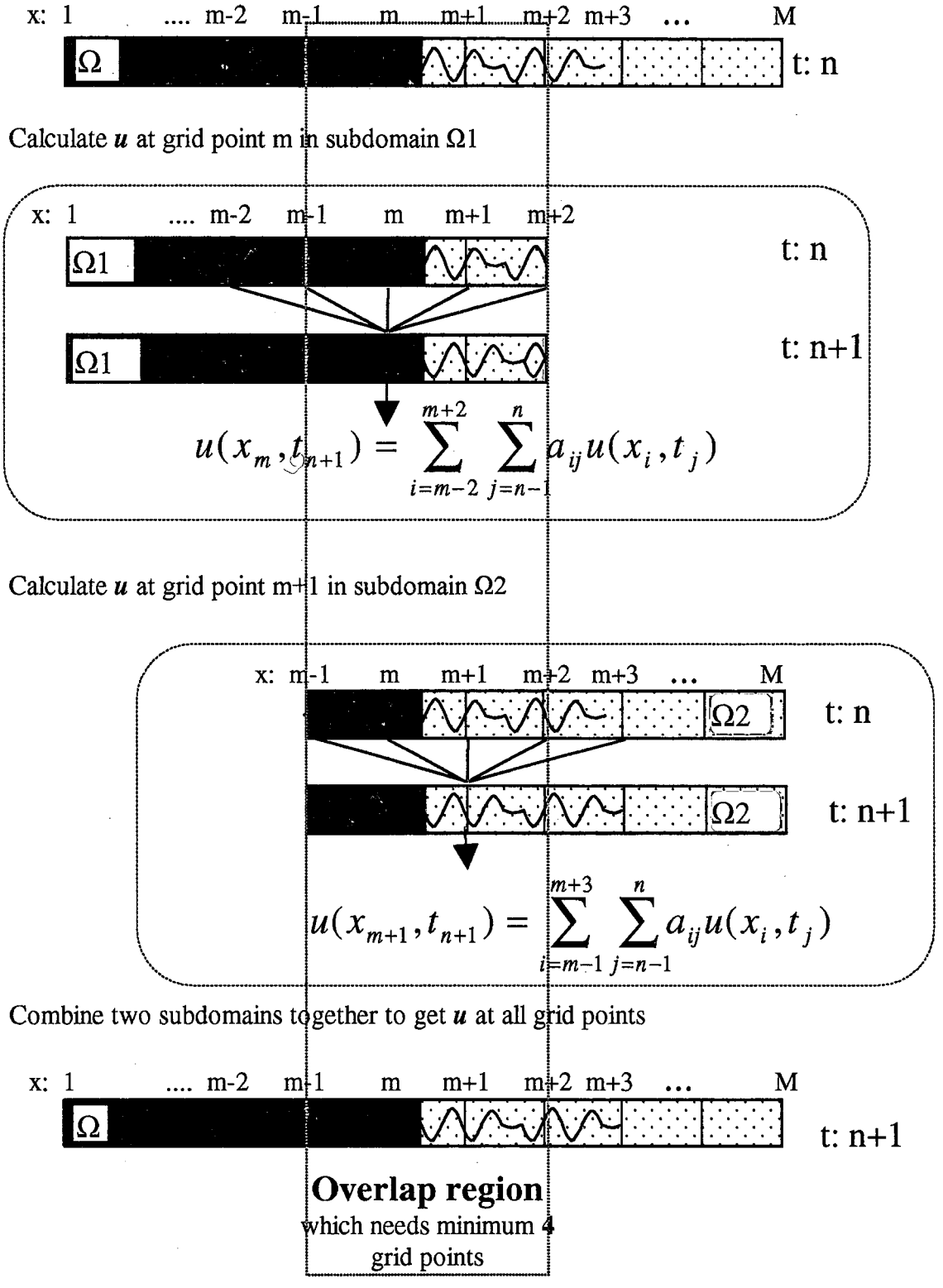

Figure 2.4. The ODD scheme for the 1-D FD method with 4th order space and 2nd order time differencing.

It should be noted that the results at grid points m+1, m+2 in Ω1 and m-1, m in Ω1 near the artificial boundaries are not used and only the uncontaminated results in the inner region are used to form the solution at time step n+1. Therefore, the artificial boundaries do not adversely affect the solution.

2.4 Application of ODD to the Fourier Pseudospectral Method

2.4.1 1-D Fourier Pseudospectral Method

The Fourier pseudospectral (PS) method has been successfully developed in recent years for acoustic and elastic wave propagation problems (Gazdag, 1981; Kosloff and Baysal, 1982; Fornberg, 1987 and 1996; Kosloff et al., 1990; Furumura et al., 1995 and 1998). Unlike the FD method, the PS method uses a Fourier transform to calculate the spatial derivatives.

Let $\hat{u}(k_l,t_n)$ denote the Fourier transform of $u(x_1,t_n),...,u(x_m,t_n),...,u(x_M,t_n)$ with respect to the variable x, and

$$\hat{u}(k_l,t_n)=\sum_{m=0}^{M-1}u(x_m,t_n)e^{-ik_lx_m}, \tag{2.4.1}$$

where $k_l = 2\pi l/(N\Delta x)$, $\Delta x = x_m - x_{m-1}$. The inverse Fourier transform of $\hat{u}(k_l,t_n)$ is given by

$$u(x_m,t_n)=\frac{1}{M}\sum_{l=0}^{M-1}\hat{u}(k_l,t_n)e^{ik_lx_m}. \tag{2.4.2}$$

From equation (2.4.2), the first and second-order spatial derivatives are

$$\frac{\partial u(x_m,t_n)}{\partial x}=\frac{1}{M}\sum_{l=0}^{M-1}(ik_l)\hat{u}(k_l,t_n)e^{ik_l x_m}, \tag{2.4.3}$$

$$\frac{\partial^2 u(x_m,t_n)}{\partial x^2}=\frac{1}{M}\sum_{l=0}^{M-1}(-k_l{}^2)\hat{u}(k_l,t_n)e^{ik_l x_m}. \tag{2.4.4}$$

The PS method solution for the 1-D wave equation (2.3.1) is then

$$u(x_m,t_{n+1})=2u(x_m,t_n)-u(x_m,t_{n-1})$$
$$+c^2\Delta t^2\left[\frac{1}{M}\sum_{l=0}^{M-1}(-k_l{}^2)\hat{u}(k_l,t_n)e^{ik_l x_m}\right]. \tag{2.4.5}$$

An important difference between the PS and the FD methods is that calculation of the derivative by the PS method requires the values of u at all the grid points. For this reason, the PS method is effectively employs higher-order spatial differencing resulting in more accurate calculation of the derivatives. However, because a Fourier transform is required for each derivative calculation, it is computationally more intensive than the FD method.

A nagging problem which arises in application of the Fourier PS method for wave propagation is the presence of wraparound boundaries (Kosloff et al., 1982; Furumura and Takenaka 1995) from the boundaries of the numerical mesh shown in Figure 2.5. When a wavefront reaching the one side of the boundaries, the wavefront comes from the other side of the boundaries due to the periodic property of the trigonometric series of Fourier transform. A tapering function was proposed by Cerjan et al. (1985) to eliminate the wraparound problems.

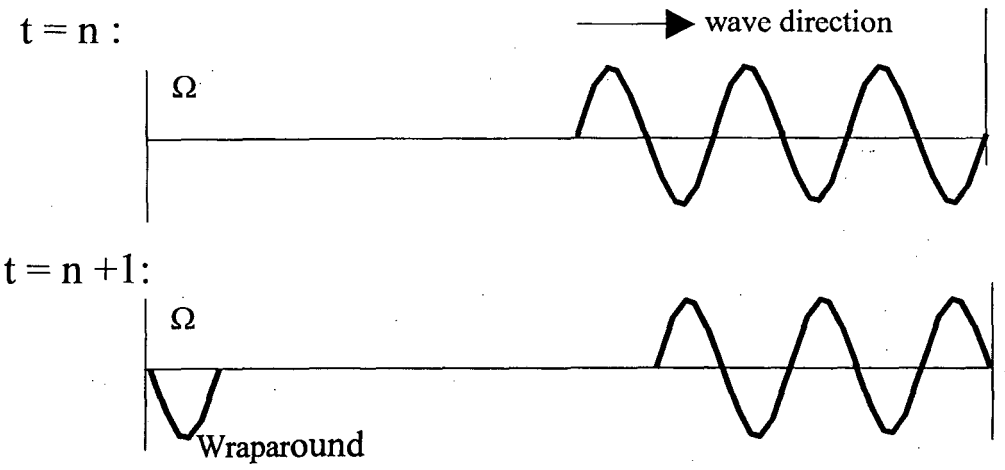

Figure. 2.5. Wraparound problem by using the Fourier pseudospectral method.

2.4.2 ODD for 1-D Fourier Pseudospectral (PS) method

The ODD technique can also be applied to the Fourier PS method. Two problems which arise when the ODD technique developed in the previous section is applied to equation (2.3.1) are: (1) the wraparound which occurs at the overlapping boundaries, and (2) the need to known the pressure at all the grid points of the previous time steps.

The wraparound effect can be circumvented by applying a taper to the wavefield at the boundaries of each subdomain (Liao and McMechan, 1993). By tapering the wavefield to zero near the boundaries of all the subdomains, the Fourier wraparound contributions become zero and the transfer of artificial waves to the other ends of the subdomains is eliminated.

Because the PS method uses values at all grid points to compute the derivatives at a single point, it may be argued that the tapering the original function might yield an incorrect result even though the value at the grid point of interest is not altered. However, mathematically, the derivatives at one point belong the local properties of the function at that point. Thus, the derivatives at the point are only dependent on the property of the local region and are not significantly affected by points far away. Since the tapering introduced in the PS ODD technique is performed only within the outer region of the overlapping area, it has little effect on the derivatives computed for a grid point within the non-overlapping region and inner overlapping regions in Figure 2.6. So, the derivatives computed for all grid points are not affected by the taper function, if the width of the overlapping region is chosen wide enough (must be greater than the length of the taper).

Figure 2.6 illustrates an example of tapering functions *T1(x)* and *T2(x)* that are applied to the subdomains. Based on the Hanning window (Oppenheim and Schafer, 1975), the two functions are defined as given below:

$$T1(x) = \begin{cases} 0 & x \in [a,\ a+\varepsilon] \\ 0.5 + 0.5\cos(\pi(x-a-\varepsilon)/l + \pi) & x \in [a+\varepsilon, a+\varepsilon+l] \\ 1 & x \in [a+\varepsilon+l, c+\varepsilon], \\ 0.5 + 0.5\cos(\pi(x-c-\varepsilon)/l) & x \in [c+\varepsilon, d-\varepsilon] \\ 0 & x \in [d-\varepsilon, d] \end{cases} \quad (2.4.6)$$

$$T2(x) = \begin{cases} 0 & x \in [b,\ b+\varepsilon] \\ 0.5 + 0.5\cos(\pi(x-b-\varepsilon)/l + \pi) & x \in [b+\varepsilon, c-\varepsilon] \\ 1 & x \in [c-\varepsilon, e-\varepsilon-l], \\ 0.5 + 0.5\cos(\pi(x-(e-\varepsilon-l))/l) & x \in [e-\varepsilon-l, e-\varepsilon] \\ 0 & x \in [e-\varepsilon, e] \end{cases} \quad (2.4.7)$$

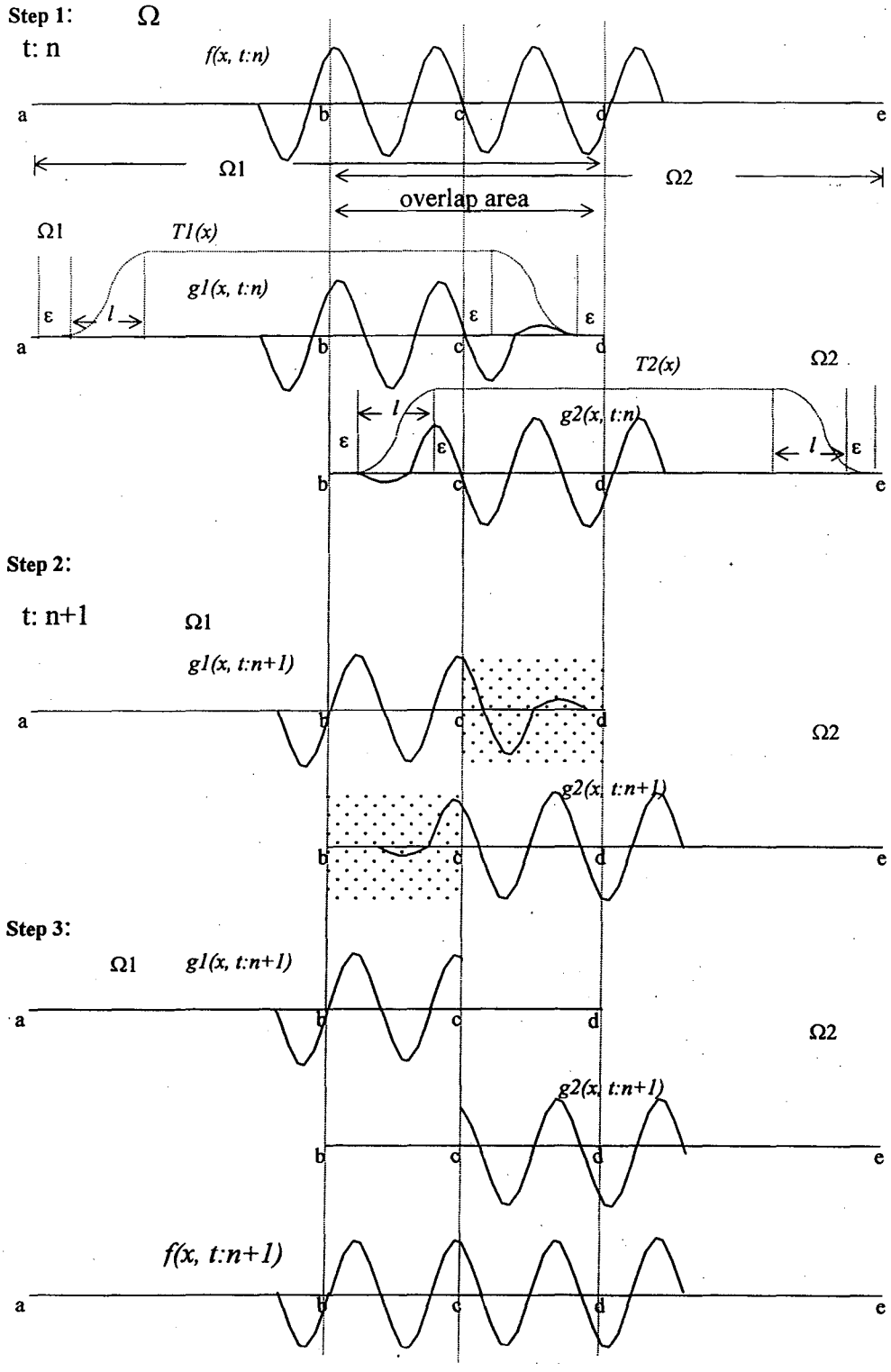

Figure 2.6. Overlap domain decomposition scheme for the 1-D PS method.

where the $2l+4\varepsilon$ is the length of the overlapping area, and ε is on the order of 2dx. The procedure of Figure 2.6 can be described as:

Step 1: Apply the taper functions $T1(x)$ and $T2(x)$ to the subdomains $\Omega 1$ and $\Omega 2$. The new wavefield functions are:

$$g1(x, t{:}n) = T1(x) \cdot f1(x, t{:}n) \qquad x \in [a, d] \text{ in } \Omega 1, \tag{2.4.8}$$

$$g2(x, t{:}n) = T2(x) \cdot f2(x, t{:}n) \qquad x \in [b, e] \text{ in } \Omega 2. \tag{2.4.9}$$

Wavefield functions $g1$ and $g2$ are not equal to $f1$ and $f2$ for the outer regions of the overlapping area $[c, d]$ in $\Omega 1$ and $[b, c]$ in $\Omega 2$. These become zero near the artificial boundaries $x=b$ and $x=d$, and are equal to $f1$ and $f2$ within the inner regions ($[a+l+\varepsilon, d-l-\varepsilon]$ in $\Omega 1$ and $[b+l+\varepsilon, e-l-\varepsilon]$ in $\Omega 2$).

Step 2: Calculations by the PS method are independently carried out in $\Omega 1$ and $\Omega 2$. There are no reflections at $x=b$ and $x=d$ since $g1$ and $g2$ are zero near the artificial boundaries.

Step 3: Take the inner regions of wavefields $[a+l+\varepsilon, c]$ in $\Omega 1$ and $[c, e-l-\varepsilon]$ in $\Omega 2$ that are not modified by the taper functions and form the final wavefield $f(x, t{:}n+1)$.

The length of the overlapping area is approximately $2l$, which is the wavelength of the cosine function used for the taper functions $T1(x)$ and $T2(x)$. For wave propagation problems, we choose the length of the overlapping area to be on the order of the wavelength of the central frequency of the source wavelet.

2.5 Application of ODD to the Mixed PS and FD Method

Because the computations within individual subdomains are carried out independently using the ODD technique, the FD and PS methods can be easily coupled together. Figure 2.7 shows how the PS in subdomain Ω1 and the FD subdomain Ω2 can be coupled. A similar procedure as in Section 2.4 is followed to compute the wavefield.

Step 1: Apply taper function $T1(x)$ to the wavefield in subdomain Ω1 where the PS method is applied. The wavefield in subdomain Ω2 is computed with the FD method. So no tapering is required. The new wavefield functions become

$$g1(x, t{:}n) = T1(x) \cdot f1(x, t{:}n) \qquad x \in [a, d] \text{ in } \Omega 1. \tag{2.5.1}$$

$$f2(x, t{:}n) \qquad x \in [b, e] \text{ in } \Omega 2. \tag{2.5.2}$$

Step 2: Separately calculate the wavefields at time step n+1 using the PS method in Ω1 and the FD4 method in Ω2. In Ω1 there is no reflection from the artificial boundary at $x=d$ where the wavefield is tapered to zero. In contrast, the reflection occurs at $x=b$ in Ω2 but there is no wraparound to the side at $x=d$ since the FD method is being used.

Step 3: Take the inner parts of wavefields within $[a+l+\varepsilon, c]$ in Ω1 and $[c, e]$ in Ω2, to form the final wavefield $f(x, t{:}n+1)$.

To obtain smooth solutions across the subdomains, the PS and FD differencing schemes used in each subdomain should have similar accuracies.

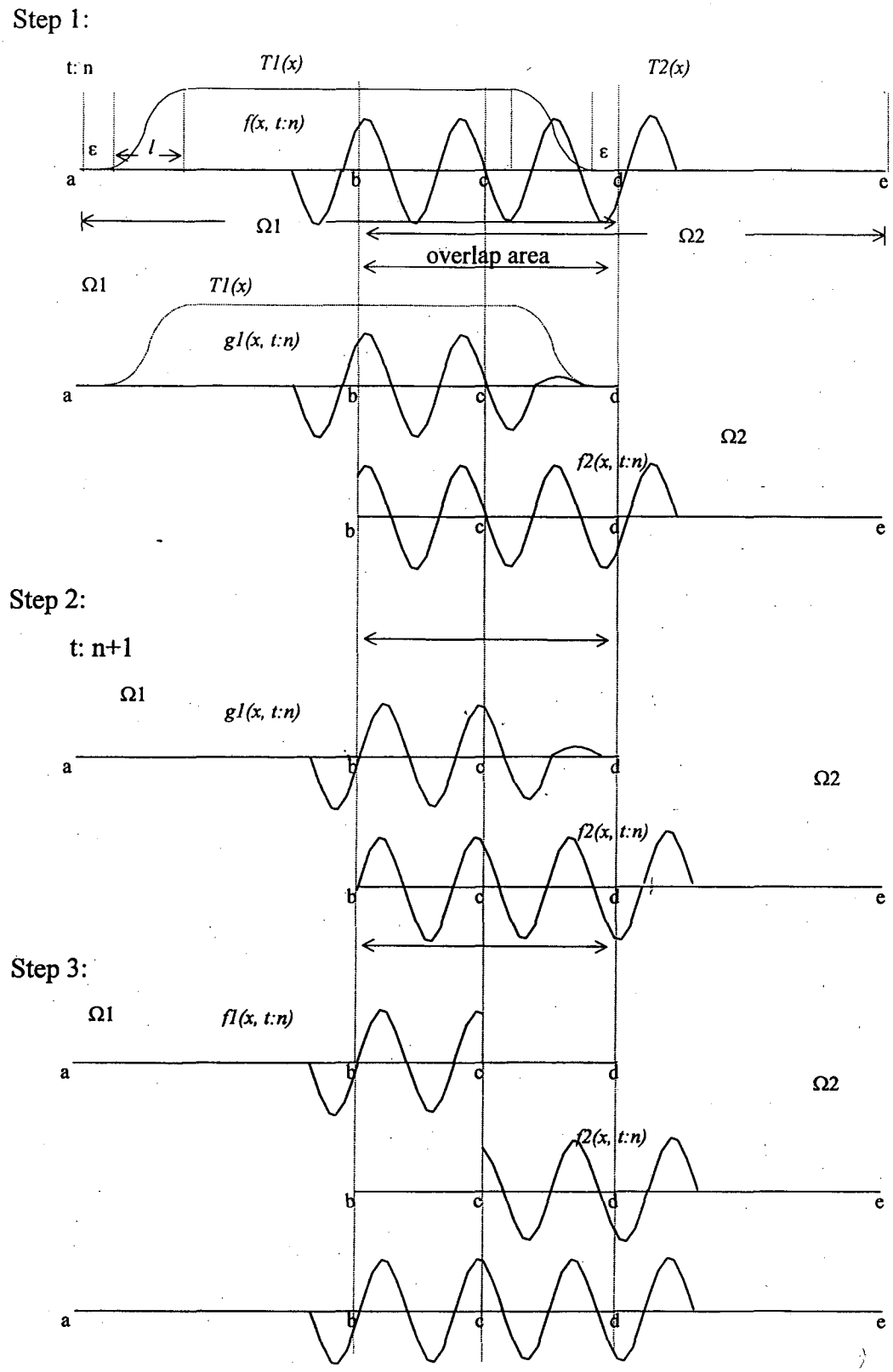

Figure 2.7. ODD scheme for the 1-D mixed PS and FD method.

2.6 Stability Conditions

In this section, the stability conditions are derived for the numerical methods used in the previous sections. Consider an isotropic, homogeneous medium, for which the density ρ and velocity C_0 are constants. If the spatial derivative is known, the solution of the wave equation (2.3.1) in the Section 2.3 with second order accuracy in time can be written as

$$u(x_m,t_{n+1}) = 2u(x_m,t_n) - u(x_m,t_{n-1}) + C_0^2\Delta t^2 \frac{\partial^2 u(x_m,t_n)}{\partial x^2}. \tag{2.6.1}$$

A parameter τ is defined as

$$\tau = C_0^2\Delta t^2 \frac{\partial^2 u(x_m,t_n)}{\partial x^2} \Big/ u(x_m,t_n). \tag{2.6.2}$$

Substituting equation (2.6.2) into equation (2.6.1) gives

$$u(x_m,t_{n+1}) = (2+\tau)u(x_m,t_n) - u(x_m,t_{n-1}). \tag{2.6.3}$$

Equation (2.6.3) can be expressed in matrix form as

$$\begin{bmatrix} u(x_m,t_{n+1}) \\ u(x_m,t_n) \end{bmatrix} = \begin{bmatrix} 2+\tau & -1 \\ 1 & 0 \end{bmatrix} \begin{bmatrix} u(x_m,t_n) \\ u(x_m,t_{n-1}) \end{bmatrix}. \tag{2.6.4}$$

Letting

$$\underline{\underline{A}} = \begin{bmatrix} 2+\tau & -1 \\ 1 & 0 \end{bmatrix}, \tag{2.6.5}$$

and

$$\underline{W}^n = \begin{bmatrix} u(x_m, t_n) \\ u(x_m, t_{n-1}) \end{bmatrix}, \tag{2.6.6}$$

equation (2.6.4) can be written as

$$\underline{W}^{n+1} = \underline{\underline{A}}\,\underline{W}^n . \tag{2.6.7}$$

The necessary condition for stability is the Von Neumann condition that requires all the eigenvalues λ_i of the amplification matrix $\underline{\underline{A}}$ be bounded by 1.0 in magnitude (Boore, 1972; Smith, 1965; Gazdag, 1980)

$$|\lambda_i| \le 1. \tag{2.6.8}$$

To obtain the eigenvalues, set

$$\left|\lambda \underline{\underline{I}} - \underline{\underline{A}}\right| = 0. \tag{2.6.9}$$

where $\underline{\underline{I}}$ is the identity matrix of order.

Substituting equation (2.6.5) into equation (2.6.9) gives

$$\begin{vmatrix} \lambda - (2+\tau) & 1 \\ -1 & \lambda \end{vmatrix} = 0, \tag{2.6.10}$$

or

$$\lambda^2 - (2+\tau)\lambda + 1 = 0. \tag{2.6.11}$$

This yields the eigenvalues

$$\lambda_i = 0.5[(2+\tau) \pm \sqrt{(2+\tau)^2 - 4}]. \tag{2.6.12}$$

By applying the above equation to equation (2.6.8), the stability condition for equation (2.6.1) can be obtained as (see Appendix C for details)

$$0 \geq \tau \geq -4. \tag{2.6.13}$$

If different numerical methods are used to compute the second order spatial derivative, the resulting τ's are assessed for their stability conditions. In the following section, stability conditions for three numerical differencing methods (2nd and 4th order finite difference and Fourier pseudospectral methods) are discussed.

2.6.1 Stability Condition for the 2nd Order FD Method

From the results of Section 2.4, the second order spatial derivatives of equation (2.6.1) can be discretized using 2nd order differences as

$$\frac{\partial^2 u(x_m,t_n)}{\partial x^2} = \frac{1}{\Delta x^2}\left[u(x_{m+1},t_n) - 2u(x_m,t_n) + u(x_{m-1},t_n)\right]. \tag{2.6.14}$$

A solution of equation (2.3.1) is assumed to have a harmonic form

$$u(x_m,t_n) = u_0 e^{i(kx-\omega t)} = u_0 e^{i(k\cdot m\Delta x - \omega\cdot n\Delta t)}, \tag{2.6.15}$$

where $x = m\cdot\Delta x$, $t = n\cdot\Delta t$ and the wavenumber k is in the spatial frequency of the numerical mesh.

Substituting this harmonic solution into equation (2.6.14) produces

$$\frac{\partial^2 u(x_m,t_n)}{\partial x^2} = \frac{u_0 e^{i(kx-wt)}}{\Delta x^2}\left[e^{ik\Delta x} - 2 + e^{-ik\Delta x}\right]$$
$$= 2\frac{u(x_m,t_n)}{\Delta x^2}[\cos(k\Delta x) - 1] \qquad (2.6.16)$$
$$= -4\frac{\sin^2(k\Delta x/2)}{\Delta x^2}u(x_m,t_n).$$

Using the definition of τ in equation (2.6.2) gives

$$\tau = -4C_0{}^2\Delta t^2\frac{\sin^2(k\Delta x/2)}{\Delta x^2}. \qquad (2.6.17)$$

Substituting the above equation into the stability condition equation (2.6.13) gives

$$0 \geq -4C_0{}^2\Delta t^2\frac{\sin^2(k\Delta x/2)}{\Delta x^2} \geq -4,$$

or

$$-1 \leq \frac{C_0\Delta t}{\Delta x}\sin(k\Delta x/2) \leq 1. \qquad (2.6.18)$$

Since $\sin(k\Delta x/2) \leq 1$, the stability condition for the 2nd order FD method is

$$\frac{C_0\Delta t}{\Delta x} \leq 1. \qquad (2.6.19)$$

2.6.2 Stability Condition for the 4th order FD method

The second order spatial derivative of equation (2.6.1) can be discretized by the fourth order finite difference as

$$\frac{\partial^2 u(x_m,t_n)}{\partial x^2}$$
$$= \frac{1}{12\Delta x^2}\left[-u(x_{m+2},t_n)+16u(x_{m+1},t_n)-30u(x_m,t_n)+16u(x_{m-1},t_n)-u(x_{m-2},t_n)\right]. \quad (2.6.20)$$

Substituting the harmonic solution in equation (2.6.15) into the above equation produces

$$\begin{aligned}\frac{\partial^2 u(x_m,t_n)}{\partial x^2} &= \frac{u_0 e^{i(kx-wt)}}{12\Delta x^2}\left[-e^{ik2\Delta x}+16e^{ik\Delta x}-30+16e^{ik\Delta x}-e^{ik2\Delta x}\right] \\ &= \frac{u(x_m,t_n)}{6\Delta x^2}\left[-(\cos(2k\Delta x)-1)+16(\cos(k\Delta x)-1)\right] \\ &= -\frac{u(x_m,t_n)}{3\Delta x^2}[16\sin^2(k\Delta x/2)-\sin^2(k\Delta x)].\end{aligned} \quad (2.6.21)$$

Using the definition of τ in equation (2.6.3), now τ has a form

$$\tau = -C_0{}^2\Delta t^2\,\frac{16\sin^2(k\Delta x/2)-\sin^2(k\Delta x)}{3\Delta x^2}. \quad (2.6.22)$$

Substitution of the above equation into the stability condition equation (2.6.13) yields

$$\frac{C_0\Delta t}{\sqrt{12}\Delta x}[16\sin^2(k\Delta x/2)-\sin^2(k\Delta x)]^{1/2} \le 1, \quad (2.6.23)$$

where

$$[16\sin^2(k\Delta x/2)-\sin^2(k\Delta x)]^{1/2} \le 4. \quad (2.6.24)$$

Therefore, the stability condition for the 4th order FD method is

$$\frac{C_0\Delta t}{\Delta x} < \frac{\sqrt{3}}{2} \approx 0.866\ . \quad (2.6.25)$$

2.6.3 Stability Condition for the Fourier PS Method

The Fourier expansion of u(x, t) can be expressed as

$$u(x_m,t_n)=\sum_{l=0}^{M-1}u_l(x_m,t_n)=\frac{1}{M}\sum_{l=0}^{M-1}\hat{u}(k_l,t_n)e^{ik_lx_m}. \tag{2.6.26}$$

The stability condition shown in equation (2.6.13) can be applied to each term of the above equation. For a single l term of equation (2.6.26), the second order derivative is

$$\begin{aligned}\frac{\partial^2 u_l(x_m,t_n)}{\partial x^2}&=\frac{1}{M}(-k_l^{\,2})\hat{u}(k_l,t_n)e^{ik_lx_m}\\&=(-k_l^{\,2})u_l(x_m,t_n).\end{aligned} \tag{2.6.27}$$

According to the definition of τ in equation (2.6.2) and the stability condition in equation (2.6.13)

$$\tau=C_0^{\,2}\Delta t^2(-k_l^{\,2})\geq -4$$

or,

$$C_0\Delta t\leq\frac{2}{k_l}. \tag{2.6.28}$$

The largest k_l is at the Nyquist spatial frequency for which $k_l=\pi/\Delta x$. A substitution of this value in the equation (2.6.28) gives the stability condition for the Fourier PS method

$$\frac{C_0\Delta t}{\Delta x}\leq\frac{2}{\pi}\approx 0.637. \tag{2.6.29}$$

Equation (2.6.29) shows that the stability condition for the PS method requires relative smaller time step compared to the stability conditions for the FD methods in equations (2.6.19) and (2.6.25).

2.7 Dispersion Condition

In a homogeneous acoustic or elastic medium, waves with any frequencies propagate with the same velocity (Graff, 1975; Aki and Richards, 1980). When solving the wave equation by the numerical methods, the wave velocities become functions of the discretization intervals of Δt and Δx. This phenomenon is called the dispersion. The previous section gives the relations between the Δt and Δx for the stability of the numerical methods. This section will states how many grid points of Δt and Δx are needed for the certain frequency and wavelength of the wave under the limited dispersion. The dispersion analysis for the second order time and fourth order space finite difference method performed in this section is similar to the method by Dablain (1984) for the second order accuracy finite difference method. The temporal and spatial dispersions are first discussed separately, and then the coupled dispersion is studied.

2.7.1 Temporal Dispersion

Consider an isotropic, homogeneous medium with constant density ρ and velocity C_0. Assume a solution of equation (2.3.1) of the form

$$u = u_0 e^{i(kx-\omega t)}, \tag{2.7.1}$$

where $x=m\Delta x$, $t=n\Delta t$, and k is the wavenumber in the band of the numerical mesh. The temporal portion of equation (2.3.1) can be discretized by second order FD as

$$\frac{\partial^2 u(x_m,t_n)}{\partial t^2} = \frac{1}{\Delta t^2}[u(x_m,t_{n+1}) - 2u(x_m,t_n) + u(x_m,t_{n-1})], \tag{2.7.2}$$

and equation (2.3.1) can be expressed as

$$\frac{1}{\Delta t^2}[u(x_m,t_{n+1})-2u(x_m,t_n)+u(x_m,t_{n-1})]=C_0^2\frac{\partial^2 u(x_m,t_n)}{\partial x^2}. \tag{2.7.3}$$

Substituting the harmonic solution of equation (2.7.1) into the above equation produces

$$\frac{1}{\Delta t^2}[e^{i\omega\Delta t}-2+e^{i\omega\Delta t}]=-C_0{}^2k^2,$$

or

$$\frac{2}{\Delta t^2}[\cos(\omega\Delta t)-1]=-C_0{}^2k^2. \tag{2.7.4}$$

By definition, the phase speed C_P is

$$C_P=\frac{\omega}{k}. \tag{2.7.5}$$

Equation (2.7.5) is now substituted into equation (2.7.4) to obtain the dispersion relationship for the temporal discretization

$$\frac{2}{\Delta t^2}[\cos(\omega\Delta t)-1]=-C_0{}^2\frac{\omega^2}{C_P{}^2},$$

or

$$\frac{C_P{}^2}{C_0{}^2}=-\frac{\theta^2}{2[\cos(\theta)-1]}, \tag{2.7.6}$$

where $\theta=\omega\Delta t$. This equation can be simplified as

$$\frac{C_P{}^2}{C_0{}^2} = \frac{\theta^2}{4\sin^2(\theta/2)}. \tag{2.7.7}$$

The normalized phase velocity dispersion relationship can be written as

$$\frac{C_P}{C_0} = \frac{\theta}{2\sin(\theta/2)}. \tag{2.7.8}$$

Assuming that low frequencies or very small time steps are taken, i.e., $\theta \sim 0$, then equation (2.7.8) can be approximated by a Taylor's series as

$$\frac{C_P}{C_0} = \frac{\theta}{2[\frac{\theta}{2} - \frac{1}{3!}(\frac{\theta}{2})^3 + \cdots]} \approx 1 + \frac{\theta^2}{24}. \tag{2.7.9}$$

Since θ can be expressed as

$$\theta = \omega\Delta t = 2\pi f\Delta t = 2\pi\frac{\Delta t}{T} = 2\pi\beta\ , \tag{2.7.10}$$

where f is frequency, T is the period, and $\beta = \Delta t/T$, $1/\beta$ is the number of time steps per period, and equation (2.7.8) can be rewritten as

$$\frac{C_P}{C_0} \approx 1 + \frac{(2\pi\beta)^2}{24} = 1 + \frac{\pi^2}{6}\beta^2 \approx 1 + 1.65\beta^2. \tag{2.7.11}$$

Equation (2.7.8) and (2.7.11) indicate that as Δt increases or the frequencies become greater, the tendency is for parts of the wavelet to be advanced with respect to the true phase velocity. Figure 2.7.1 shows the dispersion curves by equation (2.7.8) and

(2.7.11), which indicates that the relative error of phase velocity is less than 1% when β is less than 0.07 (13 time steps per period).

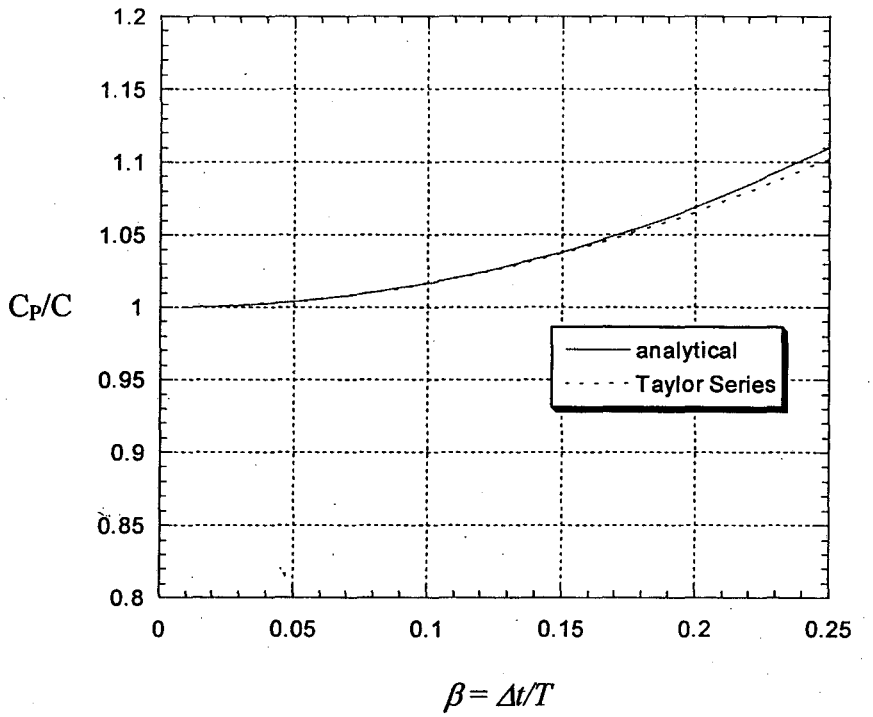

Figure 2.7.1. Temporal dispersion curves of phase velocity for finite difference solutions with second order accuracy in time.

Similarly, the dispersion analysis can be applied to group velocity. The group velocity C_G is computed by

$$C_G = \frac{d\omega}{dk}. \tag{2.7.12}$$

The equation (2.7.4) can be rewritten as

$$\frac{4\sin^2(\omega\Delta t/2)}{\Delta t^2} = {C_0}^2 k^2,$$

or

$$\frac{2\sin(\omega\Delta t/2)}{\Delta t} = C_0 k. \tag{2.7.13}$$

By taking the derivative of equation (2.7.13), the dispersion equation of group velocity is derived as

$$\cos(\omega\Delta t/2)d\omega = C_0 dk. \tag{2.7.14}$$

Combining this with equation (2.7.10) and (2.7.12), the normalized group velocity is

$$\frac{C_G}{C_0} = \frac{d\omega}{C_0 dk} = \frac{1}{\cos(\omega\Delta t/2)} = \frac{1}{\cos(\theta/2)}, \tag{2.7.15}$$

and its approximation by a Taylor's series is

$$\frac{C_G}{C_0} = \frac{1}{1-\frac{(\theta/2)^2}{2!}+\frac{1}{4!}(\theta/2)^4+\cdots} \approx 1+\frac{\theta^2}{8}, \tag{2.7.16}$$

or

$$\frac{C_G}{C_0} \approx 1+\frac{(\pi\beta)^2}{2} \approx 1+4.9\beta^2. \tag{2.7.17}$$

Equation (2.7.16) and (2.7.17) indicate that as Δt increases or the frequency becomes greater, the group velocity tends to be faster than the true velocity. Figure 2.7.2 shows the dispersion curves computed by equation (2.7.15) and (2.7.17). The figure indicates that the relative error of group velocity is less than 1% when β is less than 0.04 (25 time steps per period). This analysis reveals that the error for the group velocity is almost twice the error for the phase velocity.

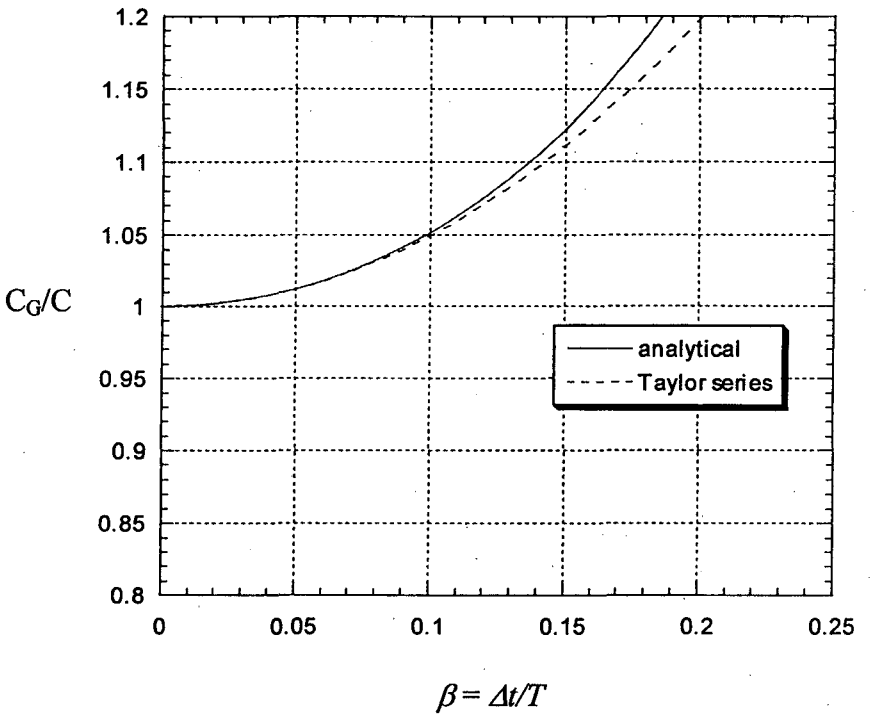

Figure 2.7.2. Temporal dispersion curves of group velocity for finite difference solutions with second order accuracy in time.

2.7.2 Spatial Dispersion

The spatial dispersion can be examined following a similar procedure as the temporal dispersion. The spatial derivative of equation (2.3.1) can be discretized by the fourth order FD as

$$\frac{\partial^2 u(x_m,t_n)}{\partial t^2} = \frac{C_0^2}{12\Delta x^2}\left[-u(x_{m+2},t_n)+16u(x_{m+1},t_n)-30u(x_m,t_n)+16u(x_{m-1},t_n)-u(x_{m-2},t_n)\right]. \tag{2.7.18}$$

Substituting the harmonic solution of equation (2.7.1) into the above equation produces

$$-\omega^2 u_0 e^{i(km\Delta x-wn\Delta t)} = \frac{C_0^2 u_0 e^{i(km\Delta x-wn\Delta t)}}{12\Delta x^2}\left[-e^{ik2\Delta x}+16e^{ik\Delta x}-30+16e^{ik\Delta x}-e^{ik2\Delta x}\right],$$

or

$$\omega^2 = \frac{C_0^2}{6\Delta x^2}\left[(\cos(2k\Delta x)-1)-16(\cos(k\Delta x)-1)\right]. \tag{2.7.19}$$

Let

$$\psi = k\Delta x. \tag{2.7.20}$$

and substituting equation (2.7.5) and (2.7.20) into equation (2.7.19). This gives the dispersion relationship

$$\frac{C_P^2}{C_0^2} = \frac{1}{6\psi^2}\left[(\cos 2\psi-1)-16(\cos\psi-1)\right]. \tag{2.7.21}$$

Then, expressing $\cos\psi$ and $\cos 2\psi$ by Taylor's series

$$\frac{C_P^2}{C_0^2}=\frac{1}{6\psi^2}\left[\left[1-\frac{1}{2!}(2\psi)^2+\frac{1}{4!}(2\psi)^4-\frac{1}{6!}(2\psi)^6\cdots-1\right]-16\left[1-\frac{1}{2!}\psi^2+\frac{1}{4!}\psi^4-\frac{1}{6!}\psi^6\cdots-1\right]\right],$$

or

$$\frac{C_P^2}{C_0^2}\approx 1-\frac{\psi^4}{90}. \tag{2.7.22}$$

The above dispersion relationship can be approximated by

$$\frac{C_P}{C_0}\approx 1-\frac{\psi^4}{180}. \tag{2.7.23}$$

Since

$$k=\frac{2\pi}{\lambda}, \tag{2.7.24}$$

where λ is the wavelength. Let

$$\alpha=\frac{\Delta x}{\lambda}, \tag{2.7.25}$$

where $1/\alpha$ is the number of grid points per wavelength. Substituting equation (2.7.24) and 2.7.25 into equation (2.7.20) gives

$$\psi=2\pi\alpha. \tag{2.7.26}$$

Therefore, equation (2.7.23) can be expressed as

$$\frac{C_P}{C_0} \approx 1 - \frac{4\pi^4}{45}\alpha^4 \approx 1 - 8.64\alpha^4 . \qquad (2.7.27)$$

Equation (2.7.23) and (2.7.27) indicate that as Δx increases or the wavelength becomes smaller, the computed phase velocity tends to be slower than the true velocity. Figure 2.7.3 shows the dispersion curves computed from equation (2.7.21) and (2.7.27). The plot indicates that the relative error in phase velocity is less than 1% when α is less than 0.17 (6 grid points per wavelength).

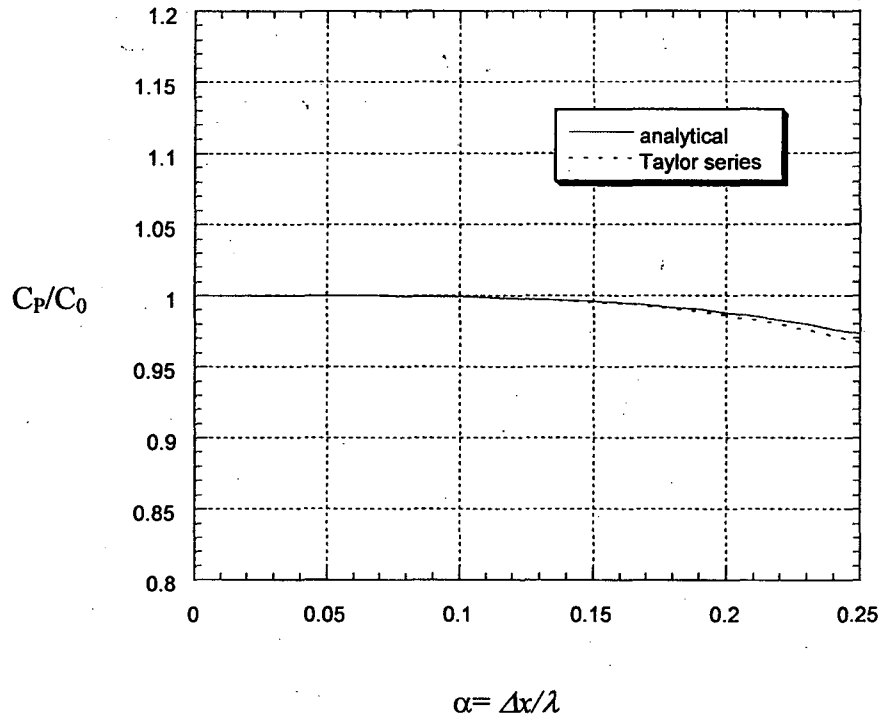

Figure 2.7.3. Spatial dispersion curves of phase velocity for finite difference solutions with fourth order accuracy in space.

The group velocity C_G can be obtained by taking the derivative of equation (2.7.19)

$$2\omega d\omega = \frac{-C_0^2}{6\Delta x^2}[2\Delta x \sin(2k\Delta x)dk - 16\Delta x \sin(k\Delta x)]dk\,, \tag{2.7.28}$$

yielding

$$C_G = \frac{d\omega}{dk} = \frac{C_0^2}{6\Delta x\omega}[8\sin\psi - \sin 2\psi]. \tag{2.7.29}$$

Substituting equation (2.7.5) into the above equation gives

$$\frac{C_G}{C_0} = \frac{1}{6\psi}[8\sin\psi - \sin 2\psi]\frac{C_0}{C_P} \tag{2.7.30}$$

or

$$\frac{C_G}{C_0} = \frac{8\sin\psi - \sin 2\psi}{\sqrt{6}[(\cos 2\psi - 1) - 16(\cos\psi - 1)]^{1/2}}. \tag{2.7.31}$$

Equation (2.7.30) can be expressed by using Taylor's series for $\sin\psi$ and $\sin 2\psi$ as

$$\frac{C_G}{C_0} \approx \frac{1}{6\psi}\left[8(\psi - \frac{1}{3!}\psi^3 + \frac{1}{5!}\psi^5) - (2\psi - \frac{1}{3!}(2\psi)^3 + \frac{1}{5!}(2\psi)^5)\right]\frac{C_0}{C_P},$$

or

$$\frac{C_G}{C_0} \approx \left[1 - \frac{\psi^4}{30}\right]\frac{C_0}{C_P}. \tag{2.7.32}$$

Substituting the equation (2.7.23) into the above equation results in

$$\frac{C_G}{C_0} \approx \left[1 - \frac{\psi^4}{30}\right] \Big/ \left[1 - \frac{\psi^4}{90}\right]. \tag{2.7.33}$$

Using the Taylor's series expression again for the denominator, we have

$$\frac{C_G}{C_0} \approx 1 - \frac{\psi^4}{45}. \tag{2.7.34}$$

Substituting equation (2.7.26) into the above equation gives

$$\frac{C_G}{C_0} \approx 1 - \frac{16\pi^4\alpha^4}{45} = 1 - 34.56\alpha^4. \tag{2.7.35}$$

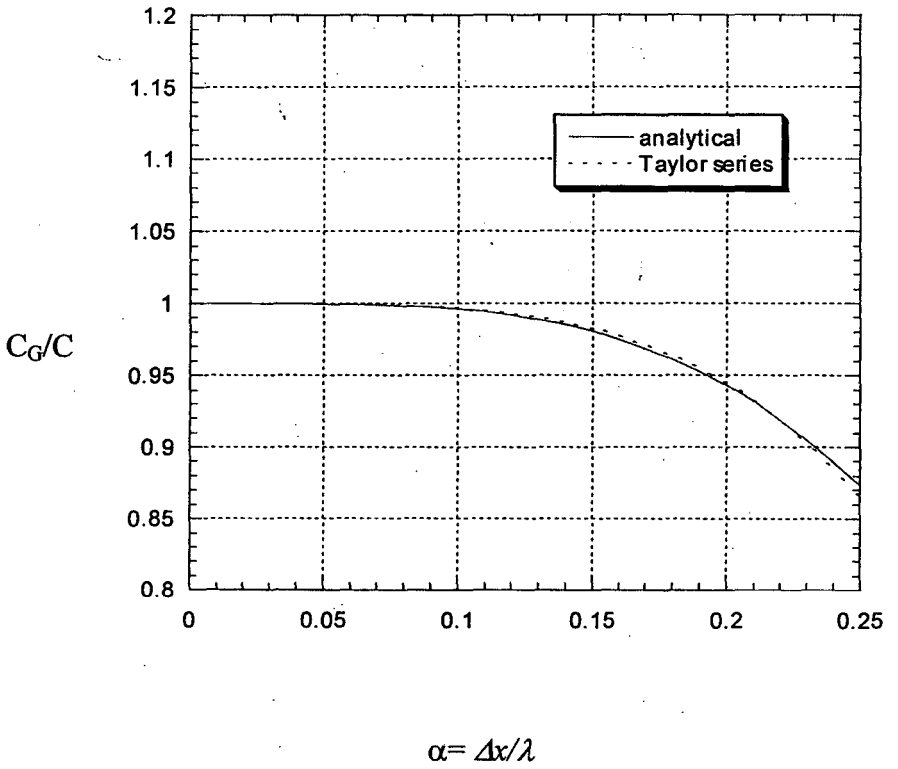

Figure 2.7.4. Spatial dispersion curves of group velocity for finite difference solutions with fourth order accuracy in space.

Equation (2.7.34) and (2.7.35) indicate the computed group velocity tends to be slower than the true velocity that as Δx increases or the wavelengths become smaller. The dispersion curves by equation (2.7.31) and (2.7.35) are showed in Figure 2.7.4. The plot indicates that the relative error in group velocity is less than 1% when α is less than 0.12 (8 grid points per wavelength). The error for group velocity is much larger than the error for phase velocity, while it is also true for the temporal dispersion discussed in last section.

2.7.3 Coupled Temporal and Spatial Dispersion

By comparing the dispersion behaviors of the computed relative phase and group velocities in preceding two sections, it is noticed that the temporal dispersion acts in the opposite sense as the spatial dispersion. Therefore, the combination of two dispersions is expected to reduce the total dispersion.

Substituting equation (2.7.1) into equation (2.3.4)

$$\frac{\sin^2(\omega\Delta t/2)}{\Delta t^2}u_0 e^{i(kx-\omega t)} = C_0{}^2\frac{16\sin^2(k\Delta x/2)-\sin^2(k\Delta x)}{12\Delta x^2}u_0 e^{i(kx-\omega t)}$$

or

$$\sin(\omega\Delta t/2) = \frac{C_0\Delta t}{\sqrt{12}\Delta x}[16\sin^2(k\Delta x/2)-\sin^2(k\Delta x)]^{1/2}, \qquad (2.7.36)$$

and

$$\omega = \frac{2}{\Delta t}\sin^{-1}[\frac{C_0\Delta t}{\sqrt{12}\Delta x}[16\sin^2(k\Delta x/2) - \sin^2(k\Delta x)]^{1/2}]. \qquad (2.7.37)$$

Combing equations (2.7.5) and (2.7.37), the phase velocity can be expressed as

$$\frac{C_P}{C_0} = \frac{\omega}{C_0 k} = \frac{2}{C_0 k\Delta t}\sin^{-1}[\frac{C_0\Delta t}{\sqrt{12}\Delta x}[16\sin^2(k\Delta x/2) - \sin^2(k\Delta x)]^{1/2}]. \qquad (2.7.38)$$

Let $p=C_0\Delta t/\Delta x$ and $k=2\pi/\lambda$, dispersion condition have a formula

$$\frac{C_P}{C_0} = \frac{2}{p\psi}\sin^{-1}[p[16\sin^2(\psi/2) - \sin^2(\psi)]^{1/2}/\sqrt{12}]. \qquad (2.7.39)$$

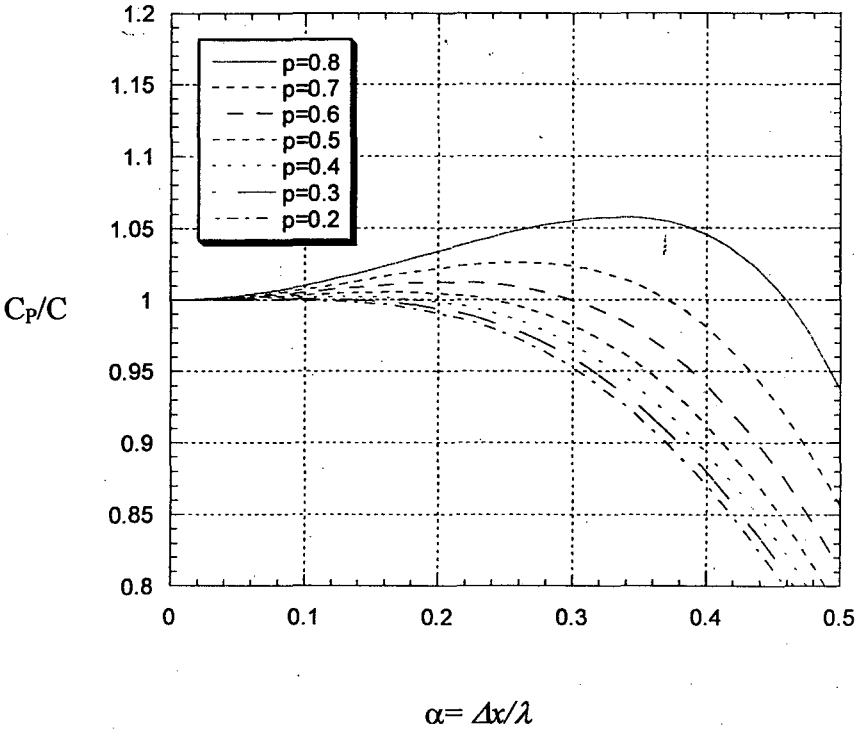

Figure 2.7.5. Dispersion curves of phase velocity for finite difference solutions with 4th order accuracy in space and 2nd order accuracy in time.

Figure 2.7.5 shows the dispersion curves computed by equation (2.7.39) for a range of p's. When $\Delta x/\lambda$ is small (Δx is small or wavelength is large), the temporal derivative (2^{nd} order) dominates the total dispersion since it has a lower accuracy than spatial derivative (4^{th} order). With decreasing p (or Δt), the spatial dispersion becomes more dominant resulting in negative dispersion. The figure also indicates that the relative error of phase velocity is less than 1% when α is less than 0.08 (12 grid points per wavelength).

To examine the dispersion of the group velocity, equation (2.7.36) is differentiated.

$$\frac{\sin(\omega\Delta t)}{\Delta t}d\omega = C_0{}^2\,\frac{8\sin(k\Delta x)-\sin(2k\Delta x)}{6\Delta x}dk. \tag{2.7.40}$$

The group velocity can be expressed as

$$\begin{aligned}\frac{C_G}{C_0}=\frac{d\omega}{C_0 dk}&=\frac{C_0\Delta t}{6\Delta x}\frac{8\sin(k\Delta x)-\sin(2k\Delta x)}{\sin(\omega\Delta t)}\\ &=\frac{C_0\Delta t}{6\Delta x}\frac{8\sin(k\Delta x)-\sin(2k\Delta x)}{\sin(\frac{C_0\Delta t}{\Delta x}k\Delta x\frac{C_P}{C_0})}\end{aligned} \tag{2.7.41}$$

or

$$\frac{C_G}{C_0}=\frac{p}{6}\frac{8\sin(\psi)-\sin(2\psi)}{\sin(p\psi\frac{C_P}{C_0})}. \tag{2.7.42}$$

Figure 2.7.6 shows the group velocity dispersion curves computed by equation (2.7.42) for a range of p's. Similar to the dispersion relationship of the phase velocity, the group velocity exhibits positive dispersion primarily due to the temporal dispersion when $\Delta x/\lambda$

is small, and negative dispersion due to the spatial dispersion for a large $\Delta x/\lambda$. With increasing p (decreasing Δt), the negative dispersion dominates due to the increasing spatial dispersion. The figure also indicates that the maximum dispersion in phase velocity is less than 1% when α is less than 0.04 (25 grid points per wavelength). It should be noted that the dispersion of group velocity is much larger than dispersion of phase velocity.

Figures 2.7.5 and 2.7.6 indicate that small p ($C_0\Delta t/\Delta x$) and α ($\Delta x/\lambda$) give less dispersion, which can guide to choose the time step Δt and grid step Δx.

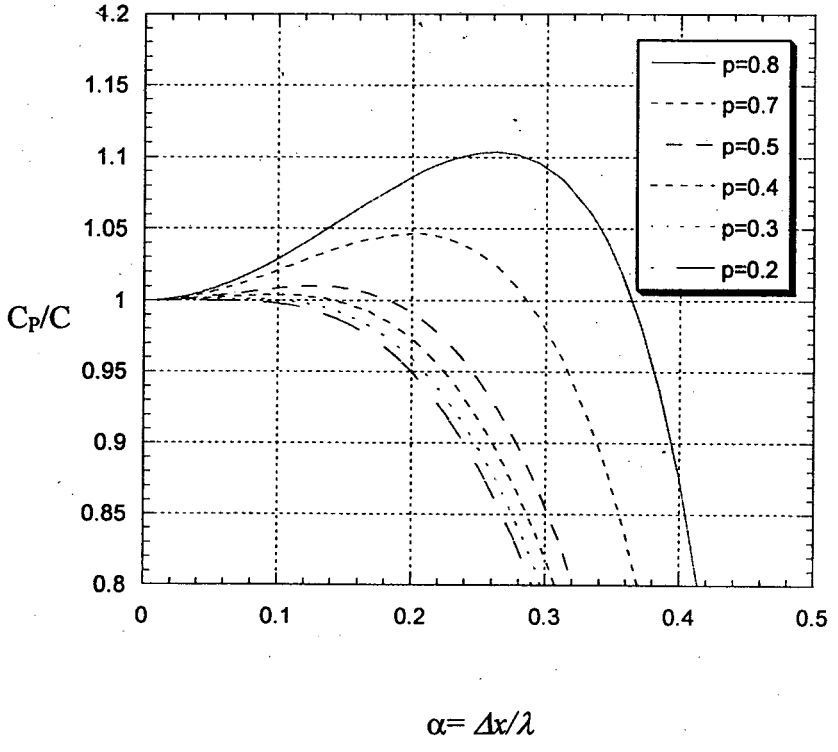

Figure 2.7.6. Dispersion curves of group velocity for finite difference solutions with 4th order accuracy in space and 2nd order accuracy in time.

2.8 Turning On & Off Subdomains Computations

For some wave propagation problems, the wavefield is concentrated within certain areas of the computational domain at a particular time step. When the domain decomposition technique is applied, some of the subdomains may not contain any wave energy at that particular time step. Figure 2.8 shows a computational domain with three subdomains at three different time steps T1, T2 and T3. At time step T1, the waves exist only within the subdomain Ω1. Therefore, only the wave within the subdomain Ω1 need to be computed. Similarly, at time step T2 or T3, only the wave within subdomain Ω2 or Ω3 is computed, respectively. Such a computational scheme saves a significant amount of computational time. The computation for a subdomain may be "turned on" or "off" according the following criteria

$$\text{If } |u(x_m, t_n)| < \varepsilon,\ x_m \in \Omega i, \text{ then turn off } \Omega i \text{ at time step } t_n;$$

$$\text{If } |u(x_m, t_n)| > \varepsilon,\ x_m \in \Omega i, \text{ then turn on } \Omega i \text{ at time step } t_n,$$

where ε is the maximum error (i.e., numerical noise generated by the finite difference approximations).

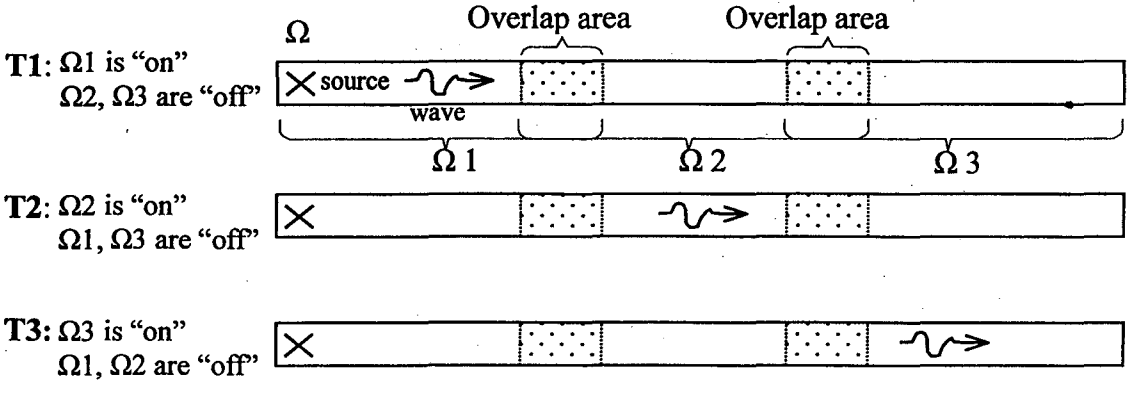

Figure 2.8. Schematic illustration of how the subdomains can be turned on and turned off during the calculation by ODD to reduce the number of computations.

2.9 Example

The finite difference method and pseudospectral method have been widely studied (Alford et al., 1974; Kelly et al., 1976; Dablain 1986; Gazdag, 1981; Kosloff and Baysal, 1982; Fornberg, 1987, 1996; Kosloff et al., 1990). Here, the solutions obtained from ODD FD and PS methods are compared with the results from conventional FD and PS methods.

The model for the 1-D comparative study is illustrated in Figure 2.9.1. The source on the left generates a Ricker wavelet (Appendix A) with a central frequency of 25 Hz. The total model is 2560 m long, the wave velocity is 3000 m/s with the wavelength of 120 m for the central frequency, and the distance between the source and receiver is 2200 m (approximately 18 wavelengths).

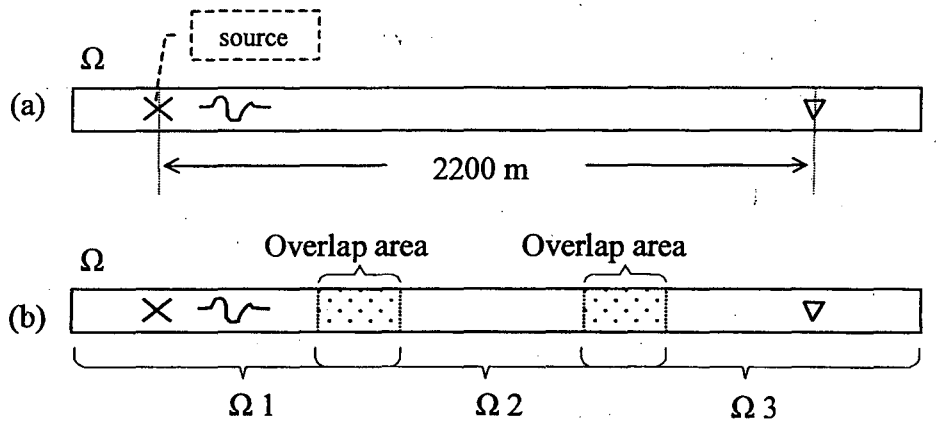

Figure 2.9.1 The 1-D model for the ODD tests: (a) single domain model and (b) three subdomain ODD model.

Figure 2.9.1(a) shows the single domain model for which the conventional 4^{th} order FD and PS are applied. Figure 2.9.1(b) shows the three subdomain model to which the ODD PS, ODD FD4, and mixed ODD PS-FD4 (PS in Ω2, FD4 in Ω1 and Ω3) methods

are applied. The ODD methods use the "turn-off" technique that computes only wavefields within subdomains with significant wave energy.

The waveforms from different methods are plotted in Figure 2.9.2. The results show a good agreement. The relative differences are less than 0.02% between the ODD and conventional methods. This example demonstrates that the domain decomposition technique and the "turn-off" technique both work very well. In the 1-D case, the time and memory required for the computation are not significant and the ODD and "turn-on-and-off" techniques do not have a significant effect. These techniques becomes very efficient for 2-D cases and, especially, for 3-D cases.

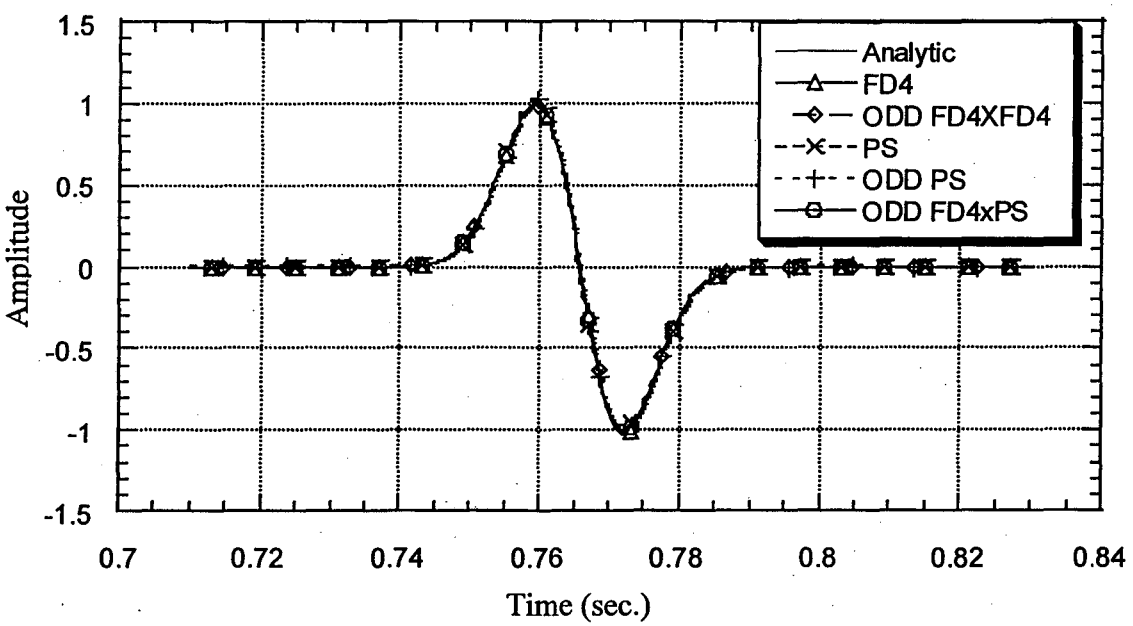

Figure 2.9.2. Comparison of waveforms for the 1-D model generated using the ODD and conventional numerical methods.

2.10 Summary

In this chapter, the ODD technique is proposed for wave propagation in a 1-D medium, and it is tested by the implementation of the ODD algorithms for the fourth order finite difference (FD4) method, pseudospectral (PS) method and mixed FD4-PS method. The results show good agreement between the ODD FD, PS, mixed FD-PS methods and the conventional FD and PS methods.

The stability conditions for the FD4 and PS methods are derived, which gives the criteria for choosing the ratio of $C_0\Delta t/\Delta x$. The temporal, spatial, and mixed temporal and spatial dispersion relations are given for the FD4 and PS methods, which indicates the minimum time steps for the certain frequency (or period) and the minimum grid points for the relative wavelength. It also shows that the dispersion for group velocity is much larger than the dispersion for phase velocity. The turning-off technique for inactive subdomain is introduced and it works well.

CHAPTER THREE

OVERLAP DOMAIN DECOMPOSITION FOR 2-D PROBLEMS

3.1 Introduction

The 1-D ODD methodology can be directly extended to 2-D wave propagation problems by overlapping in two dimensions. Since the 2-D wave equations are quite different from the 1-D wave equation especially for elastic media, necessary modifications have to be made to the ODD technique. In this chapter, first, the ODD algorithm for 2-D wave propagation problems is described. Second, acoustic and elastic wave equations are introduced. Third, the ODD implementations for FD and PS methods are explained and several examples are given.

3.2 2-D Overlap Domain Decomposition Technique

The domain decomposition for the 2-D wave propagation problems is shown schematically in Figure 3.2.1. A single domain is divided into six subdomains. The light-shaded regions are overlapping areas shared between neighboring subdomains. These overlapping areas allow transfer of the wave from one subdomain to the other. For example, the center subdomain $\Omega 2$ is considered first. The subdomain $\Omega 2$ is surrounded by four overlapping areas. Within the overlapping area, the reflecting zone are indicated by the dotted regions covering the artificial boundaries. The rest of subdomain $\Omega 2$ without the reflecting zone is called the central region of subdomain $\Omega 2$. When computing the wavefield in subdomain $\Omega 2$ at a time step, waves reflect from the artificial

boundaries when they reach the artificial boundaries. If the width of the reflecting zone is larger than $dx=vdt$, the reflecting waves are limited to the reflecting zone within a time step dt. Only the wavefield from central region of $\Omega 2$ is used to construct the wavefield in the domain Ω and the results from the reflecting zone are discarded. By not using this contaminated information, the reflections, from these artificial boundaries are eliminated. But, when the $\Omega 1$ is computed, the wavefield of the uncontaminated central region of the left neighbor $\Omega 1$ now contains (overlapps) the wavefield of the left reflecting zone of $\Omega 2$. Similarly, the wavefields of the subdomains $\Omega 3$, $\Omega 4$ and $\Omega 5$ overlap right, upper, and lower reflecting zones in $\Omega 2$. After finishing the computations in all the subdomains, the wavefield of the entire domain Ω can be constructed from the central regions of all the subdomains.

3.3 Turning on and Turning off Computations in Inactive Subdomains

If during the course of the calculation, the waves have not spread over the entire domain at a particular time step, some of subdomains will not contain any wave energy. Therefore, the calculations in these "inactive" subdomains are not necessary and can be turned off. Figure 3.3.1 shows a domain with nine subdomains at two different time steps T1 and T2. At time step T1, the wave is present only within subdomain $\Omega 6$. Therefore, computations need to be performed only in subdomain $\Omega 6$ since there is no wave energy in the other subdomains. Similarly, at time step T2, computations need only in subdomains $\Omega 1$, $\Omega 4$ and $\Omega 7$ respectively. Such a procedure can save a significant amount of computing time by turning off the inactive subdomains.

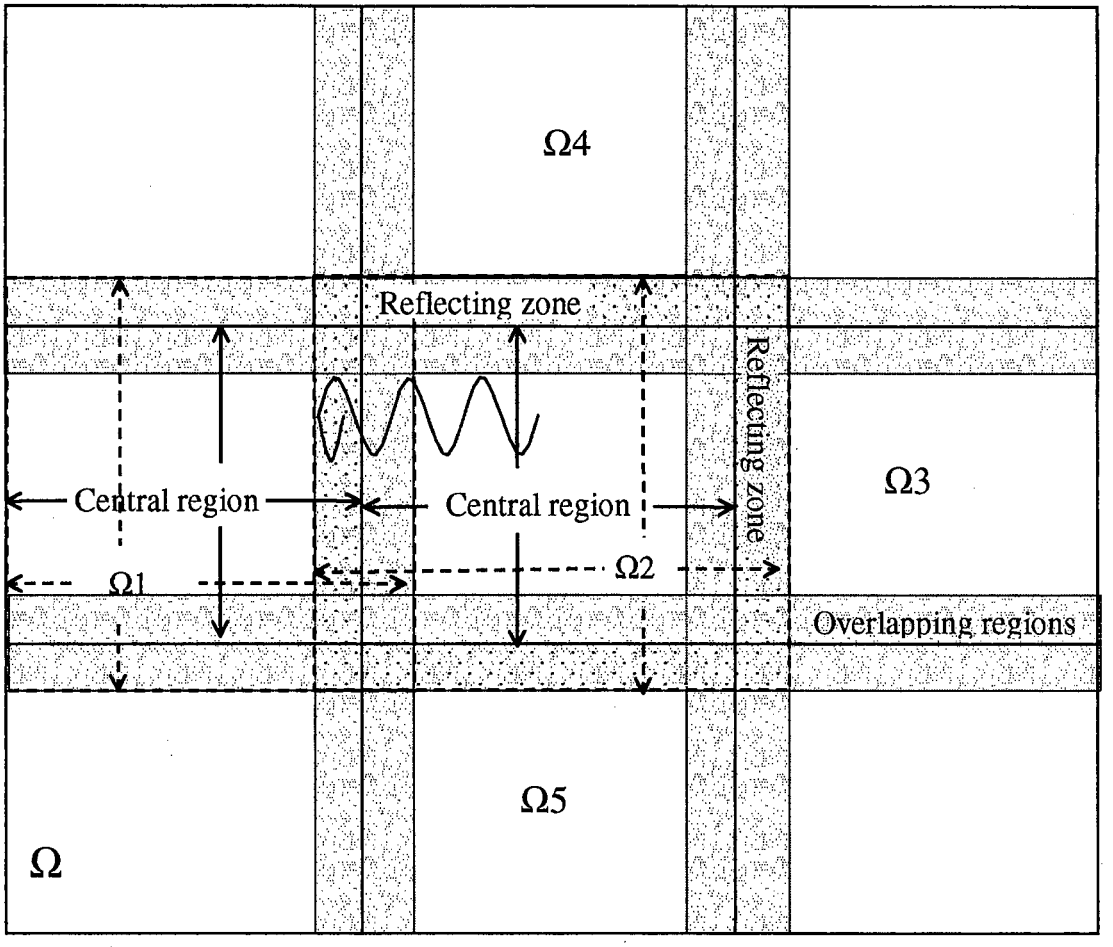

Figure 3.2.1. Diagram of the overlap domain decomposition in 2-D.

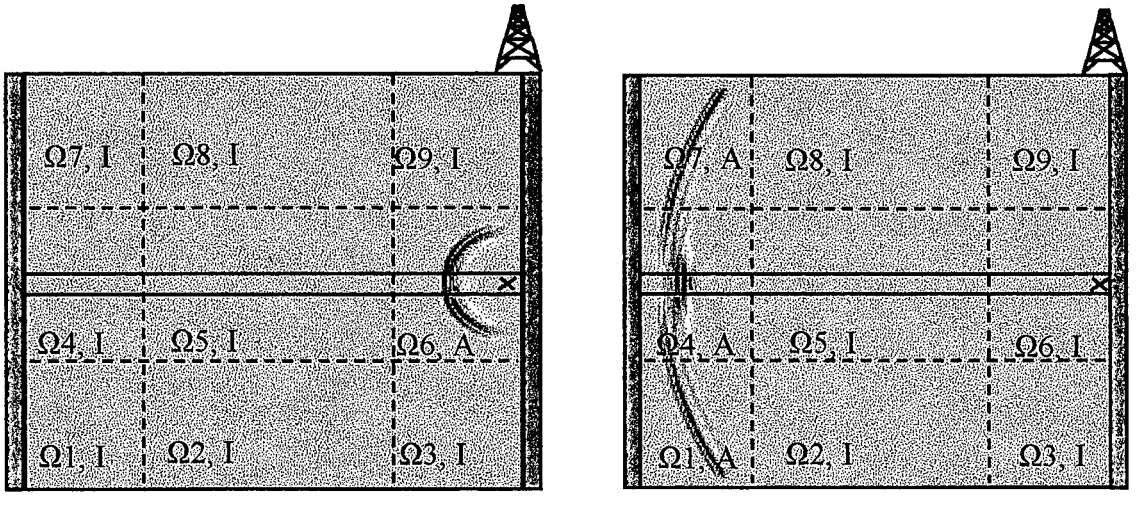

Figure 3.3.1. Active and inactive subdomains at (a) an early time step and (b) a later time step, where "A" and "I" represent "active" and "inactive", respectively.

3.4 Application of ODD to 2-D Acoustic Problems

Let x and z be the horizontal and vertical rectangular coordinates in a two-dimensional medium, and let the z-axis be positive downward. For an isotropic and homogeneous medium, the acoustic wave equation reads

$$\frac{\partial^2 P(x,z,t)}{\partial x^2}+\frac{\partial^2 P(x,z,t)}{\partial z^2}=\frac{1}{c^2}\frac{\partial^2 P(x,z,t)}{\partial t^2}+S, \tag{3.4.1}$$

where $P(x, z, t)$ represents the pressure, c the wave velocity and $S(x, z, t)$ the source term which equals the divergence of the body force divided by the density.

3.4.1 ODD for the 2-D Acoustic Finite Difference Method

The spatial derivatives in equation (3.4.1) can be discretized using the fourth order finite difference method as

$$\frac{\partial^2 P(x_l,z_m,t_i)}{\partial x^2}=\frac{1}{\Delta x^2}\sum_{j=-2}^{2}a_j P(x_{l+j},z_m,t_i)+O([\Delta x]^4), \tag{3.4.2}$$

$$\frac{\partial^2 P(x_l,z_m,t_i)}{\partial z^2}=\frac{1}{\Delta z^2}\sum_{j=-2}^{2}a_j P(x_l,z_{m+j},t_i)+O([\Delta z]^4), \tag{3.4.3}$$

where a_j are the constant coefficients of the fourth order FD such as a_{-2} = -1/12, a_{-1} = 4/3, a_0 = -5/2, a_1 = 4/3 and a_2 = -1/12. The temporal derivative for second order accuracy is

$$\frac{\partial^2 P(x_l,z_m,t_n)}{\partial t^2}=\frac{1}{\Delta t^2}[P(x_l,z_m,t_{n+1})-2P(x_l,z_m,t_n)+P(x_l,z_m,t_{n-1})]+O([\Delta t]^2). \tag{3.4.4}$$

Applying equation (3.4.2), (3.4.3) and (3.4.4) to equation (3.4.1), a FD formula can be expressed as

$$\begin{aligned} P(x_l, z_m, t_{n+1}) &= 2P(x_l, z_m, t_n) - P(x_l, z_m, t_{n-1}) \\ &+ \frac{c^2\Delta t^2}{\Delta x^2}\left[\sum_{j=-2}^{2} a_j P(x_{l+j}, z_m, t_i)\right] + \frac{c^2\Delta t^2}{\Delta z^2}\left[\sum_{j=-2}^{2} a_j P(x_l, z_{m+j}, t_i)\right] \\ &+ c^2\Delta t^2 S + O([\Delta x]^4, [\Delta z]^4, [\Delta t]^2). \end{aligned} \tag{3.4.5}$$

Equation (3.4.5) shows that the spatial derivatives at a point [*l*, *m*] need four values at neighboring grid points in each direction. According the study of Chapter 2, the minimum number of overlapping grid points should be four in each direction.

For a heterogeneous medium in which both density and seismic wave velocity are spatially variable, the acoustic wave equation is

$$\frac{\partial}{\partial x}\left(\frac{1}{\rho}\frac{\partial P(x,z,t)}{\partial x}\right) + \frac{\partial}{\partial z}\left(\frac{1}{\rho}\frac{\partial P(x,z,t)}{\partial z}\right) = \frac{1}{c^2\rho}\frac{\partial^2 P(x,z,t)}{\partial t^2} + S, \tag{3.4.6}$$

where ρ is the density and S is the body force source. Compared to equation (3.4.1), the two terms on the left-hand side now contain two first order spatial derivatives instead of a single step of the second order derivatives in both x and y directions because the density and velocity are no longer constant. Then the FD formula with 4th order accuracy in space become

$$\begin{aligned} \frac{\partial P(x_l, z_m, t_n)}{\partial x} &= \frac{1}{\Delta x}\sum_{j=-2}^{2} b_j P(x_{l+j}, z_m, t_n) + O([\Delta x]^4), \\ \frac{\partial P(x_l, z_m, t_n)}{\partial z} &= \frac{1}{\Delta z}\sum_{j=-2}^{2} b_j P(x_l, z_{m+j}, t_n) + O([\Delta z]^4), \end{aligned} \tag{3.4.7}$$

where b_j are the constant coefficients of fourth order FD giving by $b_{-2} = 1/12$, $b_{-1} = -2/3$, $b_0 = 0$, $b_1 = 2/3$ and $b_2 = -1/12$.

Now, we set

$$f(x_l, z_m, t_n) = \frac{1}{\rho(x_l, z_m)} \frac{\partial P(x_l, z_m, t_n)}{\partial x}, \tag{3.4.8}$$

$$g(x_l, z_m, t_n) = \frac{1}{\rho(x_l, z_m)} \frac{\partial P(x_l, z_m, t_n)}{\partial z}, \tag{3.4.9}$$

and spatial derivatives of equation (3.4.6) can be written as

$$\begin{aligned} &\frac{\partial}{\partial x}\left(\frac{1}{\rho(x_l,z_m)}\frac{\partial P(x_l,z_m,t_n)}{\partial x}\right)=\frac{\partial f(x_l,z_m,t_n)}{\partial x} \\ &=\frac{1}{\Delta x}\sum_{j=-2}^{2} b_j f(x_{l+j},z_m,t_n)+O([\Delta x]^4), \end{aligned} \tag{3.4.10}$$

$$\begin{aligned} &\frac{\partial}{\partial z}\left(\frac{1}{\rho(x_l,z_m)}\frac{\partial P(x_l,z_m,t_n)}{\partial z}\right)=\frac{\partial g(x_l,z_m,t_n)}{\partial z} \\ &=\frac{1}{\Delta z}\sum_{j=-2}^{2} b_j g(x_l,z_{m+j},t_n)+O([\Delta z]^4). \end{aligned} \tag{3.4.11}$$

Once f and g are computed from equation (3.4.7) to (3.4.9), two applications of spatial derivatives in equation (3.4.6) can be computed from equation (3.4.10) to (3.4.11). Since each applications of the first order spatial derivative requires four neighboring grid points in a single direction, eight grid neighboring points are used to compute the two applications of derivative. Figure 3.4.1 graphically describes the two applications of the first derivatives along the x direction and the required overlapping area containing eight grid points.

By applying equation (3.4.10), (3.4.11) and (3.4.4) into equation (3.4.6), the final FD method scheme for a heterogeneous medium can be written as

$$P(x_l,z_m,t_{n+1}) = 2P(x_l,z_m,t_n) - P(x_l,z_m,t_{n-1}) + \frac{c^2\rho\Delta t^2}{\Delta x}\sum_{j=-2}^{2} b_j f(x_{l+j},z_m,t_i) + \frac{c^2\rho\Delta t^2}{\Delta z}\sum_{j=-2}^{2} b_j g(x_l,z_{m+j},t_i) + c^2\rho\Delta t^2 S + O([\Delta x]^4,[\Delta z]^4,[\Delta t]^2). \quad (3.4.12)$$

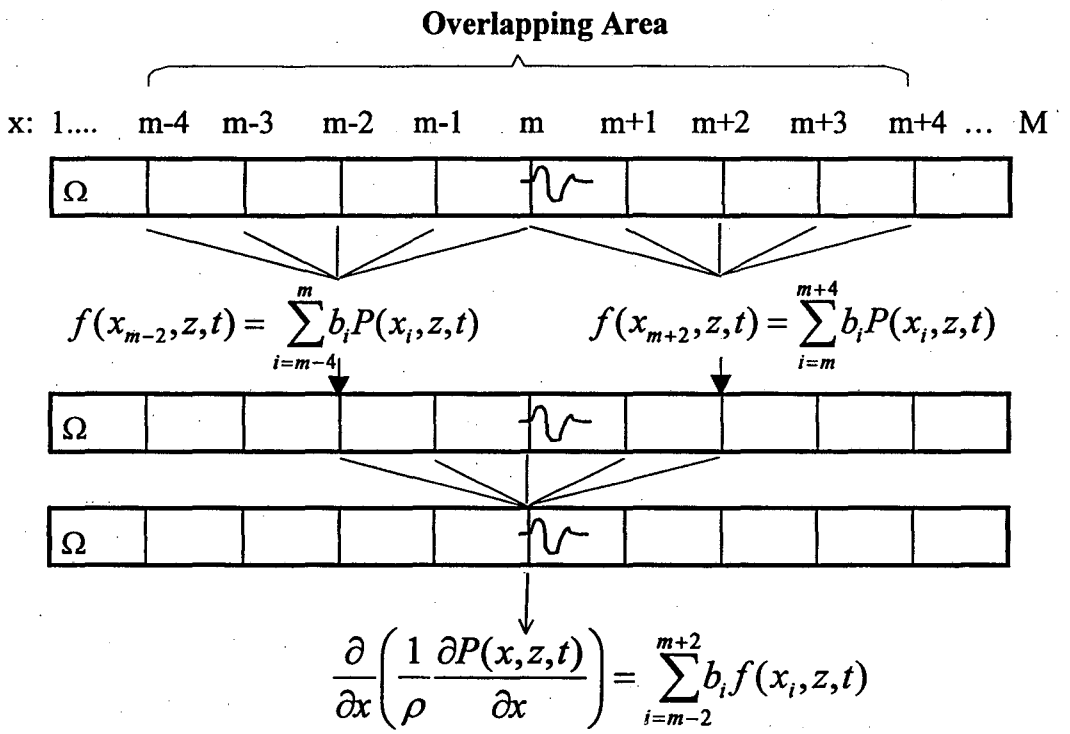

Figure 3.4.1 The overlapping area for the FD method in heterogeneous media.

3.4.2 ODD for the 2-D Acoustic Fourier Pseudospectral (PS) Method

For 2-D problems, the PS method uses a Fourier transform to calculate the spatial derivatives in the two directions. The 2-D Fourier PS method can be summarized as follows.

The 2-D Fourier transform of *P[x(0), y(0), t(n)], ..., P[x(l), y(m), t(n)], ... , P[x(L), y(M), t(n)]* can be expressed as:

$$\hat{P}[k_x(l),k_z(m),t(n)]=\sum_{j=0}^{M-1}\sum_{i=0}^{L-1}P[x(i),z(j),t(n)]e^{-ik_x(l)x(i)-ik_z(m)z(j)}, \qquad (3.4.13)$$

where the wavenumbers $k_x(l)=2\pi l/(L\Delta x)$, $k_z(m)=2\pi m/(M\Delta z)$ and $\Delta x = x_l - x_{l-1}$, $\Delta z = z_m - z_{m-1}$. The inverse Fourier transform is:

$$P[x(i),z(j),t(n)]=\frac{1}{LM}\sum_{m=0}^{M-1}\sum_{l=0}^{L-1}\hat{P}[k_x(l),k_z(m),t(n)]e^{ik_x(l)x(i)+ik_z(m)z(j)}. \qquad (3.4.14)$$

Then the first and second order spatial derivatives can be obtained from the above equation

$$\frac{\partial P[x(i),z(j),t(n)]}{\partial x}=\frac{1}{LM}\sum_{m=0}^{M-1}\sum_{l=0}^{L-1}[-ik_x(l)]\cdot\hat{P}[k_x(l),k_z(m),t(n)]e^{ik_x(l)x(i)+ik_z(m)z(j)}, \qquad (3.4.15)$$

$$\frac{\partial P[x(i),z(j),t(n)]}{\partial z}=\frac{1}{LM}\sum_{m=0}^{M-1}\sum_{l=0}^{L-1}[-ik_z(m)]\cdot\hat{P}[k_x(l),k_z(m),t(n)]e^{ik_x(l)x(i)+ik_z(m)z(j)}, \qquad (3.4.16)$$

$$\frac{\partial^2 P[x(i),z(j),t(n)]}{\partial x^2}=\frac{1}{LM}\sum_{m=0}^{M-1}\sum_{l=0}^{L-1}[-k_x^2(l)]\cdot\hat{P}[k_x(l),k_z(m),t(n)]e^{ik_x(l)x(i)+ik_z(m)z(j)}, \qquad (3.4.17)$$

$$\frac{\partial^2 P[x(i),z(j),t(n)]}{\partial z^2}=\frac{1}{LM}\sum_{m=0}^{M-1}\sum_{l=0}^{L-1}[-k_z^2(m)]\cdot\hat{P}[k_x(l),k_z(m),t(n)]e^{ik_x(l)x(i)+ik_z(m)z(j)}. \qquad (3.4.18)$$

Combining equation (3.1.7), (3.4.18) and (3.4.4), the PS scheme for a homogeneous medium wave equation (3.4.1) is

$$P[x(i),z(j),t(n+1)] = 2P[x(i),z(j),t(n)] - P[x(i),z(j),t(n-1)]$$

$$+ c^2\Delta t^2\left[\frac{1}{LM}\sum_{m=0}^{M-1}\sum_{l=0}^{L-1}[-k^2{}_x(l) - k^2{}_z(m)]\cdot \hat{P}[k_x(l),k_z(m),t(n)]e^{ik_x(l)x(i)+ik_z(m)z(j)}\right]. \quad (3.4.19)$$

For a heterogeneous medium, similar to the FD scheme, two steps are required to compute the spatial derivatives for the wave equation (3.4.12)

$$\frac{\partial}{\partial x}\left(\frac{1}{\rho[x(i),z(j)]}\frac{\partial P[x(i),z(j),t(n)]}{\partial x}\right) = \frac{\partial f[x(i),z(j),t(n)]}{\partial x}$$

$$= \frac{1}{LM}\sum_{m=0}^{M-1}\sum_{l=0}^{L-1} ik_x(l)\hat{f}[k_x(l),k_z(m),t(n)]e^{ik_x(l)x(i)+ik_z(m)z(j)}, \quad (3.4.20)$$

$$\frac{\partial}{\partial z}\left(\frac{1}{\rho[x(i),z(j)]}\frac{\partial P[x(i),z(j),t(n)]}{\partial z}\right) = \frac{\partial g[x(i),z(j),t(n)]}{\partial z}$$

$$= \frac{1}{LM}\sum_{m=0}^{M-1}\sum_{l=0}^{L-1} ik_z(m)\hat{g}[k_x(l),k_z(m),t(n)]e^{ik_x(l)x(i)+ik_z(m)z(j)}. \quad (3.4.21)$$

Applying the above two equations and equation (3.4.4) into the wave equation (3.4.12), the final PS solution for the heterogeneous medium is

$$P[x(i),z(j),t(n+1)] = 2P[x(i),z(j),t(n)] - P[x(i),z(j),t(n-1)]$$
$$+ \frac{c^2\Delta t^2}{LM}\sum_{m=0}^{M-1}\sum_{l=0}^{L-1}(\{ik_x(l)\cdot \hat{f}[k_x(l),k_z(m),t(n)]$$
$$+ ik_z(m)\cdot \hat{g}[k_x(l),k_z(m),t(n)]\}\cdot e^{ik_x(l)x(i)+ik_z(m)z(j)}). \quad (3.4.22)$$

The application of the overlap domain decomposition technique to the 2-D PS method requires that taper functions be applied to each PS subdomain in both the x and z directions. The length of the overlapping area should be about one wavelength to effectively avoid wraparound across the subdomain boundaries.

3.4.3 Acoustic Example

The layer model consists of a low-velocity (2000 m/s) layer overlying a high-velocity (3000m/s) layer (Figure 3.4.2a). The distance between the source and receiver is 400 m (five wavelengths long). The parameters for the computation are listed in the Table 3.4.1. The subdomains and their ovelapping areas for the overlap domain decomposition of this model are shown in Figure 3.4.2b. This entire domain is decomposed into 25 subdomains.

For comparison, five different combinations of computation have been performed: (1) single domain conventional 4th order finite difference (FD4) method and (2) PS method, (3) 25 subdomain ODD FD4 method and (4) PS method, and (5) hybrid ODD PS-FD4 method (PS in the source subdomain and FD in the surrounding subdomains).

Table 3.4.1 Model Parameters for the Numerical Example

Input source	Δx	Δy	Δt(s)	SFC (vdt/dx)
Ricker Wavelet	5 m	5 m	5×10^{-4}	0.2

Two snapshots of the acoustic wavefield calculated at time 0.1 s and 0.4 s with the ODD PS-FD4 method (25 subdomains) are shown in Figure 3.4.3. At 0.1 s, the wave only propagates a short distance and is still within the central subdomain. At this point in time, the calculation only needs to be applied to the central subdomain. As the wave propagates into neighboring subdomains, the subdomains are turned on and turn off depending on if there is any wave energy within these subdomains.

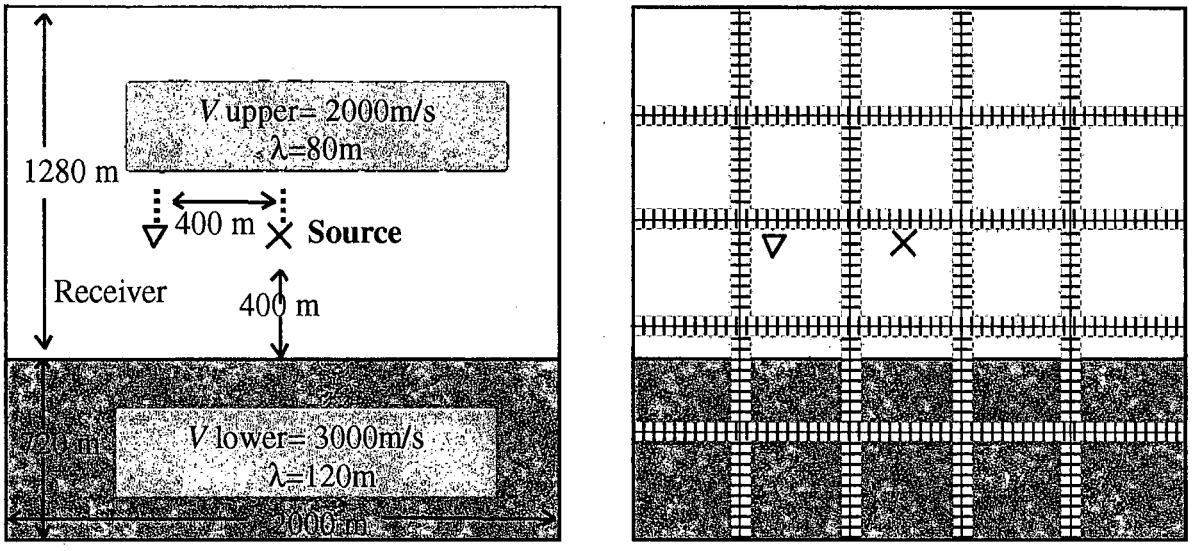

(a) (b)

Figure 3.4.2. (a) The two layer model; (b) The subdomains and overlapping areas

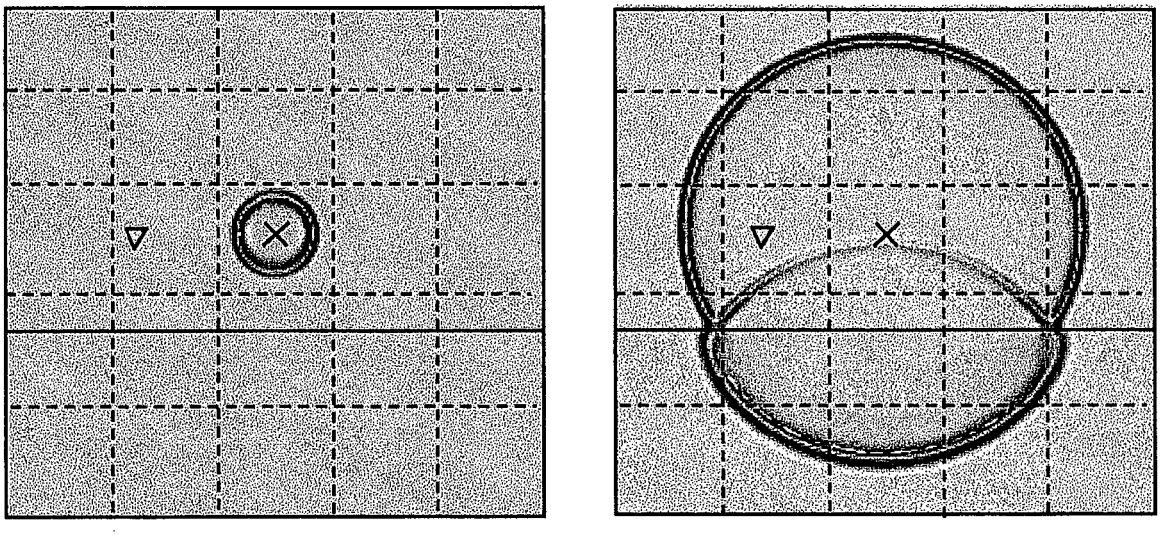

(a) (b)

Figure 3.4.3. Snapshots of acoustic wavefield (a) at 0.1 s and (b) at 0.4 s.

The waveforms calculated by different methods for the 2-D acoustic model are shown in Figure 3.4.4 and relative computing times (Pentium Pro 200 computer with 128 MB memory) are shown in Table 3.4.2. The analytical solution has been calculated by integration of the 3-D Green's function which is given in Appendix B. All numerical results match the analytical solution very well. The relative differences are less than 0.1% between the ODD and the conventional methods. However, the ODD FD4 method takes only about the half of the computing time of the conventional FD4 method and the ODD PS method takes only one third of the computing time of the conventional PS method. Furthermore, ODD methods take about two thirds of the memory requirements of conventional methods.

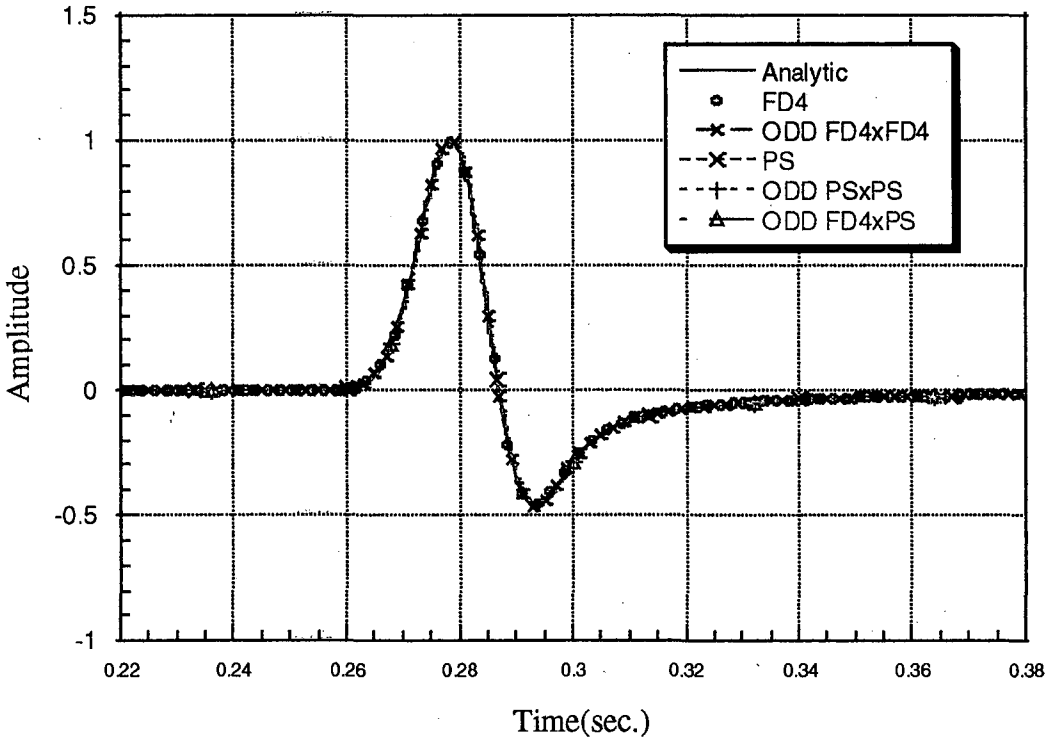

Figure 3.4.4. Waveforms from different ODD methods for 2-D acoustic model.

Table 3.4.2 Computing time of different method for an acoustic model

Methods	FD4	ODD FD4	PS	ODD PS	ODD PSxFD4
Computing time	3 hrs	1.5 hrs	19 hrs	6 hrs	4 hrs
Memory	11 mb	7.3mb	11 mb	7.3 mb	7.3 mb

3.5 Application of OOD to 2-D Elastic Problems

The elastic wave equation in a 2-D heterogeneous medium in the rectangular coordinates x and z can be written (Kolsky, 1963; Karal and Keller, 1959)

$$\begin{aligned}
&\frac{\partial}{\partial x}\left[\lambda\left(\frac{\partial u}{\partial x}+\frac{\partial w}{\partial z}\right)+2\mu\frac{\partial u}{\partial x}\right]+\frac{\partial}{\partial z}\left[\mu\left(\frac{\partial w}{\partial x}+\frac{\partial u}{\partial z}\right)\right]=\rho\frac{\partial^2 u}{\partial t^2}+S_x,\\
&\frac{\partial}{\partial z}\left[\lambda\left(\frac{\partial u}{\partial x}+\frac{\partial w}{\partial z}\right)+2\mu\frac{\partial w}{\partial z}\right]+\frac{\partial}{\partial x}\left[\mu\left(\frac{\partial w}{\partial x}+\frac{\partial u}{\partial z}\right)\right]=\rho\frac{\partial^2 w}{\partial t^2}+S_z,
\end{aligned} \tag{3.5.1}$$

where u and w are displacements in x and z directions, λ and μ are the Lame parameters which are dependent upon the space variables x and z, and S_x and S_z are the source functions. These two coupled, second order partial differential equations can be used to describe the motion of P and S waves.

For a homogeneous medium where ρ, λ and μ are constant, these equations can be written in simpler forms

$$\begin{aligned}
&(\lambda+2\mu)\left(\frac{\partial^2 u}{\partial x^2}+\frac{\partial^2 w}{\partial x\partial z}\right)+\mu\left(\frac{\partial^2 u}{\partial z^2}-\frac{\partial^2 w}{\partial x\partial z}\right)=\rho\frac{\partial^2 u}{\partial t^2}+S_x,\\
&(\lambda+2\mu)\left(\frac{\partial^2 u}{\partial x\partial z}+\frac{\partial^2 w}{\partial z^2}\right)+\mu\left(\frac{\partial^2 w}{\partial x^2}-\frac{\partial^2 u}{\partial x\partial z}\right)=\rho\frac{\partial^2 w}{\partial t^2}+S_z,
\end{aligned} \tag{3.5.2}$$

3.5.1 ODD for the 2-D Elastic Finite Difference Method

Similar to the acoustic problem, a homogeneous medium is considered first. The finite difference formulas with 4th order accuracy in space for the 2nd order spatial derivatives are

$$\begin{aligned}
\frac{\partial^2 u(x_l,z_m,t_n)}{\partial x^2} &= \frac{1}{\Delta x^2}\sum_{j=-2}^{2} a_j u(x_{l+j},z_m,t_i) + O([\Delta x]^4),\\
\frac{\partial^2 u(x_l,z_m,t_n)}{\partial z^2} &= \frac{1}{\Delta z^2}\sum_{j=-2}^{2} a_j u(x_l,z_{m+j},t_i) + O([\Delta z]^4),\\
\frac{\partial^2 w(x_l,z_m,t_n)}{\partial x^2} &= \frac{1}{\Delta x^2}\sum_{j=-2}^{2} a_j w(x_{l+j},z_m,t_i) + O([\Delta x]^4),\\
\frac{\partial^2 w(x_l,z_m,t_n)}{\partial z^2} &= \frac{1}{\Delta z^2}\sum_{j=-2}^{2} a_j w(x_l,z_{m+j},t_i) + O([\Delta z]^4,
\end{aligned} \tag{3.5.3}$$

where a_j are the constant factors of fourth order FD, a_{-2} = -1/12, a_{-1} = 4/3, a_0 = -5/2, a_1 = 4/3 and a_2 = -1/12. The other two cross second order spatial derivatives need two applications of the first order spatial derivatives by FD in two different directions. For example, the z-direction derivatives are computed as follows

$$\begin{aligned}
f(x_l,z_m,t_n) = \left.\frac{\partial u(x_l,z_m,t_n)}{\partial z}\right|_{x_l} &= \frac{1}{\Delta z}\sum_{j=-2}^{2} b_j u(x_l,z_{m+j},t_n) + O([\Delta z]^4),\\
g(x_l,z_m,t_n) = \left.\frac{\partial w(x_l,z_m,t_n)}{\partial z}\right|_{x_l} &= \frac{1}{\Delta z}\sum_{j=-2}^{2} b_j w(x_l,z_{m+j},t_n) + O([\Delta z]^4),
\end{aligned} \tag{3.5.4}$$

where b_j are the constant factors of fourth order FD: $b_{-2} = 1/12$, $b_{-1} = -2/3$, $b_0 = 0$, $b_1 = 2/3$ and $b_2 = -1/12$. The cross second order derivatives become

$$\frac{\partial^2 u(x_l, z_m, t_n)}{\partial x \partial z} = \left.\frac{\partial f(x_l, z_m, t_n)}{\partial x}\right|_{z_m} = \frac{1}{\Delta x}\sum_{j=-2}^{2} b_j f(x_{l+j}, z_n, t_i) + O([\Delta x]^4),$$

$$\frac{\partial^2 w(x_l, z_m, t_n)}{\partial x \partial z} = \left.\frac{\partial g(x_l, z_m, t_n)}{\partial x}\right|_{z_m} = \frac{1}{\Delta x}\sum_{j=-2}^{2} b_j g(x_{l+j}, z_n, t_i) + O([\Delta x]^4). \tag{3.5.5}$$

The final FD formulas for equation (3.5.2) can be written as

$$\begin{aligned} u(x_l, z_n, t_{n+1}) &= 2u(x_l, z_n, t_n) - u(x_l, z_n, t_{n-1}) \\ &+ \alpha^2 \Delta t^2 [\frac{1}{\Delta x^2}\sum_{j=-2}^{2} a_j u(x_{l+j}, z_m, t_n) + \frac{1}{\Delta x}\sum_{j=-2}^{2} b_j g(x_{l+j}, z_m, t_n)] \\ &+ \beta^2 \Delta t^2 [\frac{1}{\Delta z^2}\sum_{j=-2}^{2} a_j u(x_l, z_{m+j}, t_n) - \frac{1}{\Delta x}\sum_{j=-2}^{2} b_j g(x_{l+j}, z_m, t_n)] \\ &+ \rho \Delta t^2 S_x + O([\Delta x]^4, [\Delta z]^4, [\Delta t]^2), \end{aligned} \tag{3.5.6}$$

and

$$\begin{aligned} w(x_l, z_n, t_{n+1}) &= 2w(x_l, z_n, t_n) - w(x_l, z_n, t_{n-1}) \\ &+ \alpha^2 \Delta t^2 [\frac{1}{\Delta z^2}\sum_{j=-2}^{2} a_j w(x_{l+j}, z_m, t_n) + \frac{1}{\Delta x}\sum_{j=-2}^{2} b_j f(x_{l+j}, z_m, t_n)] \\ &+ \beta^2 \Delta t^2 [\frac{1}{\Delta x^2}\sum_{j=-2}^{2} a_j w(x_l, z_{m+j}, t_i) - \frac{1}{\Delta x}\sum_{j=-2}^{2} b_j f(x_{l+j}, z_m, t_n)] \\ &+ \rho \Delta t^2 S_y + O([\Delta x]^4, [\Delta z]^4, [\Delta t]^2), \end{aligned} \tag{3.5.7}$$

where α and β are the P and S wave velocities given by $\alpha = \sqrt{(\lambda + 2\mu)/\rho}$ and $\beta = \sqrt{\mu/\rho}$, respectively.

The ODD technique can be easily applied to the above elastic problems following the approach presented in Section 2.4. When applying the ODD to equation (3.5.3), at least four grid points for the overlapping area are required. Although equation (3.5.5) needs two applications of first order derivatives, the two applications are in different directions and the overlapping area in each direction only needs four grid points.

For a heterogeneous medium, similar finite difference formulas can be formed for equation (3.5.1). Two more functions need to be introduced besides those given in equation (3.5.4),

$$h(x_l,z_m,t_n)=\left.\frac{\partial u(x_l,t_n)}{\partial x}\right|_{z_m}=\frac{1}{\Delta x}\sum_{j=-2}^{2}b_j u(x_{l+j},z_m,t_n)+O([\Delta x]^4),$$
$$k(x_l,z_m,t_n)=\left.\frac{\partial w(x_l,t_n)}{\partial x}\right|_{z_m}=\frac{1}{\Delta x}\sum_{j=-2}^{2}b_j w(x_{l+j},z_m,t_n)+O([\Delta x]^4), \tag{3.5.8}$$

Substituting equation (3.5.4), (3.5.8) and (3.4.4) into the equation (3.5.1), we have the FD formula for a heterogeneous medium,

$$\begin{aligned}u(x_l,z_m,t_{n+1}) &= 2u(x_l,z_m,t_n)-u(x_l,z_m,t_{n-1})\\ &+\frac{\Delta t^2}{\rho}[\frac{1}{\Delta x}\sum_{j=-2}^{2}b_j\{\lambda(x_{l+j},t_n)[h(x_{l+j},t_n)+g(x_{l+j},t_n)]+2\mu(x_{l+j},t_n)h(x_{l+j},t_n)\}\\ &+\frac{1}{\Delta z}\sum_{j=-2}^{2}b_j\mu(z_{m+j},t_n)\{k(z_{m+j},t_n)+f(z_{m+j},t_n)\}+S_x]+O([\Delta x]^4,[\Delta z]^4,[\Delta t]^2),\end{aligned} \tag{3.5.9}$$

and

$$w(x_l, z_m, t_{n+1}) = 2w(x_l, z_m, t_n) - w(x_l, z_m, t_{n-1})$$
$$+\frac{\Delta t^2}{\rho}[\frac{1}{\Delta z}\sum_{j=-2}^{2} b_j\{\lambda(z_{m+j}, t_n)[h(z_{m+j}, t_n) + g(z_{m+j}, t_n)] + 2\mu(z_{m+j}, t_n)g(z_{m+j}, t_n)\} \quad (3.5.10)$$
$$+\frac{1}{\Delta x}\sum_{j=-2}^{2} b_j\mu(x_{l+j}, t_n)\{k(x_{l+j}, t_n) + f(x_{l+j}, t_n)\} + S_z] + O([\Delta x]^4, [\Delta z]^4, [\Delta t]^2),$$

To apply the ODD technique to the above equations, two applications of first order derivatives (*f, g, h, k* in equation (3.5.4) and (3.5.8) first, then u and w in equation (3.5.9) and (3.5.10)) in the same direction are required, and the overlapping areas need four grid points for each first derivatives. Thus two applications require a total of at least eight grid points for the overlapping areas in both x and z directions similar to the discussion in the Section 3.4.1.

The following table gives the minimum number of overlapping grid points for the ODD FD methods depending on their equations and approximations for different problems.

Compared to 2-D acoustic case, elastic problems have two components (u and w) instead of only one pressure component for acoustic problems; and elastic problems need to calculate fourteen spatial derivatives in equation (3.5.1) instead of four derivatives for acoustic problem in equation (3.4.6) for heterogeneous media. So elastic problems require much more memory and computation time with the same dimension of acoustic problems.

Table 3.5. The numbers of the overlapping grid points for FD ODD method

FD Methods	2^{nd} order acoustic (const ρ)	4^{th} order acoustic (const ρ)	4^{th} order elastic (const ρ)	2^{nd} order acoustic or elastic	4^{th} order acoustic or elastic
Min overlap Gird points	2	4	4	4	8

3.5.2 ODD for the 2-D Elastic Fourier Pseudospectral Method

The ODD algorithm for 2-D Fourier PS method is similar to that of the 2-D acoustic method. The implementation is described in Appendix D. The length of overlapping area required by the 2-D Fourier PS ODD method is again about one wavelength.

3.5.3 Elastic Example

The elastic model is shown in Figure 3.5.1. The geometry is the same as the acoustic model, but the media are elastic. The source is a horizontally polarized Ricker wavelet with the central frequency of 25 Hz. This whole domain is also divided into 25 subdomains as displayed in Figure 3.4.2.

Different combinations of computational methods have been applied to this model for comparison. All methods use the same parameters (Table 3.4.1) for the simulations. Figure 3.5.2a to 3.5.2.e show the snapshots of horizontal and vertical displacements at 0.4 s simulated by the FD4, ODD FD4, PS, ODD PS and mixed ODD PS-FD4 methods, where "P" and "S" indicate for direct P and S waves; "PPR" and "PSR" for P to P and P to S reflecting waves; and "PPT" and "PST" for P to P and P to S transmitting waves.

The waveforms recorded at a receiver 400 m away from the source for all the above methods are shown in Figure 3.5.3-4. The computation times are listed in Table 3.5.1.

In Figure 3.5.2a, b, the direct S wave ("S") and transmitting S waves ("SST") calculated by the FD4 and ODD FD4 method have a lot high frequency ringings due to the dispersion. However, the relative wavefields are quite smooth with very little dispersion in Figure 3.5.2c to Figure 3.5.2e calculated by the PS, ODD PS and ODD PS-FD4 methods. Figure 3.5.3 and 3.5.4 show the differences among these waveforms by comparing the numerical wavefields with an analytic solution. The waveforms from the FD4 methods have high frequency dispersion noise and the poor matches to the analytic solution (Figure 3.5.4). In general, it can be stated that the results of the PS, ODD PS and ODD PS-FD4 methods show negligible dispersion and a closer match to the analytic solution.

The reason for the lack of numerical dispersion in the PS, ODD PS and PS-FD4 methods is the higher accuracy difference provided by the PS method. In the ODD PS-FD4 simulation (Figure 3.5.2e) from the above example, the PS method is only used in the center subdomain where the source is located. The PS method yields a higher accuracy solution near the source where the gradients in the displacement are higher, especially for the S wave which has shorter wavelength. The FD4 method can, however, carry the simulations accurately in the surrounding subdomains after the wavefield is propagated from the source subdomain with PS method. Although the FD4 has lower accuracy, it is much faster than the PS method. These two numerical methods can be coupled together to form an efficient numerical algorithm to reduce computational time and to keep the high accuracy.

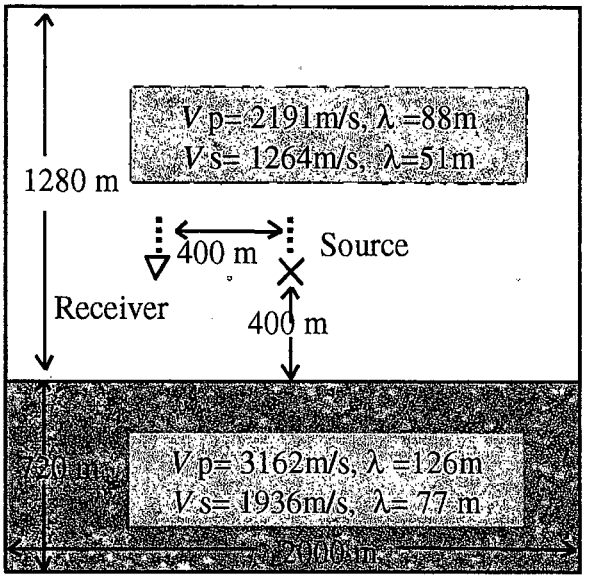

Figure 3.5.1. Model for the 2-D elastic simulation.

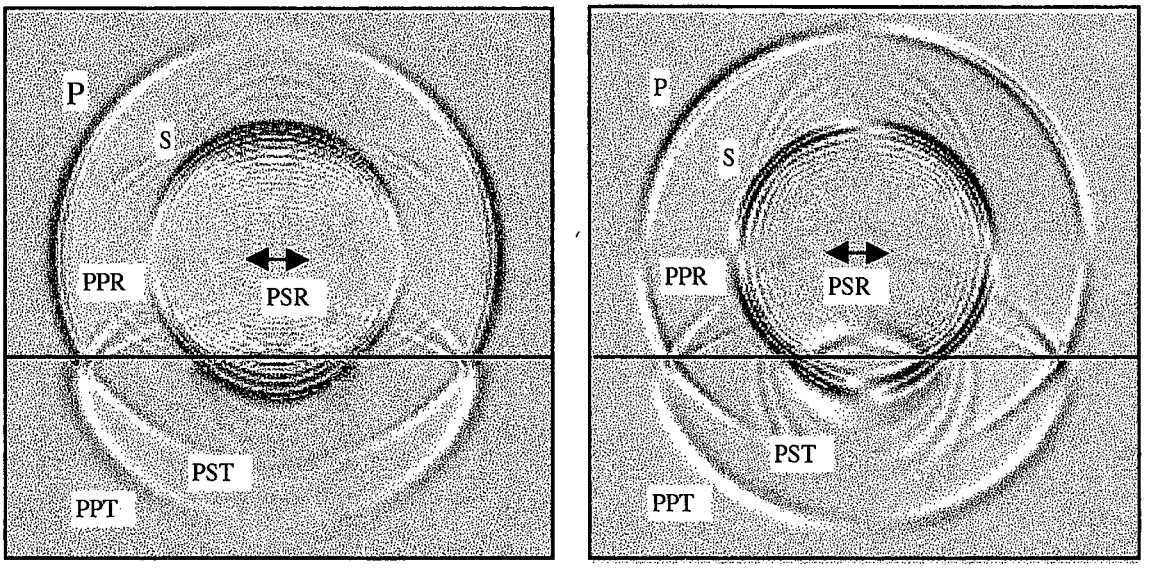

(a) horizontal displacement (b) vertical displacement

Figure 3.5.2a. Snapshots at 0.4 s computed with the FD method with a single domain.

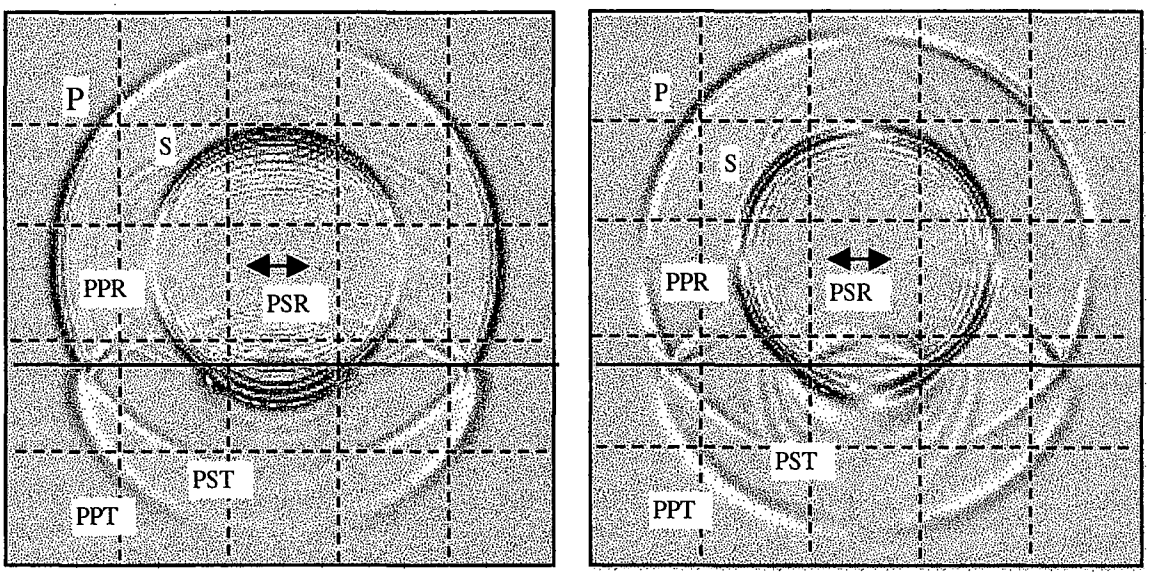

(a) horizontal displacement (b) vertical displacement

Figure 3.5.2b. Snapshots at 0.4 s computed with the ODD FD method (25 subdomains).

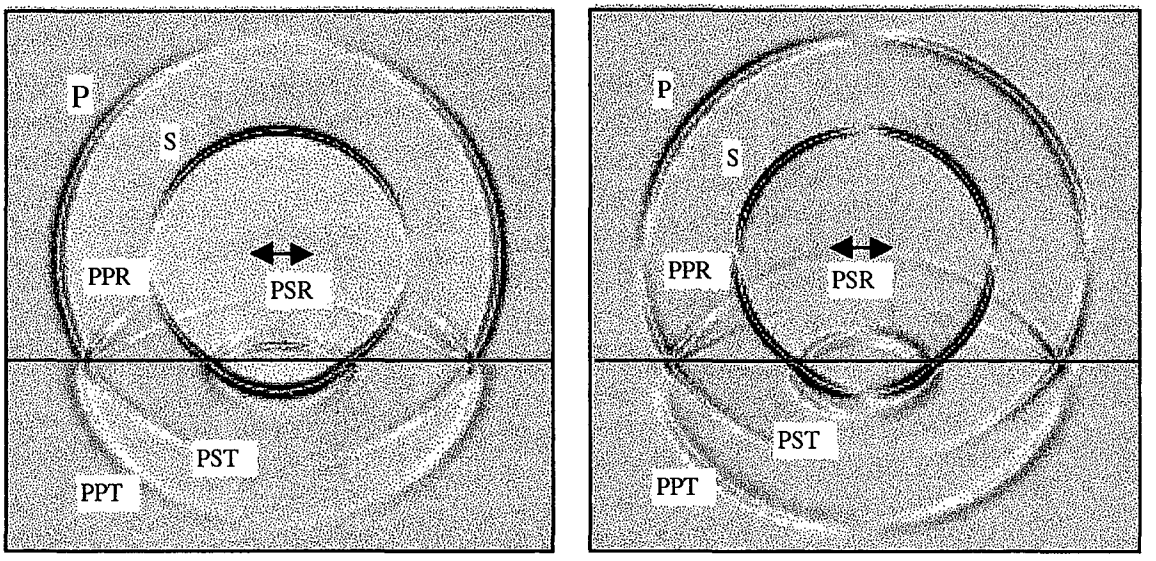

(a) horizontal displacement (b) vertical displacement

Figure 3.5.2c. Snapshots at 0.4 s computed with the PS method with a single domain.

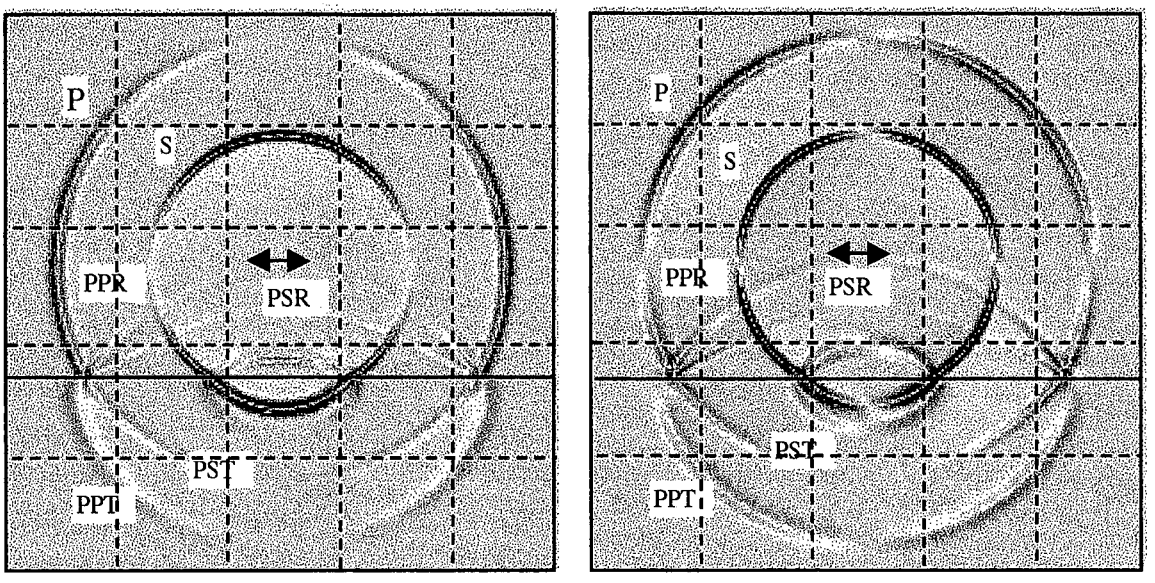

(a) horizontal displacement (b) vertical displacement

Figure 3.5.2d. Snapshots at 0.4 s computed with the ODD PS method (25 subdomains).

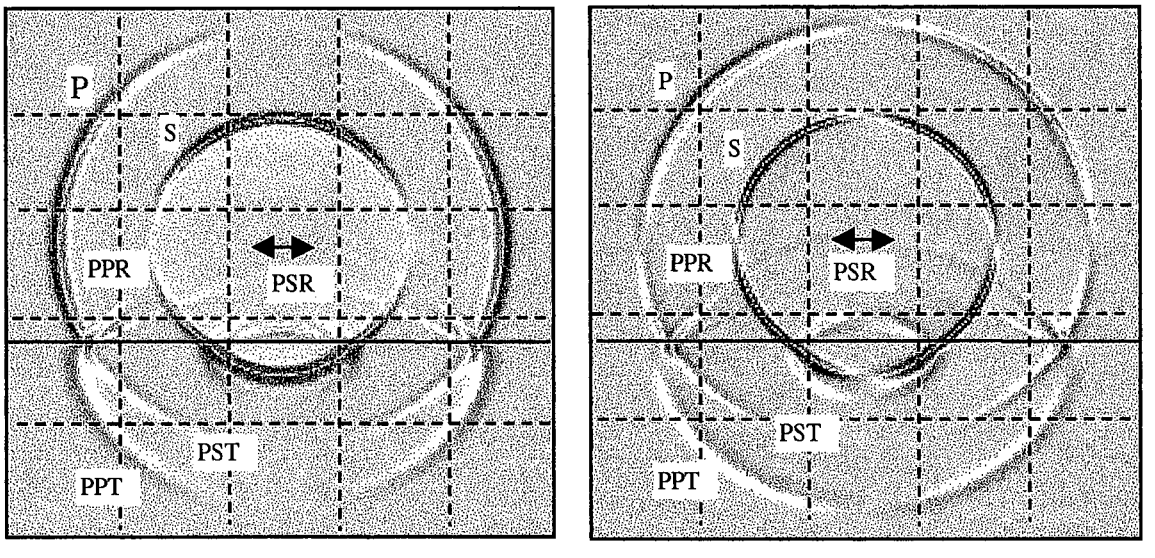

(a) horizontal displacement (b) vertical displacement

Figure 3.5.2e. Snapshots at 0.4 s computed with the ODD PS-FD4 method (25 subdomains).

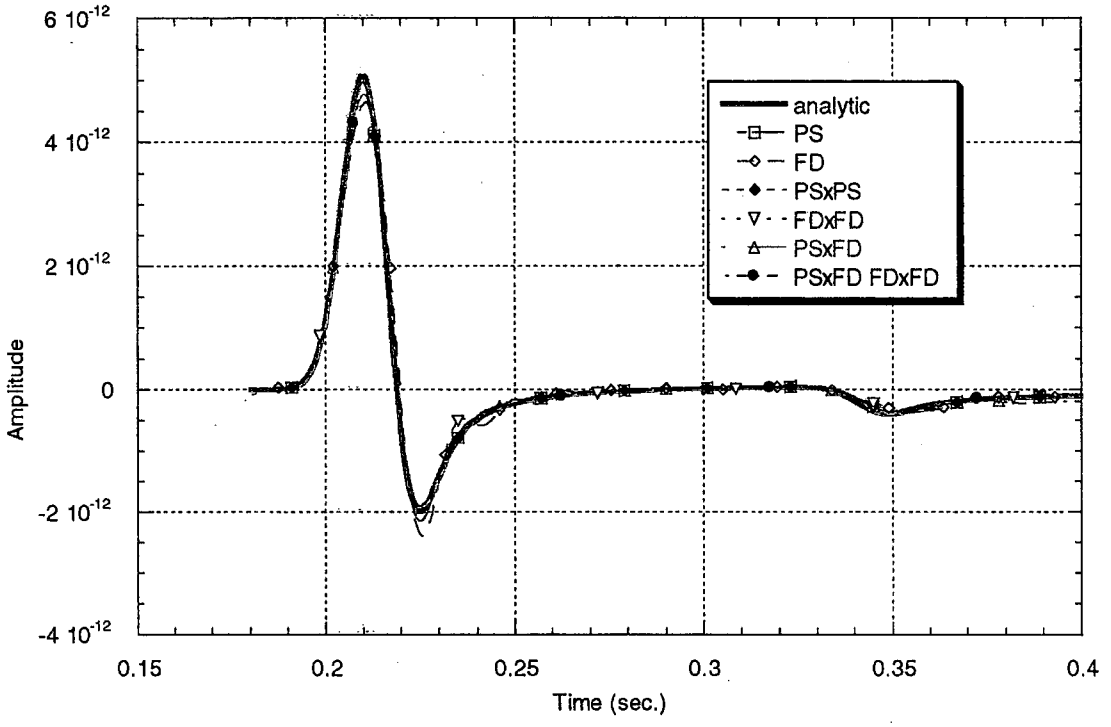

Figure 3.5.3. Waveforms from different methods for 2-D elastic model.

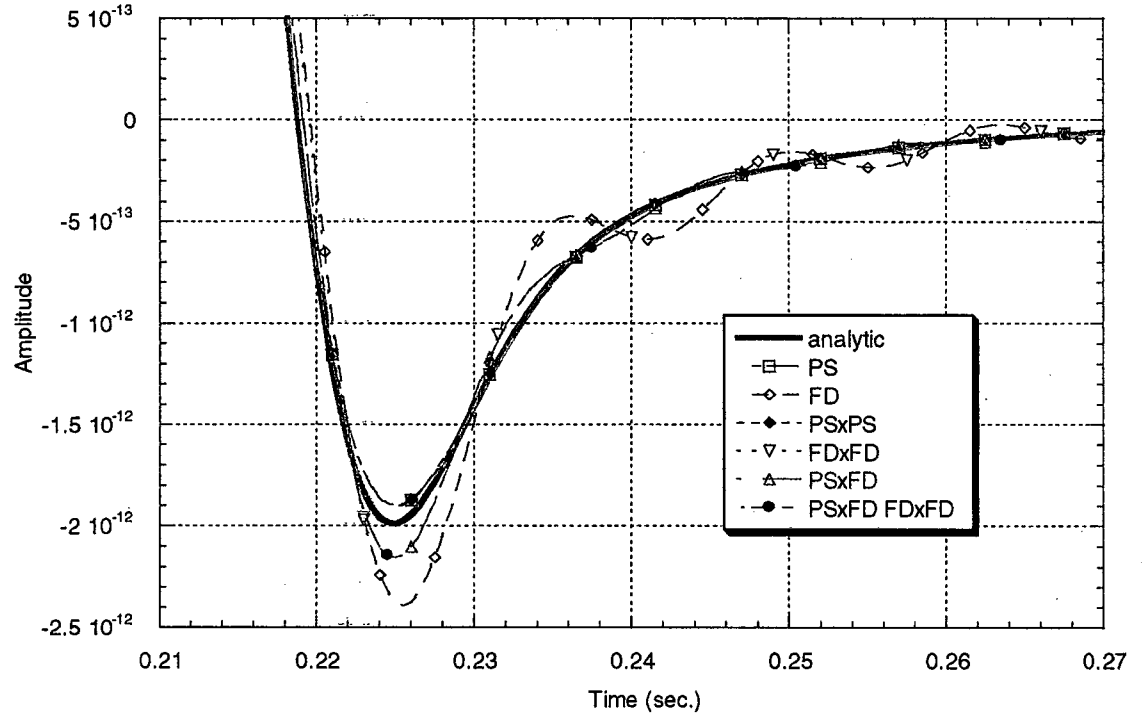

Figure 3.5.4. Expanded view of the lower part of curves in Figure 3.5.3.

Table 3.5.1 shows the computing time and memory usage by the different methods (Pentium Pro 200 computer with 128 MB memory). The ODD FD4 and ODD PS methods without turning-off technique are little slower than the conventional one domain FD4 and PS methods because of the communication time between the subdomains. However, the ODD FD4 and ODD PS methods with turning-off technique are faster than the conventional FD4 and PS methods. The ODD mixed PS-FD4 method with turning-off technique has the higher accuracy and faster speed. All the ODD methods use less memory. The FD4 employs lower accuracy differencing and, thus, requires a fine grid to properly handle the strong gradients produced by the point source. To get the results by FD4 method with the same accuracy as the PS and ODD PS-FD4 methods, the spatial grid interval for FD4 could be used as a quarter of the interval for PS method (Fornberg, 1987, 1996). It would increase memory needed for the example by a factor of 16, which is beyond the capacity of the computer. This example demonstrates that the ODD method can be used to speed up the computation, decrease the usage of memory, in addition, to couple different numerical methods together to increase the accuracy of simulation.

Table 3.5.1. Computation times and memory usage by the different methods.

Methods	FD4	ODD FD4	PS	ODD PS	ODD FD4 & PS
Computing time	0.67 hrs	0.5 hrs	13 hrs	8 hrs	1.1 hrs
Memory (MB)	34.88	23.84	36.91	23.84	23.84
Computing time (comparison)	faster	fastest	slower	slow	fast
Accuracy	low	low	high	high	high

3.6 Stability and Dispersion Condition

The general wave propagation equation for 2-D problems can be written as:

$$\frac{\partial^2 P(x,z,t)}{\partial t^2} = L[P(x,z,t)], \tag{3.6.1}$$

where L is a spatial derivative operator. The second order accuracy time FD is

$$P(x,z,t_{n+1}) = 2P(x,z,t_n) - P(x,z,t_{n-1}) + \Delta t^2 L[P(x,z,t_n)]. \tag{3.6.2}$$

Similar to Section 3.6, τ is defined as

$$\tau = \frac{\Delta t^2}{P(x,z,t)} L[P(x,z,t)]. \tag{3.6.3}$$

Substituting equation (3.6.3) into equation (3.6.2) gives

$$P(x,z,t_{n+1}) = (2+\tau)P(x,z,t_n) - P(x,z,t_{n-1}). \tag{3.6.4}$$

Since equation (3.6.4) has the same form as the 1-D case in equation (3.6.3), following the discussion in Section 3.6, the stability condition for 2-D problems is the same as for 1-D case in equation (3.6.13),

$$0 \geq \tau \geq -4. \tag{3.6.5}$$

3.6.1 Stability Condition for 2-D Acoustic Problems

From the 2-D acoustic wave equation (3.4.1) and definition of τ in equation (3.6.3), we have

$$\tau = \frac{C_0^2 \Delta t^2}{P(x,z,t)}\left[\frac{\partial^2 P(x,z,t)}{\partial x^2} + \frac{\partial^2 P(x,z,t)}{\partial z^2}\right]. \qquad (3.6.6)$$

For the fourth order FD method using a harmonic solution of the form given in equation (3.6.4), τ becomes

$$\tau = -C_0{}^2 \Delta t^2 [\frac{16\sin^2(k_x \Delta x/2) - \sin^2(k_x \Delta x)}{3\Delta x^2} + \frac{16\sin^2(k_z \Delta z/2) - \sin^2(k_z \Delta z)}{3\Delta z^2}], \qquad (3.6.7)$$

where k_x and k_z are the wave numbers in the two directions. Letting $\Delta x = \Delta z$ in equation (3.6.7) gives

$$\tau = -\frac{2C_0{}^2 \Delta t^2}{3\Delta x^2}[16\sin^2(k_x \Delta x/2) - \sin^2(k_x \Delta x)] \qquad (3.6.8)$$

Substituting equation (3.6.24) and 3.6.8 into equation (3.6.5) gives the stability condition

$$\frac{C_0 \Delta t}{\Delta x} < \frac{\sqrt{3}}{2}\frac{1}{\sqrt{2}} \approx 0.612 \ , \qquad (3.6.9)$$

Compared to the 1-D stability condition in equation (3.6.23), the 2-D stability is more demanding by a factor of $1/\sqrt{2}$.

For the Fourier pseudospectral method, τ is obtained as

$$\tau = -C_0{}^2 \Delta t^2 [k_x^2 + k_z^2]. \qquad (3.6.10)$$

Substituting the preceding equation into equation (3.6.5) gives,

$$C_0\Delta t \le \frac{2}{\sqrt{k_x^2 + k_z^2}}, \tag{3.6.11}$$

where $k_x=\pi/\Delta x$ and $k_z=\pi/\Delta z$, which are the largest values at the spatial Nyquist frequency.

Substitution of these values in equation (3.6.7) gives the stability condition

$$\frac{C_0\Delta t}{\Delta x} \le \frac{2}{\pi}\frac{1}{\sqrt{2}} = \frac{\sqrt{2}}{\pi} \approx 0.45. \tag{3.6.12}$$

This shows that the 2-D stability condition differs from the 1-D condition by a factor of $1/\sqrt{2}$.

3.6.2 Stability Condition for 2-D Elastic Problems

The elastic wave equation (3.5.2) can be rewrite without the source terms as

$$\alpha^2\left(\frac{\partial^2 u}{\partial x^2}+\frac{\partial^2 w}{\partial z^2}+\frac{\partial^2 (u+w)}{\partial x \partial z}\right)+\beta^2\left(\frac{\partial^2 u}{\partial z^2}+\frac{\partial^2 w}{\partial x^2}-\frac{\partial^2 (u+w)}{\partial x \partial z}\right)=\frac{\partial^2 (u+w)}{\partial t^2}. \tag{3.6.13}$$

Using the definition of τ in equation (3.6.3), we have

$$\tau = \frac{\Delta t^2}{(u+w)}\left[\alpha^2\left(\frac{\partial^2 u}{\partial x^2}+\frac{\partial^2 w}{\partial z^2}+\frac{\partial^2 (u+w)}{\partial x \partial z}\right)+\beta^2\left(\frac{\partial^2 u}{\partial z^2}+\frac{\partial^2 w}{\partial x^2}-\frac{\partial^2 (u+w)}{\partial x \partial z}\right)\right]. \tag{3.6.14}$$

Substituting a solution of equation (3.5.3) of harmonic form

$$\begin{aligned} u(x,z,t) &= u_0 e^{i(k_x x + k_z z - \omega t)}, \\ w(x,z,t) &= w_0 e^{i(k_x x + k_z z - \omega t)} \end{aligned} \tag{3.6.15}$$

into equation (3.6.14) with fourth order spatial finite differencing gives

$$\begin{aligned}\tau = &-\frac{\alpha^2\Delta t^2}{u+w}\left[\frac{16\sin^2(k_x\Delta x/2)-\sin^2(k_x\Delta x)}{3\Delta x^2}u+\frac{16\sin^2(k_z\Delta z/2)-\sin^2(k_z\Delta z)}{3\Delta z^2}w\right.\\ &\left.+\frac{8\sin(k_x\Delta x)-\sin(2k_x\Delta x)}{6\Delta x}\frac{8\sin(k_z\Delta z)-\sin(2k_z\Delta z)}{6\Delta z}(u+w)\right]\\ &-\frac{\beta^2\Delta t^2}{u+w}\left[\frac{16\sin^2(k_x\Delta x/2)-\sin^2(k_x\Delta x)}{3\Delta x^2}w+\frac{16\sin^2(k_z\Delta z/2)-\sin^2(k_z\Delta z)}{3\Delta z^2}u\right.\\ &\left.-\frac{8\sin(k_x\Delta x)-\sin(2k_x\Delta x)}{6\Delta x}\frac{8\sin(k_z\Delta z)-\sin(2k_z\Delta z)}{6\Delta z}(u+w)\right]\end{aligned} \quad (3.6.16)$$

Letting $\Delta x = \Delta z$ in the above equation gives

$$\begin{aligned}\tau = &-\frac{\alpha^2\Delta t^2}{\Delta x^2}\left[\frac{16\sin^2(k_x\Delta x/2)-\sin^2(k_x\Delta x)}{3}+\frac{\sin^2(k_x\Delta x)(4-\cos(k_x\Delta x))^2}{9}\right]\\ &-\frac{\beta^2\Delta t^2}{\Delta x^2}\left[\frac{16\sin^2(k_x\Delta x/2)-\sin^2(k_x\Delta x)}{3}-\frac{\sin^2(k_x\Delta x)(4-\cos(k_x\Delta x))^2}{9}\right].\end{aligned} \quad (3.6.17)$$

Since $\sin(k_x\Delta x)\le 1$ and $(4-\cos(k_x\Delta x))\le 5$, gives

$$\sin^2(k_x\Delta x)(4-\cos(k_x\Delta x))^2 \le 25. \quad (3.6.18)$$

Using equation (3.6.24) and equation (3.6.18), then

$$\frac{16\sin^2(k_x\Delta x/2)-\sin^2(k_x\Delta x)}{3}\pm\frac{\sin^2(k_x\Delta x)(4-\cos(k_x\Delta x))^2}{9}\le\frac{16}{3}+\frac{25}{9}\le\frac{73}{9}. \quad (3.6.19)$$

Substituting equation (3.6.17) into equation (3.6.5) and using equation (3.6.19), we get the stability condition

$$\frac{\sqrt{\alpha^2+\beta^2}\Delta t}{\Delta x}<\frac{6}{\sqrt{73}}\approx 0.702\ . \quad (3.6.20)$$

This inequality can also be written in more revealing forms

$$\Delta t < 0.702 \frac{\Delta x}{\sqrt{\alpha^2 + \beta^2}}, \tag{3.6.21}$$

or

$$\frac{\alpha \Delta t}{\Delta x} < 0.702 \sqrt{1 + \frac{\beta^2}{\alpha^2}}. \tag{3.6.22}$$

For the Fourier pseudospectral method, we have

$$\tau = \frac{-\Delta t^2}{(u+w)} \left[\alpha^2 \left(k_x^2 u + k_z^2 w + k_x k_z (u+w) \right) + \beta^2 \left(k_x^2 w + k_z^2 u - k_x k_z (u+w) \right) \right]. \tag{3.6.23}$$

Substituting the above equation into equation (3.6.5), we have

$$\Delta t^2 \le 4(u+w) \left[\alpha^2 \left(k_x^2 u + k_z^2 w + k_x k_z (u+w) \right) + \beta^2 \left(k_x^2 w + k_z^2 u - k_x k_z (u+w) \right) \right]^{-1}. \tag{3.6.24}$$

Letting $k_x = \pi/\Delta x$ and $k_z = \pi/\Delta z$, which are the largest value at the spatial Nyquist frequency, and $\Delta x = \Delta z$, equation (3.6.24) becomes,

$$\Delta t \le \frac{2\Delta x}{\sqrt{2}\pi\alpha}, \tag{3.6.25}$$

and the stability condition is

$$\frac{\alpha \Delta t}{\Delta x} \le \frac{2}{\pi} \frac{1}{\sqrt{2}} = \frac{\sqrt{2}}{\pi} \approx 0.45. \tag{3.6.26}$$

3.6.3 Dispersion for 2-D Acoustic Problems

Substituting the harmonic solution equation (3.6.4) into equation (3.4.4) gives the dispersion condition for the second order time and fourth order space accuracy finite difference method,

$$\frac{C_P}{C_0}=\frac{2}{p\psi}\sin^{-1}\{\frac{p}{\sqrt{12}}[16\sin^2(\frac{k_x\Delta x}{2})-\sin^2(k_x\Delta x)+16\sin^2(\frac{k_z\Delta z}{2})-\sin^2(k_z\Delta z)]^{1/2}\}\ , \quad (3.6.27)$$

where $\psi = k\Delta x$ from equation (2.7.19). Letting $k_x = k\cos\varphi$ and $k_x = k\sin\varphi$, in the above equation gives

$$\frac{C_P}{C_0}=\frac{2}{p\psi}\sin^{-1}\{\frac{p}{\sqrt{12}}[16\sin^2(\frac{\psi\cos\varphi}{2})-\sin^2(\psi\cos\varphi)+16\sin^2(\frac{\psi\sin\varphi}{2})-\sin^2(\psi\sin\varphi)]^{1/2}\}. \quad (3.6.28)$$

Figure 3.6.1 shows the dispersion curve predicted by equation (3.6.28). The maximum relative error of phase velocity occurs when the wave propagates along the x-axis and z-axis, and the minimum error occurs along the direction with the angle of 45° to the x-axis. The relative error in the phase velocity is less than 1% when α is less than 0.2 (5 grid points per wavelength).

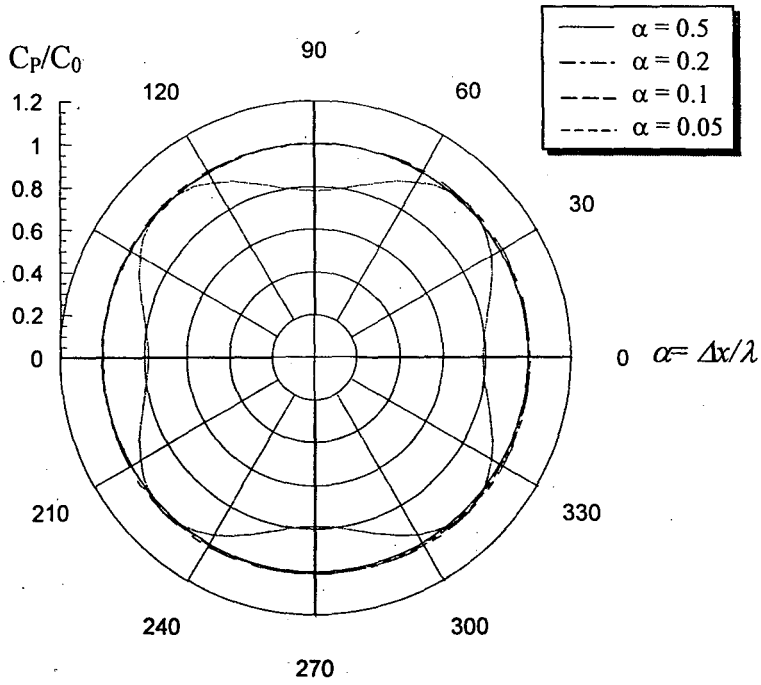

Figure 3.6.1. Phase velocity dispersion curves for the 2-D finite difference solution with fourth order accuracy in space and second order accuracy in time.

3.6.4 Dispersion for 2-D Elastic Problems

The general dispersion relation for 2-D elastic problems is quite complicated. Therefore, two special cases are examined here. When a wave propagates along the x- and z-axes, the problem becomes the 1-D case. Next, if Δx is equal to Δz, the wave propagates in the direction 45° from the x and z directions. The dispersion relation for such a wave is

$$4\sin^2(\omega\Delta t/2) = \frac{\alpha^2\Delta t^2}{\Delta x^2}\left[\frac{16\sin^2(k_x\Delta x/2)-\sin^2(k_x\Delta x)}{3}+\frac{\sin^2(k_x\Delta x)(4-\cos(k_x\Delta x))^2}{9}\right] + \frac{\beta^2\Delta t^2}{\Delta x^2}\left[\frac{16\sin^2(k_x\Delta x/2)-\sin^2(k_x\Delta x)}{3}-\frac{\sin^2(k_x\Delta x)(4-\cos(k_x\Delta x))^2}{9}\right]. \quad (3.6.29)$$

where α and β are the P and S wave velocities. If $\alpha = 2\beta, p = \beta\Delta t / \Delta x$ and $k = 2\pi\lambda$, equation (3.6.29) becomes

$$4\sin^2(\omega\Delta t/2) = 5p^2 \frac{16\sin^2(k_x\Delta x/2) - \sin^2(k_x\Delta x)}{3} + p^2 \frac{\sin^2(k_x\Delta x)(4-\cos(k_x\Delta x))^2}{3}. \quad (3.6.30)$$

Using the definition of phase velocity in equation (2.7.4) gives

$$\frac{C_P}{C_\alpha} = \frac{\omega}{C_\alpha k} = \frac{\omega}{C_\alpha \sqrt{2} k_x}. \quad (3.6.31)$$

Combining the above two equations, the dispersion relation is obtained as

$$\frac{C_P}{C_\alpha} = \frac{1}{\sqrt{2}p\psi} \sin^{-1}\left(\frac{p}{2}[5\frac{16\sin^2(\psi/2) - \sin^2(\psi)}{3} + \frac{\sin^2(\psi)(4-\cos(\psi))^2}{3}]^{1/2} \right), \quad (3.6.32)$$

where $\psi = k\Delta x$ from equation (2.7.18).

Figure 3.6.2 shows the dispersion curve predicted by equation (3.6.32), which indicates that as Δx increases or the wavelength become smaller, the phase velocity tends to be faster than the true velocity. When α is less than 0.08 (6 grid points per wavelength), the relative error in the phase velocity is less than 1%.

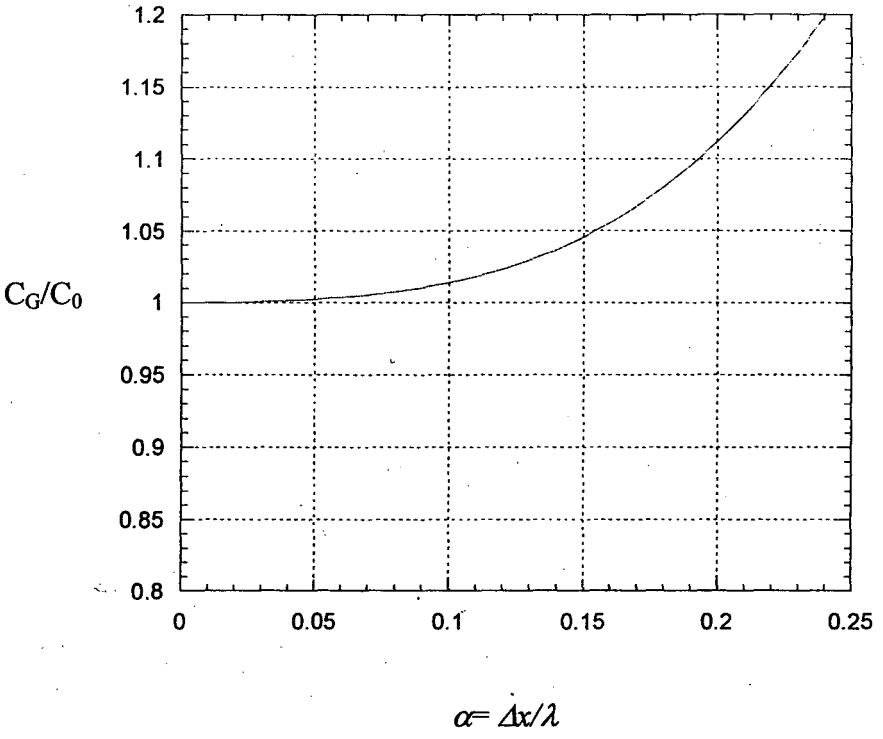

Figure 3.6.2. Phase velocity dispersion curve for the 2-D finite difference solution with fourth order accuracy in space for a wave propagating along the direction 45° to the x- and z-axes.

3.7 Summary

This chapter extended the ODD technique for 2-D acoustic and elastic media. The algorithms for the finite difference and pseudospectral method were described. The relative stability conditions and dispersion conditions are given, which indicated that smaller time steps and grid points are required for 2-D problems compared to 1-D problems.

The examples demonstrated that the ODD technique couple different numerical methods together to increase the accuracy of simulation and speed up the computation, where the accurate but computationally expensive PS method can be used in the subdomains which need a high accurate method (containing the source and the low velocity layer) and the faster FD method is applied to the rest subdomains. In addition, the number of grid points can be reduced by using the higher accurate method, which can decrease the usage of memory.

CHAPTER FOUR

SIMULATION OF GUIDED WAVES USING THE ODD TECHNIQUE

4.1 Introduction

The term waveguides or guided waves refers to a class of waves which propagate within thin layers, free surface, or along interfaces between two media (Miklowitz, 1951; 1978; Brekhovskikh 1980). Interfaces can be discontinuous planes of contacts such as joints and faults. Guided waves that travel along these interfaces are called interface waves such as Stoneley interface waves (Love, 1911; Aki and Richards, 1980) and fracture interface waves (Pyrak-Nolte and Cook, 1987). Guided waves which propagate in thin and low velocity layers are typically called channel waves (Buchanan et al., 1981; Krohn, 1990).

The distinctive characteristics of the guided wave is that the seismic energy is localized within a narrow zone which may extend only a few wavelengths outside of the interface or layer. As a consequency of this localization, the guided wave can travel long distances with less loss in amplitude than body waves. The potential use of guided waves is to interpret the properties of interfaces and thin layers that play an important role for underground fluid flow, mining and oil and gas production. Channel waves have been used extensively in the coal mining industry to locate discontinuities in coal seams that disrupt the longwall mining process (Dresen et al., 1985; Buchanan and Jackson, 1986; Gritto and Dresen, 1992). More recently, guided waves have been employed to determine the continuity of flow units and bounding surfaces in oil and gas reservoirs

(Krohn, 1992; Lines et al., 1992). Interface waves have been studied by Pyrak-Nolte and Cook (1987) using the displacement-discontinuity model. These interface waves also have been observed in the laboratory (Pyrak-Nolte et al., 1992) and in numerical boundary element simulations (Gu, 1994).

In this chapter, channel waves traveling along a low velocity layer are simulated using the ODD technique with the PS-FD4 method. These results are compared to physical measurements.

4.2 Numerical Simulations and Experimental Measurements of Channel Waves

A physical low velocity layer model was built with acrylic plates to form a 2-D (plane stress) model for investigating channel waves in the laboratory. The experiments are conducted by measuring the wave along a profile crossing the channel. Based on the same model, numerical simulations are conducted by the overlap domain decomposition technique. The results of the physical and numerical modeling are compared for particle motions and frequency characteristics.

4.2.1 Experimental Model Setup

Figure 4.1 shows the experimental setup for the low velocity channel. A Lexan strip (Polycarbonate, Vp=1550 m/s, Vs=897 m/s) has been used for a 30 mm wide low-velocity channel which was glued (Cyanoacrylate adhesive) with two higher velocity acrylic plates (Vp=2235 m/s, Vs=1333 m/s). Both plates have the densities of 1200 kg/m^3. The distance between the source and receiver was 0.55 m.

The source was a radial expansion mode PZT piezoelectric crystal which was bonded to the edge of the plastic plate at the center of the channel. The transducer was excited by a high voltage electric pulse with a single cycle of a 45 kHz sine wave. A miniature piezoelectric accelerometer (PCB 309A Piezotronics) was used as the receiver. Particle motions were measured by varying the positions and orientations of the accelerometer along the plate. For the acrylic plate, the 45 kHz source generated P waves with a 52 mm wavelength and S waves with a 30 mm wavelength. For the Lexan plate, the wavelengths were 34 mm and 20 mm for P and S waves, respectively. These wavelengths enabled the 3 mm wide accelerometer to accurately detect the particle motions on the plastic plates.

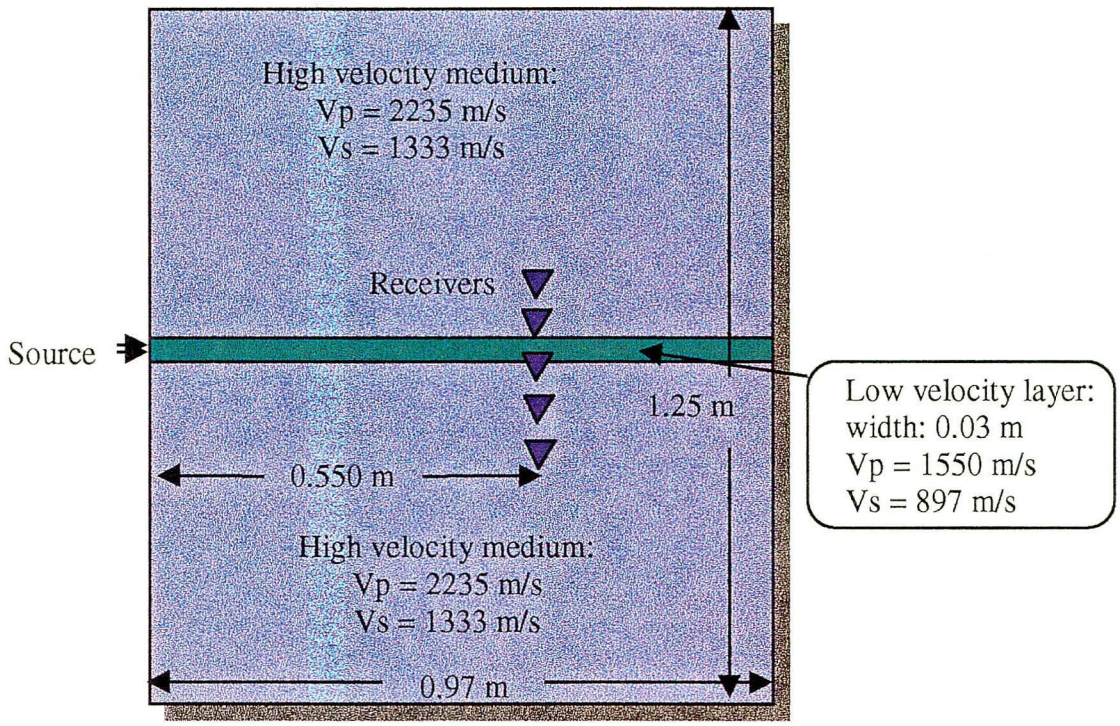

Figure 4.1. Experimental setup for the low velocity channel model.

4.2.2 Numerical Model Setup for the ODD technique

Using the same physical parameters from the experiment, numerical simulations were conducted using the overlap domain decomposition technique. The ODD numerical model with nine subdomains is shown in Figure 4.2. The central horizontal zone has the low velocity layer which contains both the source and the interfaces with the surrounding higher velocity media. This zone needs an accurate numerical method to properly handle the shorter wavelengths. Therefore, the PS method is used in the middle subdomains which cover the low velocity layer, and the FD4 method is applied to the surrounding subdomains. Without using the ODD technique to couple the PS and FD4 methods, the memory usage can be 16 times more by FD method and the computing time can be 10 times longer by PS method to calculate the same accurate results. Table 4.1 shows the parameters used for the numerical simulations for the channel model.

Figure 4.3 shows the two snapshots for the mixed ODD PS-FD4 and conventional FD4 methods at a time 0.4 ms for the horizontal component of the wavefield. Both approaches use the same parameters for the computations. It is very clear that the accuracy of the ODD method is higher than that of the FD method, which shows strong numerical dispersion. Therefore, the mixed ODD PS-FD4 method is used for all the numerical simulations. The details of differences between two approaches are shown in Appendix E.

Table 4.1. Parameters for the numerical computations.

Input source	Δx	Δy	Δt	λ_p/dx	λ_s/dx
Ricker Wavelet	5 mm	5 mm	5e-7 sec	20	12

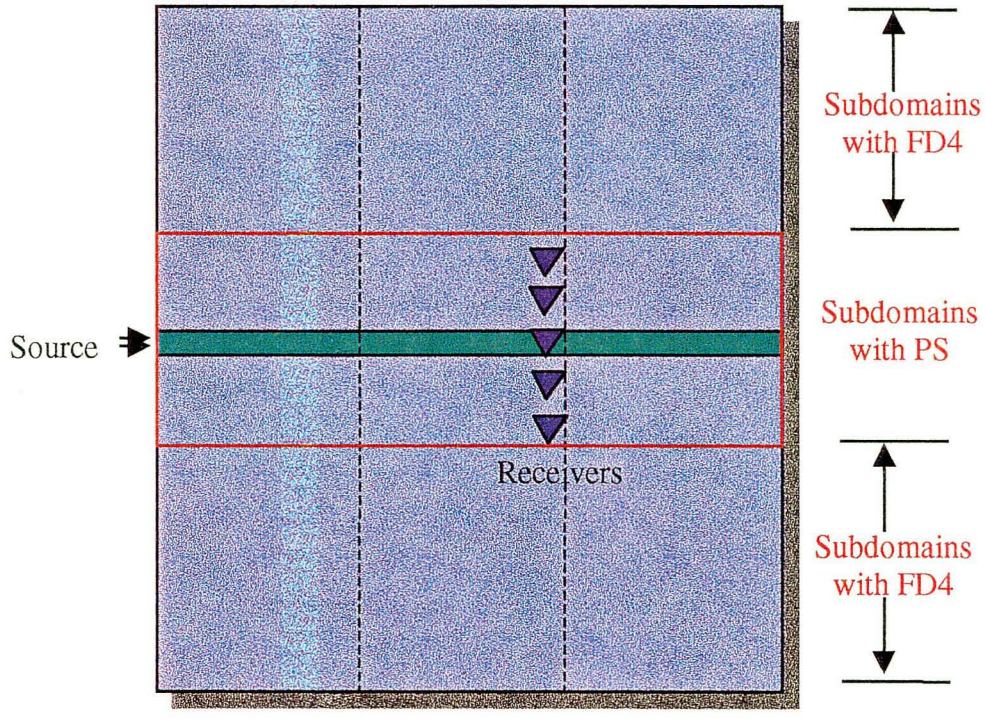

Figure 4.2. The subdomains used in the ODD numerical modeling.

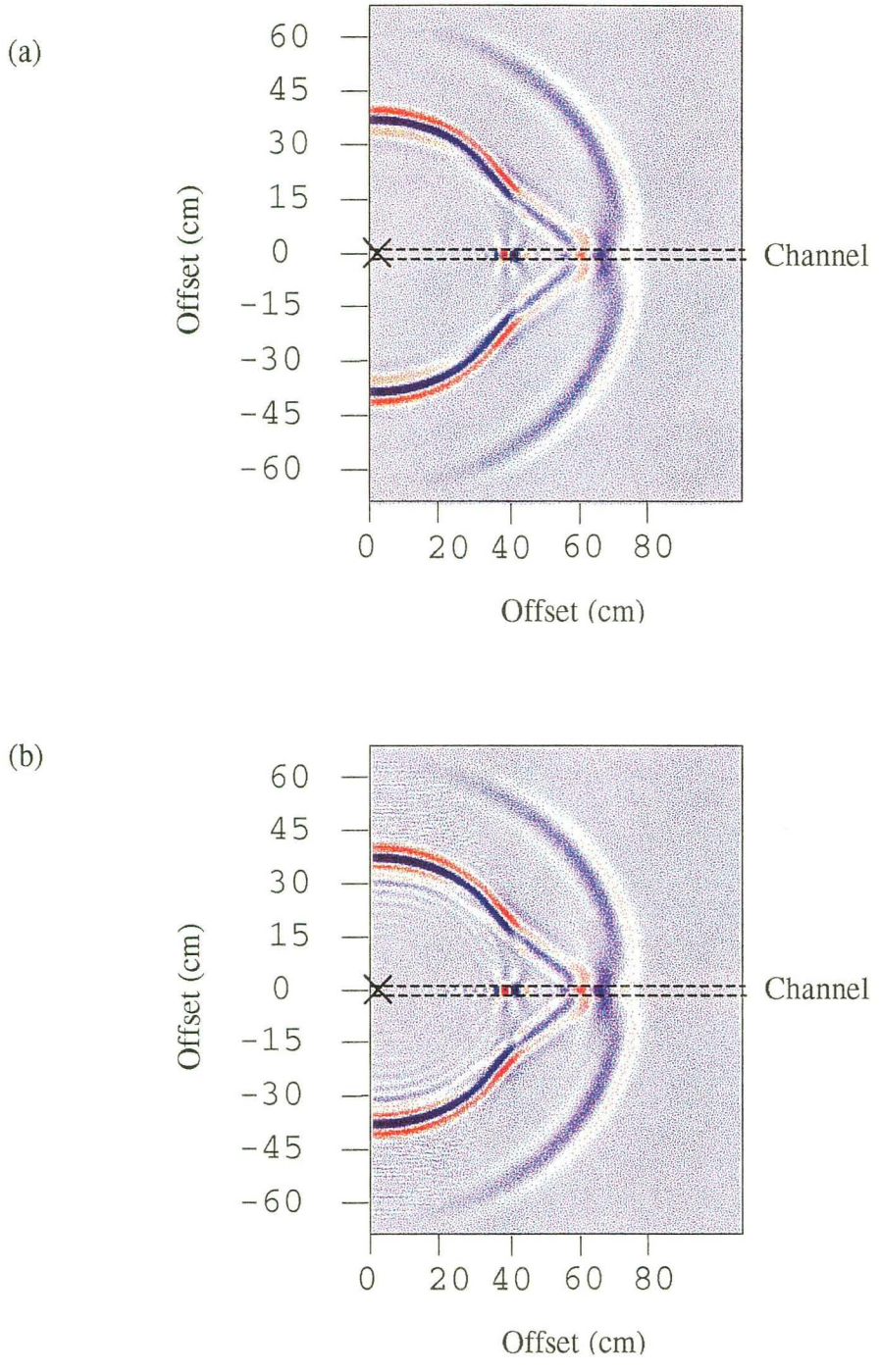

Figure 4.3. Snapshots of horizontal components from the numerical simulations: (a) six subdomain ODD PS-FD4 method and (b) FD4 method.

4.2.3 Comparison of Results from Experiments and Numerical Simulations

The wavefield was measured along a vertical profile crossing the channel located 55 cm from the source for two receiver orientations at an interval of 0.3 cm (Figure 4.1). Figure 4.4 and 4.5 show the horizontal and vertical components of the wavefield from the experimental measurements and numerical simulations.

Two types of waves were generated by the horizontally polarized P type source located at the center of the channel. The first-arriving wave is a P-wave that mainly has particle motion (energy) in the horizontal direction. The later-arriving wave is a Rayleigh channel wave, which unlike an S-wave, has large wavemotion in both horizontal and vertical directions. The experimental measurement and the numerical simulation show good agreement for both waves. The waveforms show clear symmetry for the horizontal components with respect to the center of the channel and anti-symmetry for the vertical components. This is expected as a horizontally polarized source located at the center of the channel will generate primarily symmetric extensional modes.

From the measured and computed arrivals of the waves, it can be seen that both waves travel slower within and near the low velocity channel. In Figure 4.4 and 4.5, the P1, S1 and P2, S2 indicate the predicted arrival times of P and S waves propagating in the homogeneous higher velocity medium and lower velocity medium, respectively. The arrivals of the P type wave within and near the channel are after P1, but before P2, i.e. the velocities of the waves are between V1 and V2. Similarly, the R type wave travels with a velocity between S1 and S2.

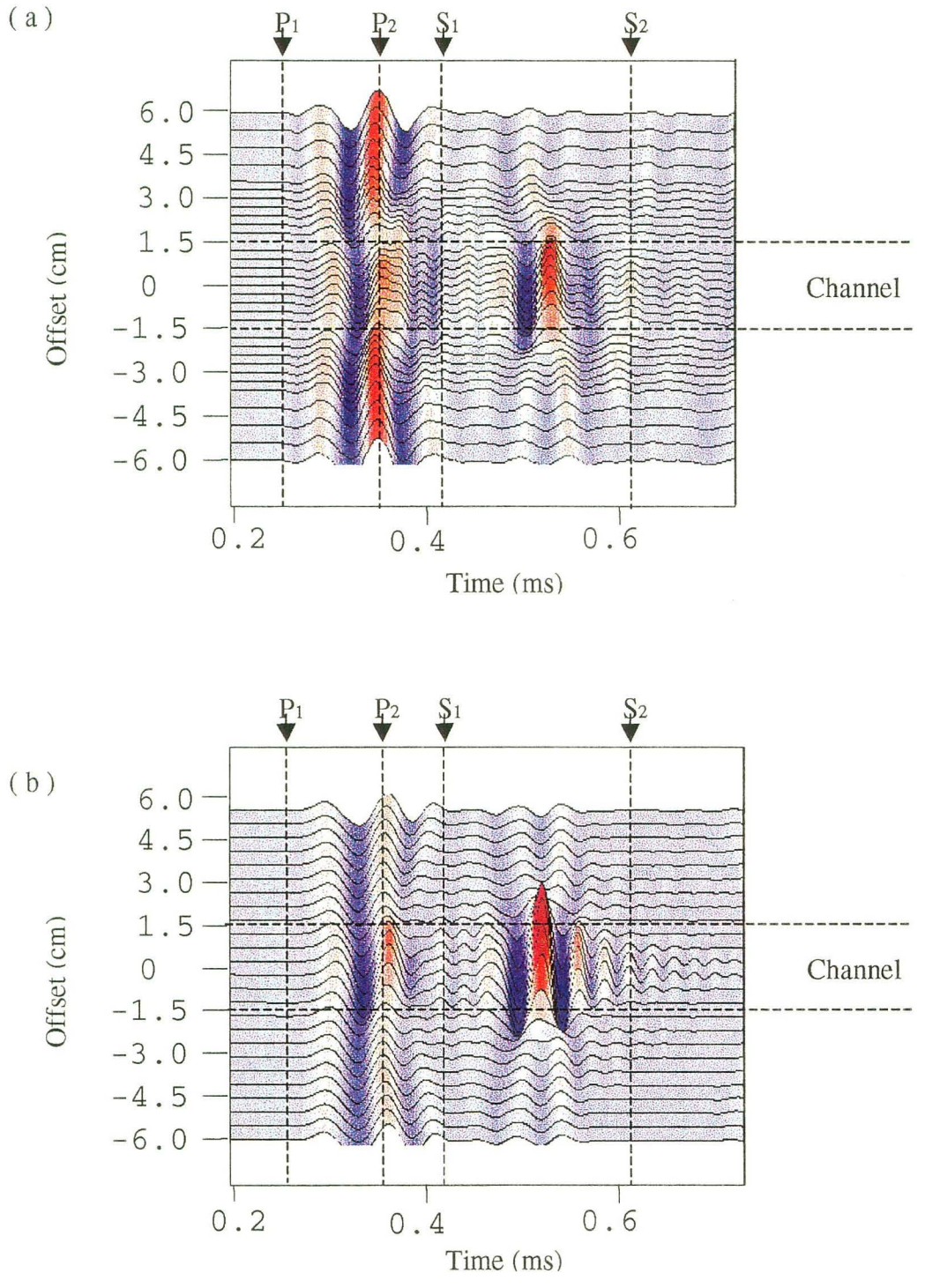

Figure 4.4. Horizontal components of the wavefield measured along a vertical profile crossing the channel: (a) experimental measurement and (b) PS-FD computation.

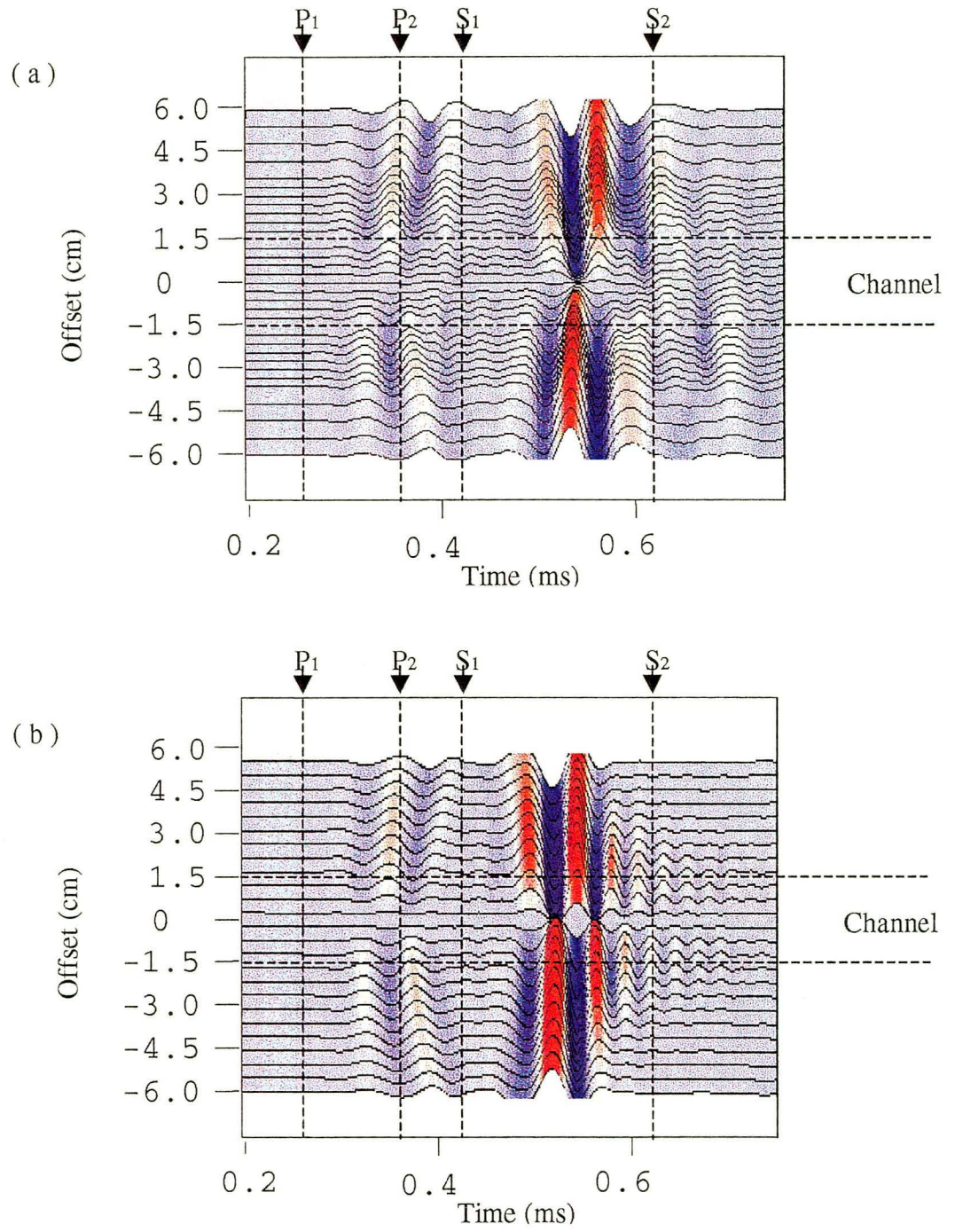

Figure 4.5. Vertical components of the wavefield measured along a vertical profile crossing the channel: (a) experimental measurement and (b) PS-FD computation.

The amplitudes of the waves change dramatically across the channel. To examine the changes quantitatively, the maximum amplitudes and energy of the P and R type waves were measured at a range of offsets from the center of the channel and are displayed in Figure 4.6 to 4.9 for both the horizontal and vertical components. The maximum amplitude is the normalized difference between the maximum and the minimum peak values of each time series. The energy is computed from the normalized square of the amplitudes along the windowed arrival for the P and R type waves.

For the horizontal component, the maximum amplitude of the P arrival has a peak value at the center of the channel. With increasing offset, the amplitude first decreases to a minimum value at the interfaces, then increases in the high-velocity media. In contrast, although the maximum amplitude of R type wave has the maximum value at the center of the channel, with increasing offset, the amplitude first decreases rapidly within the low-velocity channel and then continues to decrease slowly in the high-velocity media. For the vertical component, the maximum amplitudes of both P and R type wave have minimum values at the center (anti-symmetry), and with increasing offset, the amplitudes first increase and reach peaks outside of the channel (near the interfaces), then decrease in the high-velocity media. The profiles of the vertical components for the experimental and numerical results match well.

There are several disagreements between the experimental measurements and numerical simulations. The experimental results are not perfectly symmetric and anti-symmetric as in the numerical simulations. This is most likely due to the variability in the physical model (e.g., non-uniform bonding of the Lexan to acrylic) and errors in the measurements. The amplitudes of the P and R type waves from the experiments are

smaller than the amplitudes from the numerical simulations. A potential reason for this is that the lower Lexan plastic layer is more attenuating than the high acrylic plastic halfspaces (i.e., the numerical model did not have attenuation). In Figure 4.7, the peaks of the vertical component from the experimental results are slightly further away from the interfaces than the peaks from the numerical results. This probably results because the receivers could not be put on the glued interfaces as the surfaces were not flat enough to take reliable measurements with the accelerometer.

The energy profiles (Figure 4.8 and 4.9) show similar properties as the maximum amplitude profiles. The total energy (P+R) is also shown in the plots. It is quite clear that the energy is concentrated within the channel for the horizontal component and near the channel for the vertical component.

The spectra of the waveforms measured across the channel are shown in Figure 4.10 and 4.11. The most significant characteristics in the plot are the high frequency waves within the channel for the horizontal component and along the interfaces of the channel for the vertical component. As a consequence, the wave energy is distributed in a region of triangular shape in the spectral profiles across the channel.

The above comparison between the experimental measurements and numerical simulations demonstrate that the numerical simulations using the ODD technique can reproduce the basic results observed in the laboratory experiments. Since the construction of a physical model and the measurement of the wavefield is both difficult and time consuming, numerical simulations can be used as an alternative way to study properties of channel waves.

(a)

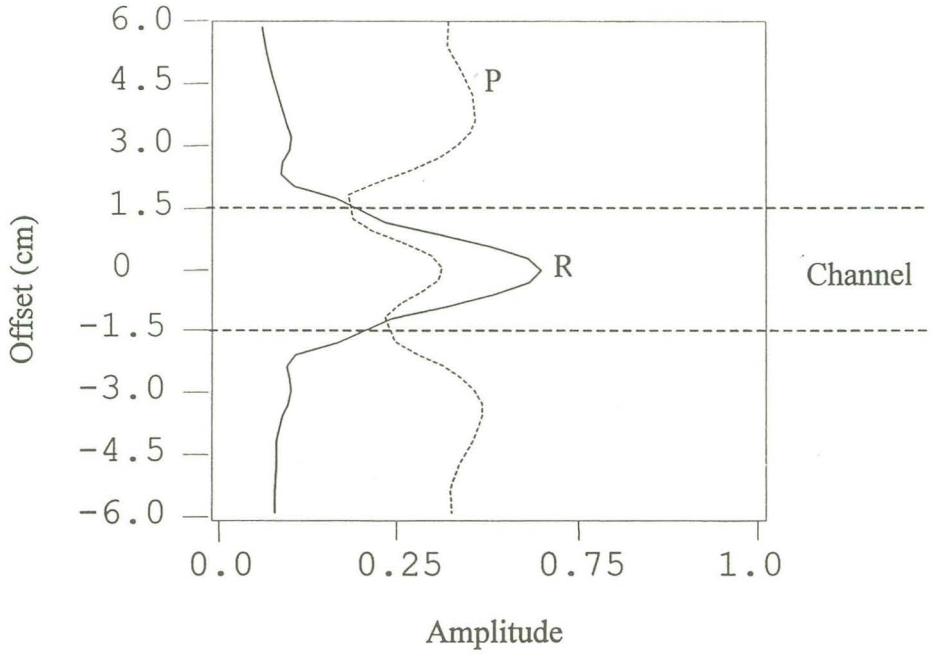

(b)

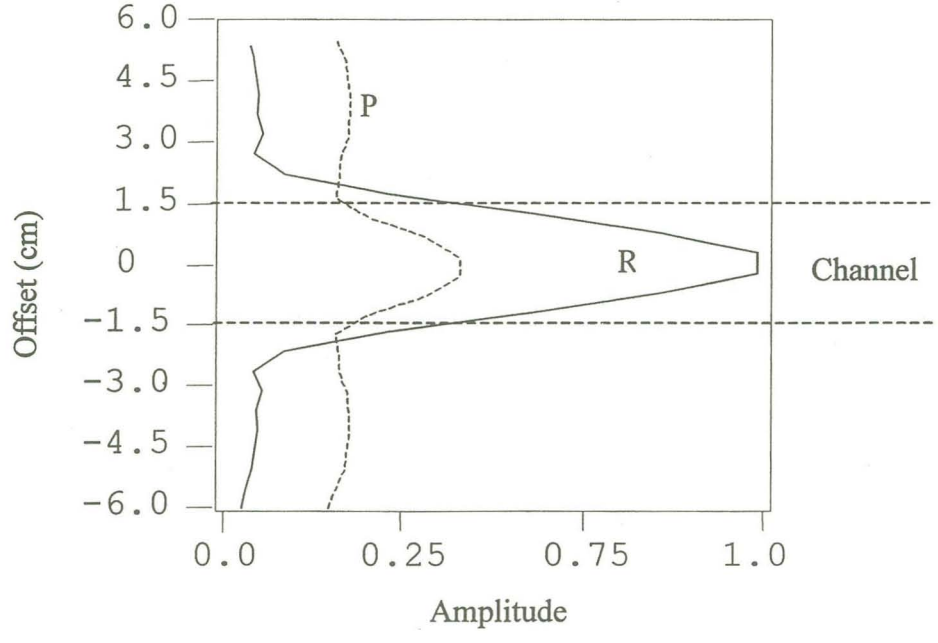

Figure 4.6. Profiles of maximum amplitude of the horizontal component: (a) experimental measurement and (b) PS-FD computation.

(a)

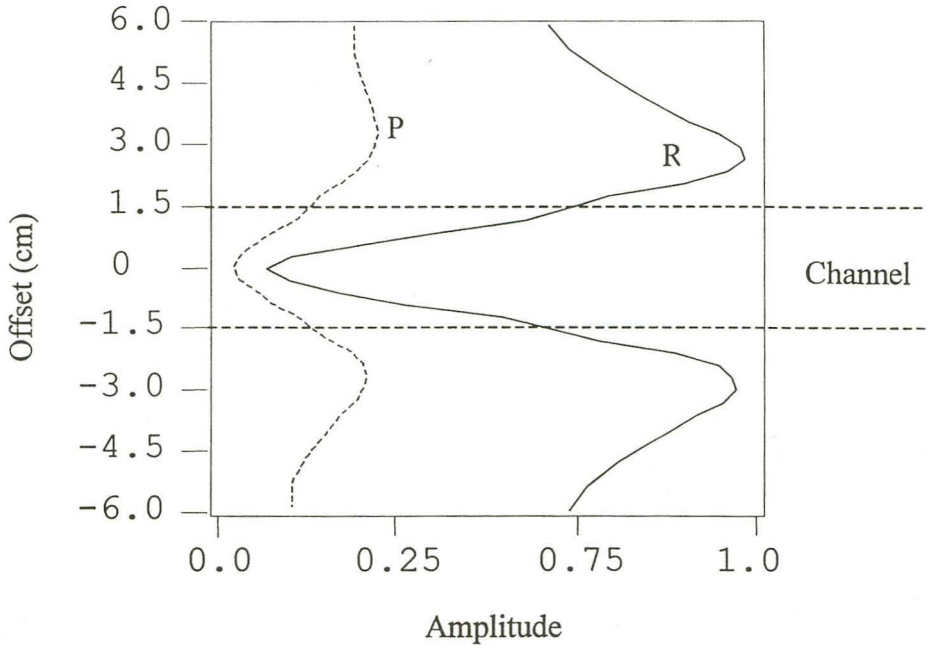

(b)

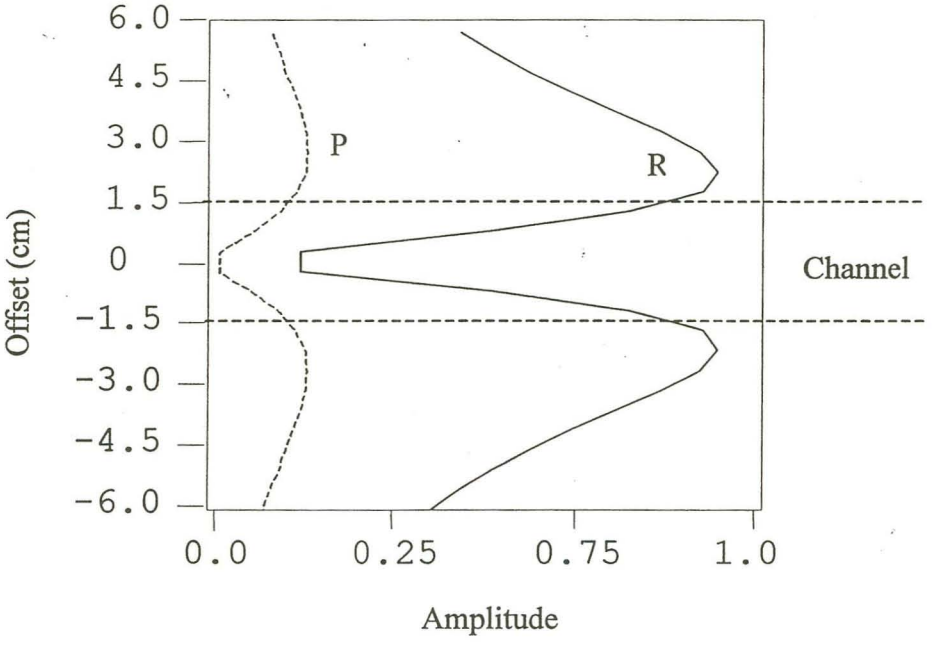

Figure 4.7. Profiles of maximum amplitude of the vertical component: (a) experimental measurement and (b) PS-FD computation.

(a)

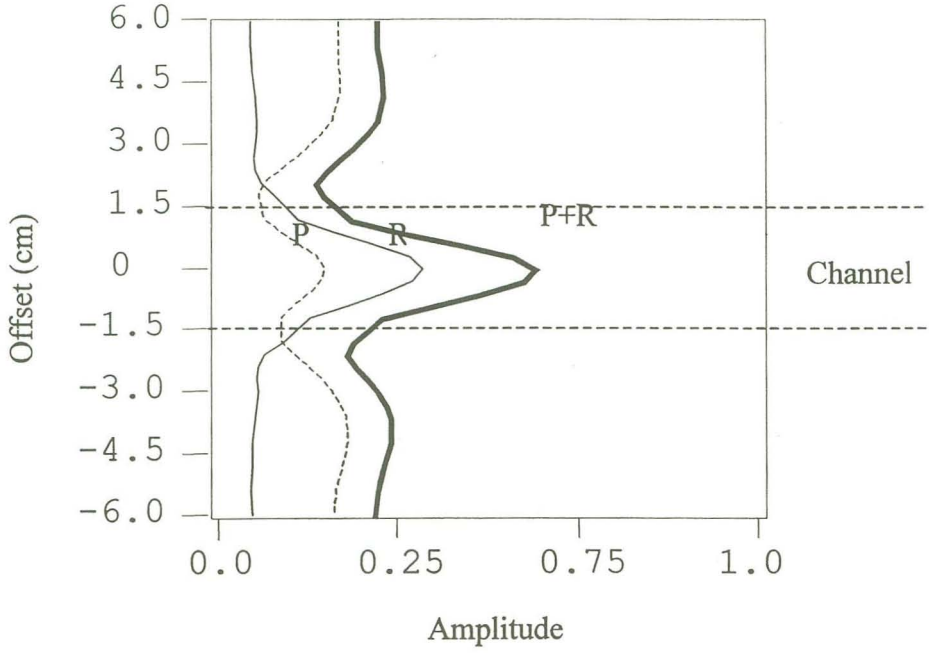

(b)

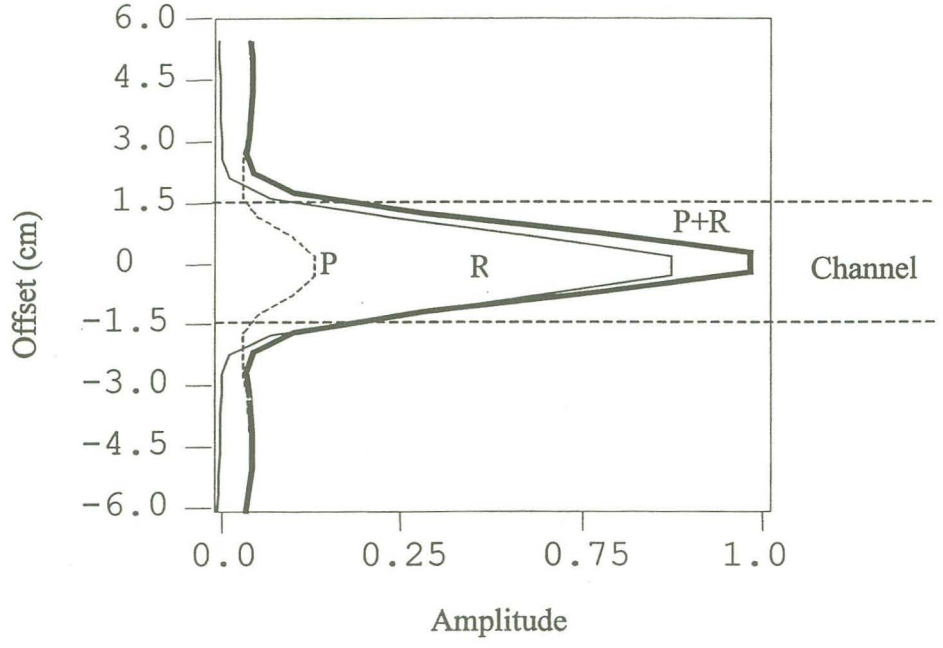

Figure 4.8. Energy profiles of the horizontal component:
(a) experimental measurement and (b) PS-FD computation.

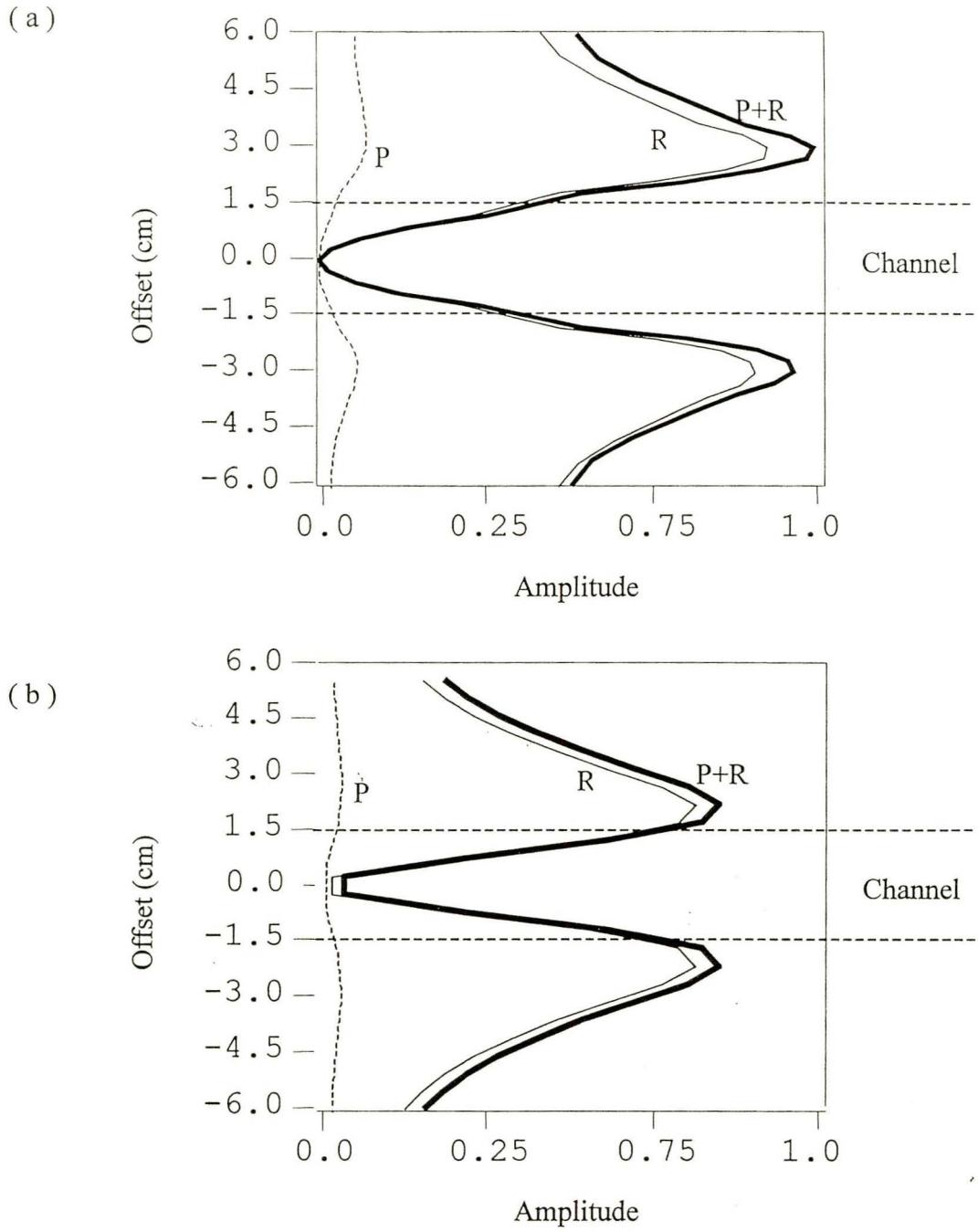

Figure 4.9. Energy profiles of the vertical components:
(a) experimental measurement and (b) PS-FD computation.

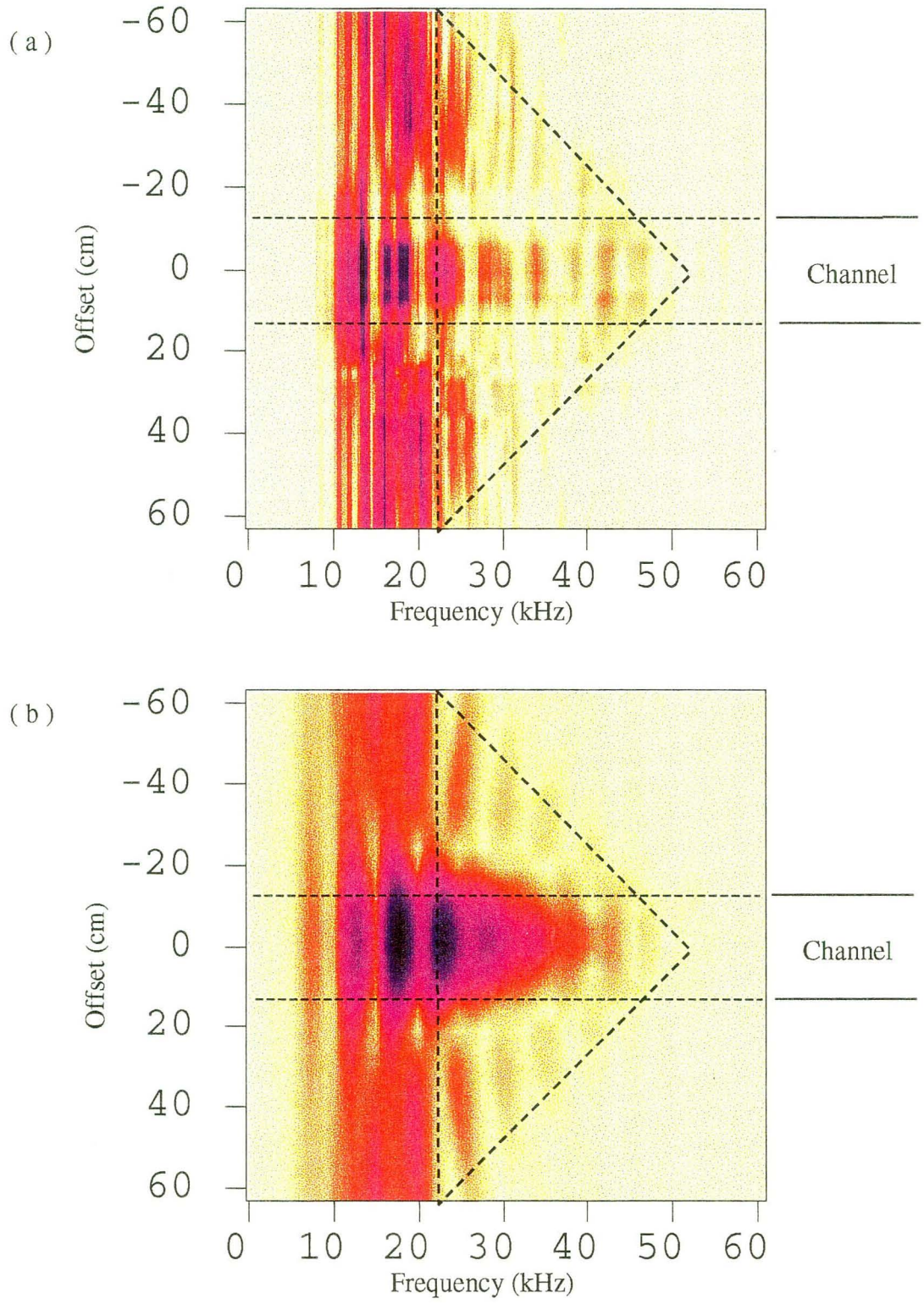

Figure 4.10. The spectra of the horizontal component of the wavefield: (a) experimental measurement and (b) PS-FD computation.

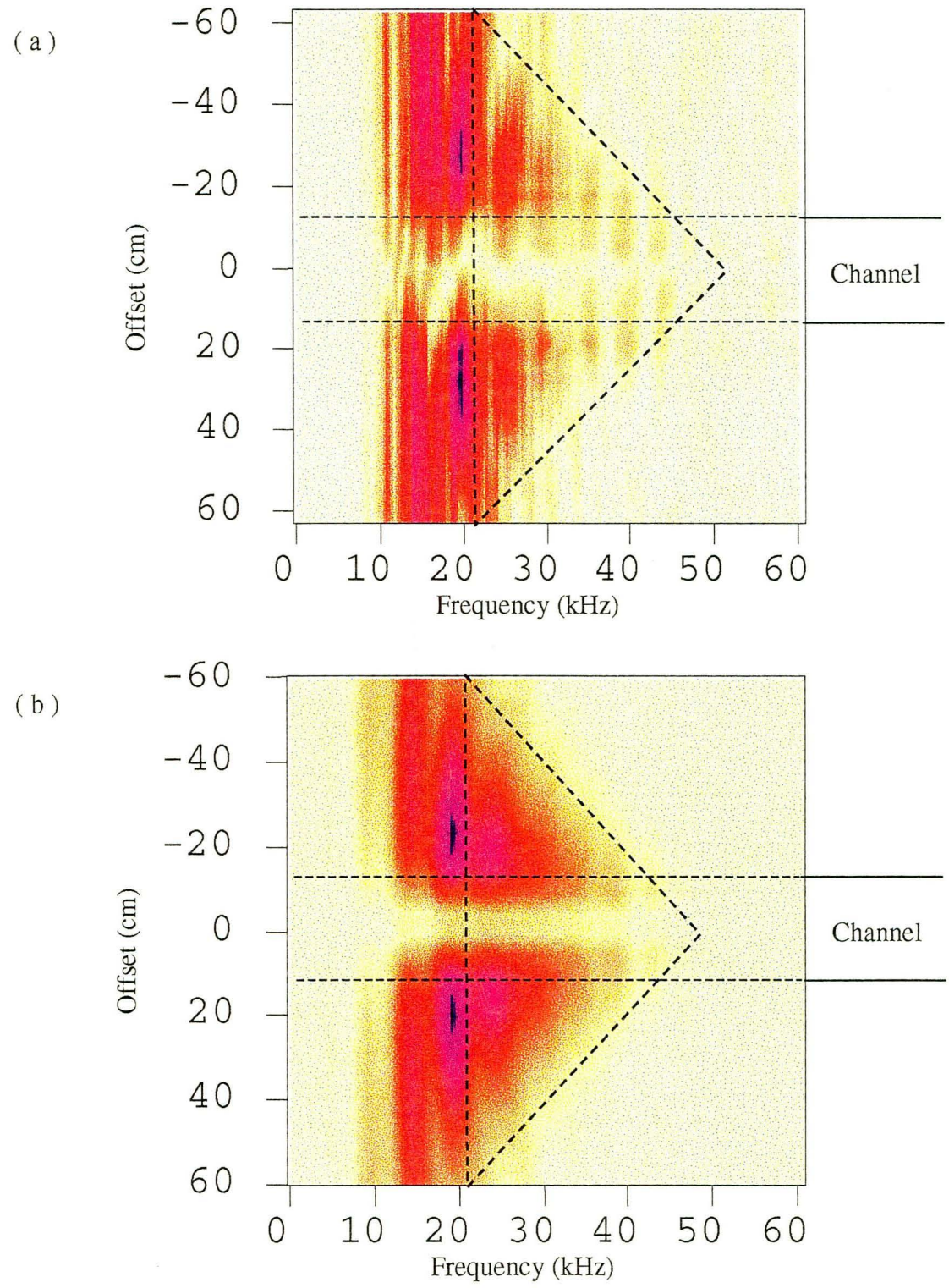

Figure 4.11. The spectra of the vertical component of the wavefield: (a) experimental measurement and (b) PS-FD computation.

4.3 Summary

In this chapter simulations of guided wave propagation in a low velocity layer is performed by the ODD technique, where the high accurate PS method is used in the subdomain encompassing the low velocity layer where the wavelength is shorter and the source is located, and the FD method is applied to surrounding high velocity medium in which waves have longer wavelengths. This example again demonstrates the flexibility and efficiency of the ODD technique.

The numerical results show that the wave energy and high frequency components are concentrated along the low velocity layer. The results are compared to experimental results from physical modeling and they show a good agreement.

CHAPTER FIVE

OVERLAP DOMAIN DECOMPOSITION FOR 3-D ACOUSTIC PROBLEMS

5.1 Introduction

Recent advances in computational technology have made it possible to perform relative large-scale seismic modeling. A typical single CPU computer can handle a model with a dimension of 570x350x110 (about 22 millions grid points) and take several days for a finite-difference simulation (Graves, 1998). If the grid spacing is 10 m, the physical dimension of the model is 5.7 km x 3.5 km x 1.1 km. A model of 13.9 km x 13.9 km x 8.0 km with a 20 m spaced grid (a total grid size of 695x695x400, about 200 million grid points, taking over 5 GB computer memory in a finite-difference method) can be simulated only by using domain decomposition and parallel computing techniques (Aminzadeh et al., 1994 and 1995, Bradley et al. 1997). Consequently, domain decomposition techniques become more important for 3-D simulations.

5.2 3-D Acoustic Finite Difference Method

Let x, y and z be rectangular coordinates in a three-dimensional medium, and let the z-axis be positive downward. For an isotropic medium with both density and seismic wave velocity that are spatially constant, the acoustic wave equation is

$$\frac{\partial^2 P(x,y,z,t)}{\partial x^2}+\frac{\partial^2 P(x,y,z,t)}{\partial y^2}+\frac{\partial^2 P(x,y,z,t)}{\partial z^2}=\frac{1}{c^2}\frac{\partial^2 P(x,y,z,t)}{\partial t^2}+S, \quad (5.1)$$

where $P(x, y, z, t)$ represents the pressure, c the wave velocity, and $S(x, y, z, t)$ the source

term, which equals the divergence of the body force divided by the density.

The spatial derivatives can be expressed by the fourth-order FD as

$$\begin{aligned}
\frac{\partial^2 P(x_l,t_i)}{\partial x^2} &= \frac{1}{\Delta x^2}\sum_{j=-2}^{2} a_j P(x_{l+j},t_i) + O([\Delta x]^4) \\
\frac{\partial^2 P(y_m,t_i)}{\partial y^2} &= \frac{1}{\Delta y^2}\sum_{j=-2}^{2} a_j P(y_{m+j},t_i) + O([\Delta y]^4) \\
\frac{\partial^2 P(z_n,t_i)}{\partial z^2} &= \frac{1}{\Delta z^2}\sum_{j=-2}^{2} a_j P(z_{n+j},t_i) + O([\Delta z]^4),
\end{aligned} \tag{5.2}$$

where a_j are the constant factors of fourth-order FD: $a_{-2} = -1/12$, $a_{-1} = 4/3$, $a_0 = -5/2$, $a_1 = 4/3$ and $a_2 = -1/12$. The temporal derivative has the second order FD form

$$\frac{\partial^2 P(x_l,y_m,z_n,t_i)}{\partial t^2} = \frac{1}{\Delta t^2}[P(x_l,y_m,z_n,t_{i+1}) - 2P(x_l,y_m,z_n,t_i) + P(x_l,y_m,z_n,t_{i-1})] + O([\Delta t]^2), \tag{5.3}$$

If $\Delta x = \Delta y = \Delta z$, the solution can be obtained for the grid point [*l, m, n*] at next time step $i+1$ by substituting equations (5.2) and (5.3) to equation (5.1)

$$\begin{aligned}
P(x_l,y_m,z_n,t_{i+1}) &= 2P(x_l,y_m,z_n,t_i) - P(x_l,y_m,z_n,t_{i-1}) \\
&+ \frac{1}{\Delta x^2}\sum_{j=-2}^{2} a_j [P(x_{l+j},y_m,z_n,t_i) + P(x_l,y_{m+j},z_n,t_i) + P(z_{n+j},y_m,z_n,t_i)] \\
&+ c^2\Delta t^2 S + O([\Delta x]^4,[\Delta z]^4,[\Delta t]^2),
\end{aligned} \tag{5.4}$$

For a heterogeneous medium in which both density and seismic wave velocity are spatially variable, the acoustic wave equation is

$$\frac{\partial}{\partial x}\left(\frac{1}{\rho}\frac{\partial P}{\partial x}\right) + \frac{\partial}{\partial z}\left(\frac{1}{\rho}\frac{\partial P}{\partial y}\right) + \frac{\partial}{\partial z}\left(\frac{1}{\rho}\frac{\partial P}{\partial z}\right) = \frac{1}{c^2\rho}\frac{\partial^2 P}{\partial t^2} + S, \tag{5.5}$$

where $P = P(x, y, z, t)$ is the pressure and $\rho = \rho(x, y, z, t)$ is the density. Compared to equation (5.1), the two passes of the first order spatial derivatives are required instead of the one application of second order derivatives in x, y and z directions since the density and velocity are no longer constant. The finite difference formulas for 4th order accuracy in the spatial derivatives are

$$\begin{aligned}
\frac{\partial P(x_l, y_m, z_n, t_i)}{\partial x} &= \frac{1}{\Delta x}\sum_{j=-2}^{2} b_j P(x_{l+j}, y_m, z_n, t_i) + O([\Delta x]^4) \\
\frac{\partial P(x_l, y_m, z_n, t_i)}{\partial y} &= \frac{1}{\Delta y}\sum_{j=-2}^{2} b_j P(x_l, y_{m+j}, z_n, t_i) + O([\Delta x]^4) \\
\frac{\partial P(x_l, y_m, z_n, t_i)}{\partial z} &= \frac{1}{\Delta z}\sum_{j=-2}^{2} b_j P(x_l, y_m, z_{n+j}, t_i) + O([\Delta z]^4),
\end{aligned} \tag{5.6}$$

where b_j are the constant factors of fourth-order FD: $b_{-2} = 1/12$, $b_{-1} = -2/3$, $b_0 = 0$, $b_1 = 2/3$ and $b_2 = -1/12$. Now we set

$$\begin{aligned}
f(x_l, y_m, z_n, t_i) &= \frac{1}{\rho(x_l, y_m, z_n)}\frac{\partial P(x_l, y_m, z_n, t)}{\partial x} \\
g(x_l, y_m, z_n, t_i) &= \frac{1}{\rho(x_l, y_m, z_n)}\frac{\partial P(x_l, y_m, z_n, t)}{\partial y} \\
h(x_l, y_m, z_n, t_i) &= \frac{1}{\rho(x_l, y_m, z_n)}\frac{\partial P(x_l, y_m, z_n, t)}{\partial z},
\end{aligned} \tag{5.7}$$

and the spatial derivatives of equation (5.5)

$$\begin{aligned}
&\frac{\partial}{\partial x}\left(\frac{1}{\rho(x_l, y_m, z_n)}\frac{\partial P(x_l, y_m, z_n, t_i)}{\partial x}\right) = \frac{\partial f(x_l, y_m, z_n, t_i)}{\partial x} \\
&= \frac{1}{\Delta x^2}\sum_{j=-2}^{2} b_j f(x_{l+j}, y_m, z_n, t_i) + O([\Delta x]^4).
\end{aligned} \tag{5.8}$$

Similar equations can be written for the derivatives of g and h, allowing the final FD solution for a heterogeneous 3-D medium to be written as

$$\begin{aligned} P(x_l, y_m, z_n, t_{+1i}) &= 2P(x_l, y_m, z_n, t_i) - P(x_l, y_m, z_n, t_{i-1}) \\ &+ \frac{1}{\Delta x} \sum_{j=-2}^{2} b_j [f(x_{l+j}, y_m, z_n, t_i) + g(x_{l+j}, y_{m+j}, z_n, t_i) + h(x_l, y_m, z_{n+j}, t_i)] \\ &+ c^2 \rho \Delta t S + O([\Delta x]^4, [\Delta z]^4, [\Delta t]^2). \end{aligned} \tag{5.9}$$

5.3 Application of ODD for the 3-D Acoustic Finite Difference Method

Similar to the 2-D case, the overlap domain decomposition technique can be easily applied to three directions. Figure 5.1 shows 3-D subdomains and overlap areas. For the homogeneous problems, equation (5.2) indicates that the spatial derivative at point [*l, m, n*] needs only four nearby grid points values in each direction. The minimum number of overlap grid points should be four in each direction according to the study of Chapter 2. For heterogeneous problems using equation (5.2), the overlapping area should cover at least eight grid points in each direction.

Figure 5.2 shows snapshots from a simulation of seismic waves through a homogeneous cube of material with a point source at the center. Figure 5.2(a) is a single-domain FD4 snapshot, while Figure 5.2(b) is a snapshot from an eight-subdomain ODD FD4 run. The two results are identical, demonstrating that the ODD technique can also be applied to 3-D problems.

To demonstrate the value of the ODD technique, computation times and memory requirements are calculated for the 3-D migration geometry shown in Figure 5.3. Assuming a spatial grid interval of 5 m for a FD4 method, the number of grid points is

1000x600x600 (360 million). By using the ODD technique, a PS method can be applied for the low velocity layer and a FD4 method for the remaining volume, the spatial grid interval can be increased by a factor of 4 to 20 m while still preserving numerical accuracy (Fornberg, 1987). The number of grid points is reduced by a factor of 64 (4x4x4) to 250x175x175 (5.625 million). The computing time also can be reduced dramatically by decreasing the number of grid points and coupling the PS and FD4 method. Based on estimations by Fornberg (1987) and Marfurt (1984), the relative memory usage and computing time between the ODD PS-FD4 and conventional FD4 are shown in Table 5.1, where N is the number of the grid points in one direction.

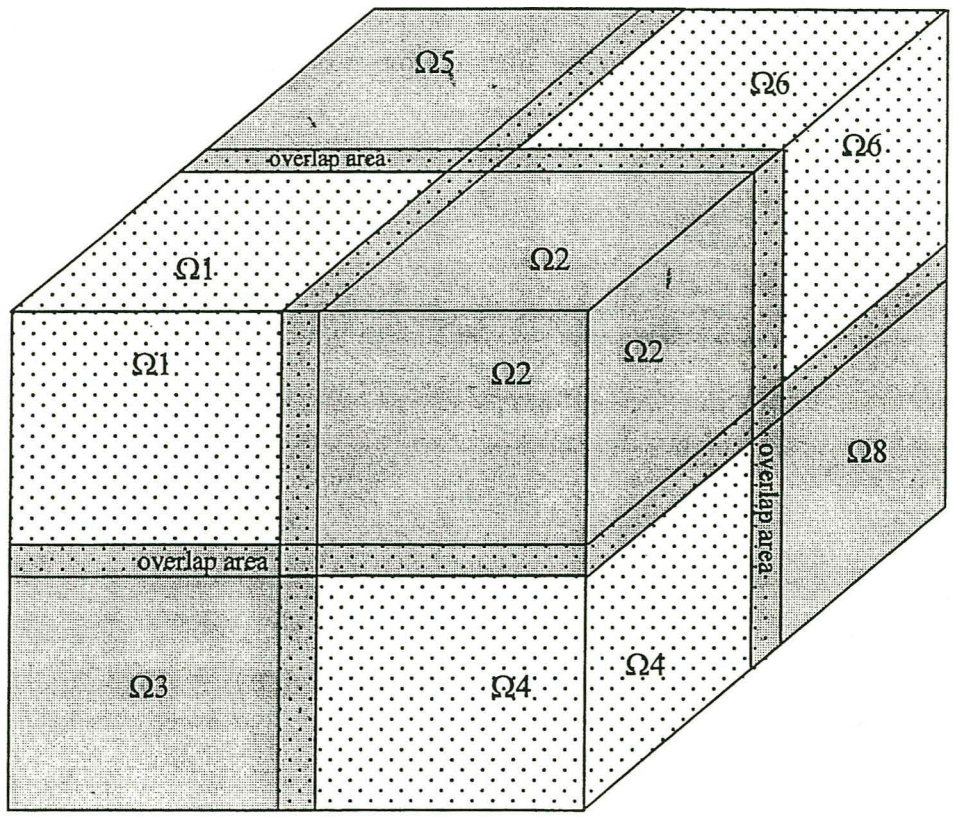

Figure 5.1. Subdomains and overlap areas for the 3-D overlap domain decomposition.

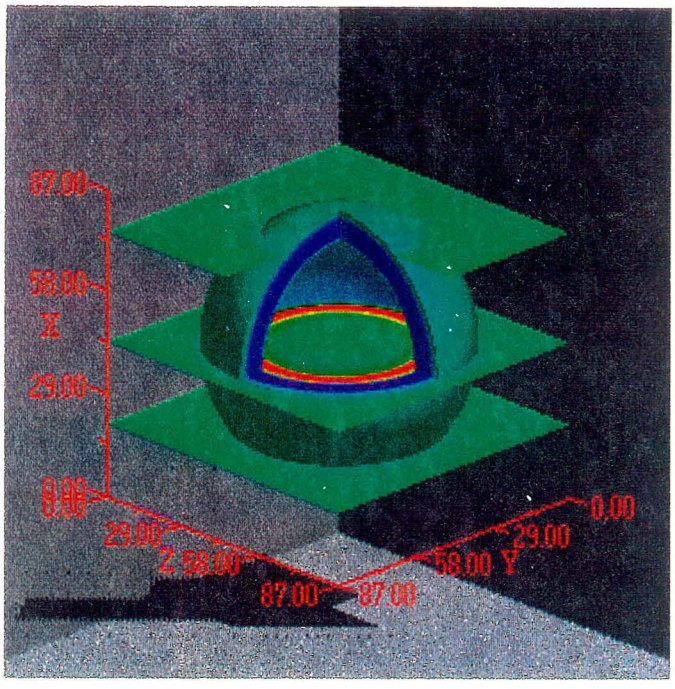

(a) One domain conventional FD method

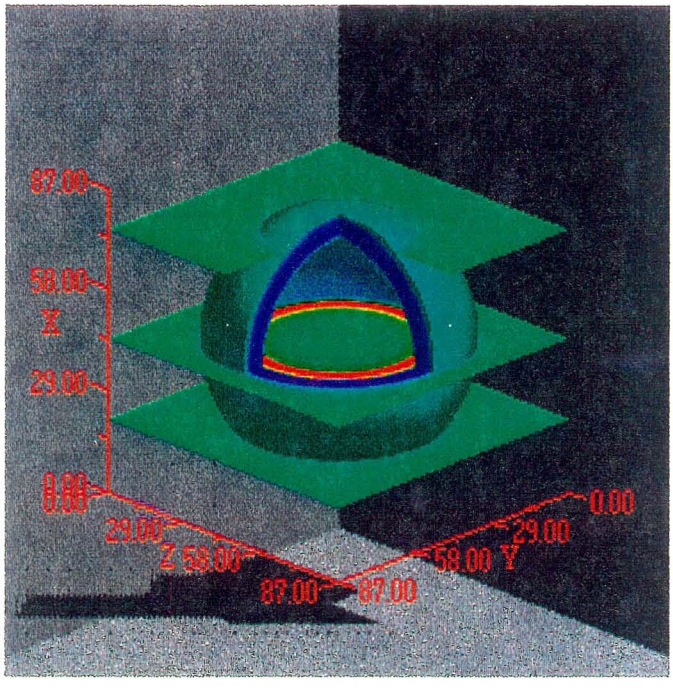

(b) Eight subdomain ODD FD method

Figure 5.2. Snapshots from a 3-D acoustic simulation with a point source.

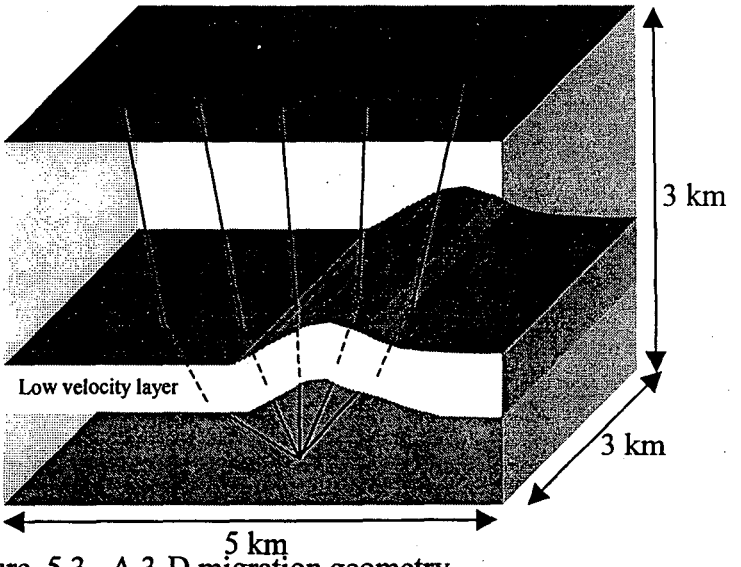

Figure. 5.3. A 3-D migration geometry.

Table 5.1. The potential of the 3-D computation times and memory usage by the different methods.

Method	Number of grid points at each spatial direction	Relative computer cost	
		CPU time	Memory
Conventional PS	N	1	1
ODD PS (w/o turning-off)	N	1	0.7
ODD PS (turning-off)	N	0.5	0.7
Conventional FD4	4N	8	64
ODD FD4 (w/o turning-off)	4N	10	43
ODD FD4 (turning-off)	4N	6	43
ODD PS-FD4 (w/o turning-off)	N	0.15	0.7
ODD PS-FD4 (turning-off)	N	0.1	0.7

5.2 Summary

This chapter described the ODD technique for 3-D problems and shown an acoustic example. The relative savings of the computing time and memory usage by using the ODD technique and "turning-off" technique are estimated.

CHAPTER SIX

CONCLUSIONS AND FUTURE WORK

6.1 Conclusions

This work has presented a general overlap domain decomposition (ODD) technique based on Huygens' Principle for numerical modeling of wave propagation. The ODD technique is described in detail for 1-D cases and extended to 2-D and 3-D cases. The finite difference (FD) method and Fourier pseudospectral (PS) method for solving wave equations incorporated into the ODD framework and the resulting algorithms are given. The lengths of the overlap areas for different methods in 1-D, 2-D, and 3-D are presented. The ODD algorithms are well suited for the FD method, the PS method, and the coupled FD and PS method. By using the ODD technique, calculations can be turned-off in subdomains that do not have appreciable wave activity, resulting in savings of computing time and memory use. The object-oriented ODD FD and PS code implemented by C++ language based on the ODD algorithm has been developed for wave simulations in which either FD or PS method can be selected in each subdomain. The examples show the advantages of the using ODD technique for modeling wave propagation.

The ODD technique for the FD method gives identical solutions as the conventional FD method does. The overlap areas of the ODD FD method with fourth order accuracy need at least four grid points for a homogeneous acoustic or elastic medium and at least eight grid points for a heterogeneous acoustic or elastic medium. The number of grid points per wavelength for the FD method to achieve stable and nondispersive results is

about 10 to 35, depending on the model complexity. In the application of the ODD technique to the PS method, a tapering technique for each subdomain was introduced to avoid the wraparound problem which results from the periodic property of Fourier transform. The wavelength of the taper functions should match the wavelength of the wave (i.e., the length of overlapping area should be about one wavelength). The number of grid points per wavelength for the PS method to achieve stable and nondispersive results is about 5 to 20. To couple the FD and PS methods, subdomains with the PS method require taper functions, while subdomains with the FD method do not need taper functions. Examples show that the results of the ODD technique match very well with the results by conventional method, and that the ODD technique can save computation time and reduce memory requirements.

An example of channel wave propagation in a low velocity layer demonstrates the flexibility and efficiency of the ODD technique. The accurate but computationally expensive PS method can be used in the subdomains containing the source and the low velocity layer (where the wavelength is shorter). The faster FD method is applied to the surrounding high velocity media (which has longer wavelength). The results are compared to experimental results from physical modeling and they show a good agreement. Both models show that the wave energy and high frequency components are concentrated along the low velocity layer.

6.2 Future Work

Because the ODD technique breaks a large problem into many independent subdomain computations, it is well suited to parallel computation. This promises to give even more

power to the ODD technique. The ODD technique is based on Huygens' Principle, and it only requires exchange of the final computing results between two neighboring subdomains through the overlap areas. Therefore, the ODD technique itself is not restricted to a specific numerical method and it can be easily applied to different numerical methods such as the staggered grid finite difference method, the finite element method and boundary element method for solving the wave equation. In addition, different methods can be used in each subdomain to achieve a desired level of accuracy and computing speed. The application of the ODD technique to implicit FD or PS method could reduce a significant computing time by breaking down the size of matrices. Optimization of the domain decomposition turn-on & off technique may be achieved by artificial intelligence.

Due to the high costs (computing time and memory usage) of the 3-D finite-difference scheme, current 3-D prestack migration typically uses a ray-tracing scheme (i.e. Kirchhoff migration). However, calculations of migration tables based on Kirchhoff methods may result in significant traveltime errors in complex geometries (Nichols, 1996). The low cost and highly accurate mixed ODD pseudospectral and finite-difference scheme could be quite suitable for 3-D migration.

BIBLIOGRAPHY

Alford, R. M., Kelly, K. R. and Boore, D. M., 1974, Accuracy of finite difference modeling of the acoustic wave equation: Geophysics, **39**, 834-842.

Alterman, Z. and Kornfeld, P., 1968, Finite difference solution for pulse propagation in a sphere: Israel J. Of Technology, **6**, 138-149.

Alterman, Z. and Karal, F. C., Jr., 1968, Seismic waves in a quarter and three-quarter plane: Bull. Seis. Soc. Am., **59**, 347-368.

Alterman, Z. and Rotenberg, A., 1969, Propagation of elastic waves in layered media by finite difference methods: Bull. Seis. Soc. Am., **58**, 367-398.

Aminzadeh, F., Rocca, F., Wyatt, K., Lailly, P., Burkhard, N., Kunz, T., Chen, K. H., and Mulder, M., 1994, Progress report from the SEG/EAEG modeling: The Leading Edge, **13**, 2, 110-112.

Aminzadeh, F., Burkhard, N., Nicoletis, L., Rocca, F., and Wyatt, K., 1994, SEG/EAEG 3-D modeling project: 2nd update: The Leading Edge, **13**, 9, 949-952.

Aminzadeh, F., Burkhard, N., Kunz, T., Nicoletis, L., and Rocca, F., 1995, 3-D modeling project: 3rd report: The Leading Edge, **13**, 9, 949-952.

Aminzadeh, F., Burkhard, N., Long, J., Kunz, T., and Duclos, P., 1996, There dimensional SEG/EAEG models – an update: The Leading Edge, **15**, 131-134.

Bayliss, A., Jordan, K. E., LeMesurier, B. J., and Turkel, E., 1986, A fourth-order accurate finite-difference scheme for the computation of elastic waves: Bull. Seis. Soc. Am., **76**, 1115-1132.

Boore, D. M., 1972, Finite-difference methods for seismic wave propagation in heterogeneous materials, Methods in computational physics: B. Alder, S. Fernbach and M. Rotenberg, Editors, New York, Academic Press, **2**, 21-22.

Bradley, C., House, L., Fehler, M., Pearson, J., and TenCate, J., 1997, Numerical and measured data from the 3D salt canopy physical modeling project: 67th Ann. Internat. Mtgl, Soc. Expl. Geophys., Expanded Abstracts, 1476-1479.

Brekhovskikh, L. M., 1980, Waves in layered media: Academic Press.

Buchanan, D. J., Davis, R., Jackson, P. J., and Taylor, P. M., 1981, Fault location by channel wave seismology in United Kingdom coal seams: Geophysics, **46**, 994-1002.

Buchanan, D. J., and Jackson, P. J., 1986, Coal Geophysics, Geophysics reprint series No.6: Society of Exploration Geophysics.

Cai, X.-C., 1995, A family of Overlapping Schwarz algorithms for nonsymmetric and indefinite elliptic problems, Domain-based parallelism and problem decomposition methods in computational science and engineering, edited by David E. Keyes, Youcef Saad, Donald G. Truhlar. 1-20.

Canuto, C., Hussaini, M.Y., Quarteroni, A., and Zang, T. A., 1988, Spectral methods in fluid dynamics, Springer series in computational physics, Springer-Verlag.

Carcione, J., 1991, Domain decomposition for wave propagation problems: J. Sci. Comput., **6**, 453-472.

Cerjan, C., Kosloff, D., Kosloff, R., and Reshef, M., 1985, A nonreflecting boundary condition for discrete acoustic and elastic wave equations: Geophysics, **50**, 705-708.

Cerveny, V., Molotkov, I. A., and Psencik, I., 1977, Ray method in Seismology: Monograph. Univerzita Karlova, Praha.

Chen, H, and Lazarov, R., 1994, Domain splitting algorithm for mixed finite element approximations to parabolic problems: East-West J. Numer. Math., **1**, No. 1., 1-14.

Cruse, T. A., 1968, A direct formulation and numerical solution of the general transient elastodynamic problem, II: I. J. Math. And Appl., **22**, 341-355.

Cruse, T. A. and F. J. Rizzo, 1968, A direct formulation and numerical solution of the general transient elastodynamic problem: I. J. Math. And Appl., **22**, 244-259.

Cruse, T. A., 1987, Advanced boundary element methods: Proceedings of the IUTAM Symposium, San Antonio, Texas, April 13-16, 1987, T. A. Cruse, Editor.

Dablain, M. A., 1986, The application of high-order differenceing to the scalar wave equation: Geophysics, **51**, 54-66.

Dix, C. H., 1981, Seismic prospecting for oil: International Human Resources Development Corporation, Boston, P.352-358.

Drake, L. A., 1972, Love and Rayleigh waves in nonhorizontally layered media: Bull. Seis. Soc. Am., **62**, 1241-1258.

Dryja, M., and Widlund, O. B., 1990, Towards a unified theory of domain decompostion algorithms for elliptic problems, *in* Third international symposium on domain

decomposition methods for partial differential equations, Chan, T., Glowinski, R. Periaux, J., and Willund, O., Editors: SIAM, Philadelphia.

Duff, I. S., Erisman, A. M., and Reid, J. K., 1986, Direct methods for sparse matrices: Clarendon Press.

Faccioli, E., Maggio, F., Quarteroni, A., and Tagliani, A., 1996, Spectral-domain decomposition methods for the solution of acoustic and elastic wave equations: Geophysics, **61**, 1160-1174.

Fornberg, B., 1972, On a Fourier method for the integration of hyperbolic equations: Soc. Ind. Appl. Math., J. Numer. Anal., 12, 509-528.

Fornberg, B., 1987, The pseudospectral method: comparisons with finite differences for the elastic wave equation: Geophysics, **52**, 483-501.

Fornberg, B., 1996, A practical guide to pseudospectral method: Cambridge University Press.

Friedlander, F. G., 1958, Sound Pulses, Cambridge University Press.

Furumura, T. and Takenaka, H., 1995, A wraparound elimination technique for the pseudospectral wave synthesis using an antiperiodic extension of the wavefield: Geophysics, **60**, 302-307.

Furumura, T. Kennett, B. L. N. and Takenaka, H., 1998, Parallel 3-D pseudospectral simulation of seismic wave propagation: Geophysics, **63**, 279-288.

Gazdag, J., 1981, Modeling of the acoustic wave equation with transform methods: Geophysics, **46**, 854-859.

George, A., and Liu, J. W. H., 1981, Computer solution of large sparse positive-definite systems: Prentice Hall.

Graff, K. F., 1975, Wave motion in elastic solids: Dover Publications, Inc., New York.

Graves, R W., 1996, Simulating seismic wave propagation in 3D elastic media using staggered-grid finite differences: Bull. Seism. Soc. Am, **86**, 4, 1091-1106.

Graves, R W., 1998, Three-dimensional finite-differences modeling of the San Andreas Fault: source parameterization and ground-motion levels: Bull. Seism. Soc. Am, **88**, 4, 881-897.

Gritto, R., and Dresen, L., 1992, Seismic modelling of seam waves excited by energy transmission in to a seam: Geophysical Prospecting, **40**, 671-699.

Hestholm, S., 1997, 3-D finite-difference viscoelatic wave modeling including surface topography: 67th Ann. Internat. Mtgl, Soc. Expl. Geophys., Expanded Abstracts, 1448-1451.

Hilbert, L. B., 1995, Substructuring and domain decomposition techniques for analysis of discontinuous media: Ph.D. thesis, Univ. of California at Berkeley.

House, L., Fehler, M., Aminzadeh, F., Barhen, J, and Larsen, S., 1996, A national laboratory-industry collaboration to use SEG/EAEG model data sets: The Leading Edge, **15**, 135-136.

Israeli, M., Vozovoi, L. And Averbuch, A., 1992, Domain decomposition methods with local Fourier basis for parabolic problems: Domain decomposition Methods in science and engineering, Quarteroni, A. et al. Editors.

Kelly, K. R., Ward, R. W., Treitel, S. Alford, R. M., 1976, Synthetic seismograms: a finite difference approach, Geophysics, **41**, 2-27.

Keyes, D. E. and Xu, J., 1993, Domain decomposition methods in science and engineering, Proceedings of the 7th International conference on domain decomposition: American Mathematical Society.

Komatisch, D., and Vilotte, J.-P., 1998, The spectral element method: an efficient tool to simulate the seismic response of 2D and 3D geological structures: Bull. Seism. Soc. Am, **88**, 2, 368-392.

Kosloff, D., and Baysal, E., 1982, Forward modeling by a Fourier method: Geophysics, **47**, 1402-1412.

Kosloff, D., Kessler, D., Filho, A. Q., Tessmer, E., Behle, A., and Strahilevitz, R., 1990, Solution of the equations of dynamics elasticity by a Chebychev spectral method: Geophysics, **55**, 734-748.

Kreiss, H. O., and Oliger, J., 1972, Comparison of accurate methods for the integration of hyperbolic equation: Tellus, **24**, 199-215.

Krohn, C. E., 1992, Cross-well continuity logging using guided seismic waves: The Leading Edge, 11, No. 7, 39-45.

Kuznetsov, Yu. A., 1988, New algorithm for approximate realization of implicit difference scheme: Sov. J. Numer. Anal. Math. Modeling, **3**, 95-114.

Lamb, H., 1904, On the propagation of tremors over the surface of an elastic solid: Philosophical Transactions of the Royal Society of London, A203, 1-42.

Lamb, H., 1960. Statics: Cambridge University Press, New York, N.Y.

Lewis, J., 1984, The nested dissection multifrontal method for large 2D grids: Presented at the Garlinburg IX Conference on numerical linear Algebra, Waterloo, Ontario and at the Soc. Ind. Appl. Math. Summer meeting, Seattle, Wash.

Liang, G.-P., and He, J. H., 1993, The non-conforming domain decomposition method for elliptical problems with Lagrange multipliers: Chinese J. Num. Meth. Appl., **15**, 8-19.

Liao, Q. and McMechan. G., 1993, 2-D Pseudo-spectral viscoacoustic modeling in a distributed-memory multi-processor computer: Bull. Seism. Soc. Am, **83**, 5, 1345-1354.

Lines, L. R., Kelly, K. R. and Queen, J., 1992, Channel waves in cross-borehole data: Geophysics, 57, 334-342.

Louis, I. F., 1997, Avery cost-efficient solution for the parallel implementation of 3D seismic modelling algorithms in an environment of heterogeneous computers using PVM: 67th Ann. Internat. Mtgl, Soc. Expl. Geophys., Expanded Abstracts, 1437-1440.

Love, A. E. H., 1911, Some problems of geodynamics: Cambridge University Press, Cambridge, 165-178.

Love, A. E. H., 1944, Mathematical theory of elasticity: Dove, New York, 4th Edtion.

Lysmer, J., and Drake, L. A., 1971, A finite element method for seismology, *in* Method in Computational physics, *11*, Seismology, Alder, B., Fernbach, S., and Bolt, B. A., Editors: Academic Press, New York.

Madariaga, R., 1990, Dynamics of an expanding circular fault: Bull. Seis. Soc. Am., **66**, 639-666.

Mandel, J., Farhat, C., and Cai, X.-C., 1997, Domain decomposition methods 10, the tenth International conference on domain decomposition methods: American Mathematical Society.

Marfurt, Kurt J., 1984, Seismic modeling: A frequency-domain finite-element approach: 54th Annual Internat. Mtg., Soc.Expl. Geophys., Expanded Abstracts, 84, Session: S15.6.

Miklowitz, Julius, 1951, Waveguides handbook: McGraw-Hill Book Company, Inc.

Miklowitz, Julius, 1978, The theory of elastic waves and waveguides: North-Holland Publishing Company.

Nichols, D. E., 1996, Maximum energy traveltimes calculated in the seismic frequency band: Geophysics, **61**, 253-263.

Oppenheim, A. V. and Schafer, R. W., 1975, Digital signal processing: Prentice-Hall, Inc.

Orazag, S. A., 1972, Comparison of pseudospectral and spectral approximation: Stud. Appl. Math., 51, 253-259.

Priolo, E., Carcione, J, M., and Seriani, 1994, Numerical simulation of interface waves by high-order spectral modeling technique: J. Acoust. Soc. Am., 95, 681-693.

Ricker, N., 1953, The form and laws of propagation of seismic wavelets: Geophysics, 18, No. 1, 10-40.

Quarteroni, Alfio, 1995, Domain decomposition methods for wave propagation problems, Domain-based parallelism and problem decomposition methods in computational science and engineering, edited by David E. Keyes, Youcef Saad, Donald G. Truhlar. 21-38.

Saatcilar, R., S. Ergintav and N. Canitez, 1990, The use of the Hartley transform in geophysical applications: Geophysics, **55**, 1488-1495.

Saatcilar, R. and S. Ergintav 1991, Solving elastic wave equations with the Hartley method: Geophysics, **56**, 274-278.

Schlue, J. W., 1979, Finite element matrices for seismic surface waves in three-dimensional structures: Bull Seism. Soc. Am., **69**, 1425-1438.

Schwarz, H. A., 1890, Gesammelte Mathematiscshe Abhandlungen, **2**, 133-143. Springer, Berlin. First published in Vierteljahrsschrift Nauturforsch. Ges. Zurich, 15:272-286, 1870.

Sengbush, R. L., 1983, Seismic exploration methods: International Human Resources Development Corporation, Boston, 17-18.

Shubin, G. R., and Bell, J. B., 198, A modified equation approach to constructing fourth order methods for acoustic wave propagation: Soc. Ind. Appl. Math. J. Sci. Stat. Comp., **8**, 135-151.

Smith, F. G., and Thomson, J. H., 1971, Optics: John Wiley & Sons Ltd.

Smith, G. D., 1965, Numerical solution of partial differential equations: Oxford University Press, London. P.70.

Tessmer, E., Kessler, D., Kosloff, K., and Behle, A., 1992, Multi-domain Chebychev-Fourier method for the solution of the equations of motion of dynamic elasticity: J. Comput. Phys., **100**, 355-363.

Tessmer, E., Kosloff, D., and Behle, A., 1994, 3-D elastic modeling with surface topography by a Chebychev spectral method: Geophysics, **59**, 464-473.

Virieux, Jean, 1984, SH-wave propagation in heterogeneous media: velocity-stress finite-difference method: Geophysics, **49**, 1933-1942.

Wu, W. J., Lines, L. R., and Lu, H. X., 1996, Analysis of higher-order, finite-difference schemes in 3-D reverse-time migration: Geophysics, **61**, 845-856.

Xu, T and McMechan. G., 1998, Efficient 3-D viscoelastic modeling with application to near–surface land seismic data, Geophysics: **63**, 601-612.

APPENDIX A

RICKER WAVELET

(a) Ricker Wavelet

The formula of the Ricker wavelet (Ricker, 1953; and Bayliss et al., 1986) is

$$f_1(t) = 2[(\frac{t - t_0}{\tau})^2 - 0.5]e^{-(\frac{t-t_0}{\tau})^2} \quad t \in [0, T], \tag{A-1}$$

where T is the period of the source function, t is time from 0 to T, τ is $T/7$ and t_0 is $0.5T$. The central frequency f_c is about $2.25/T$. Figure A.1 shows the source wavelet with a central frequency f_c = 25 Hz (T =2.25/25 = 0.09 s) and Figure A.2 shows its spectra.

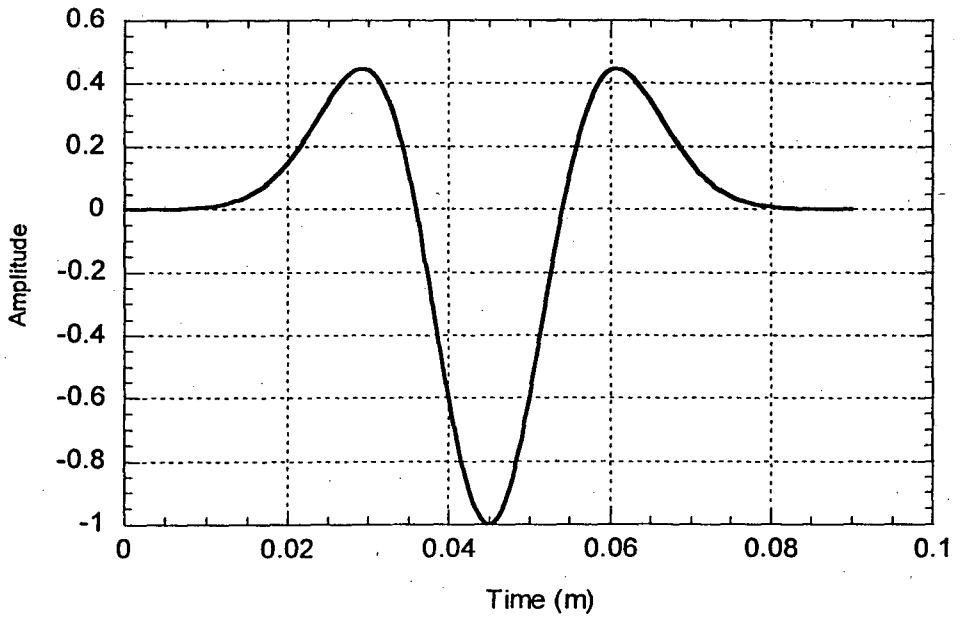

Figure A.1. The wavelet of the Ricker wavelet.

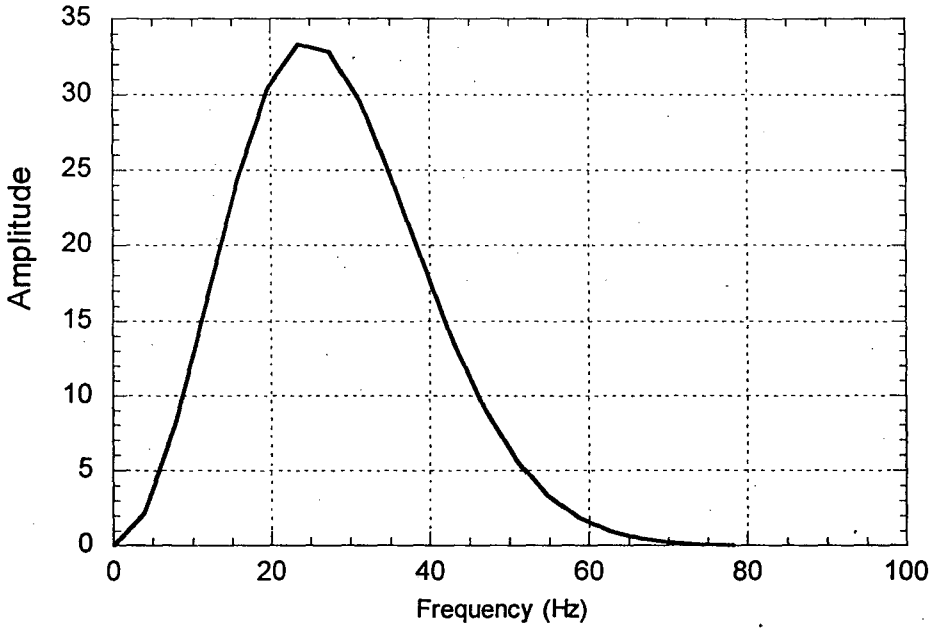

Figure A.2. The spectra of the Ricker wavelet.

(b) Integrated Ricker Wavelet

The formula of the integrated Ricker wavelet (Ricker, 1953; and Bayliss et al., 1986) is

$$f(t) = -2\frac{(t-t_0)}{\tau^2} e^{-(\frac{t-t_0}{\tau})^2} / e^{-(0.5)^2} \quad t \in [0, T], \tag{A-2}$$

The central frequency f_c now is about $1.6/T$. Figure A.3 shows the wavelet of the source function for a central frequency f_c = 25 Hz (T =1.6/25 = 0.064 s), and Figure A.4 shows its spectra. Compared to the Ricker wavelet in Figure A.1, the integrated Ricker wavelet has a shorter period, but a wider frequency range when the central frequencies are the same.

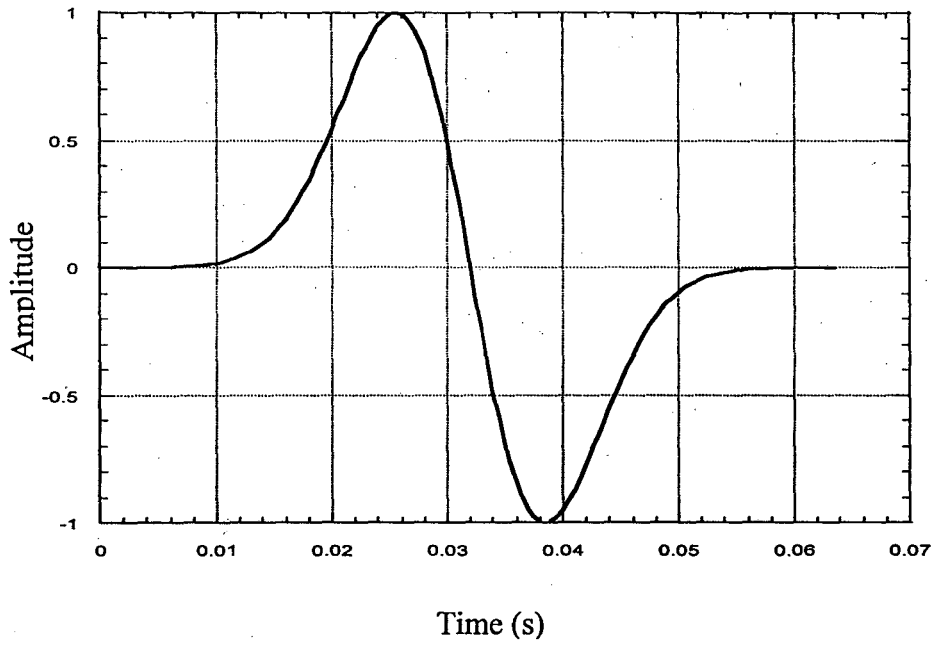

Figure A.3. The integrated Ricker wavelet.

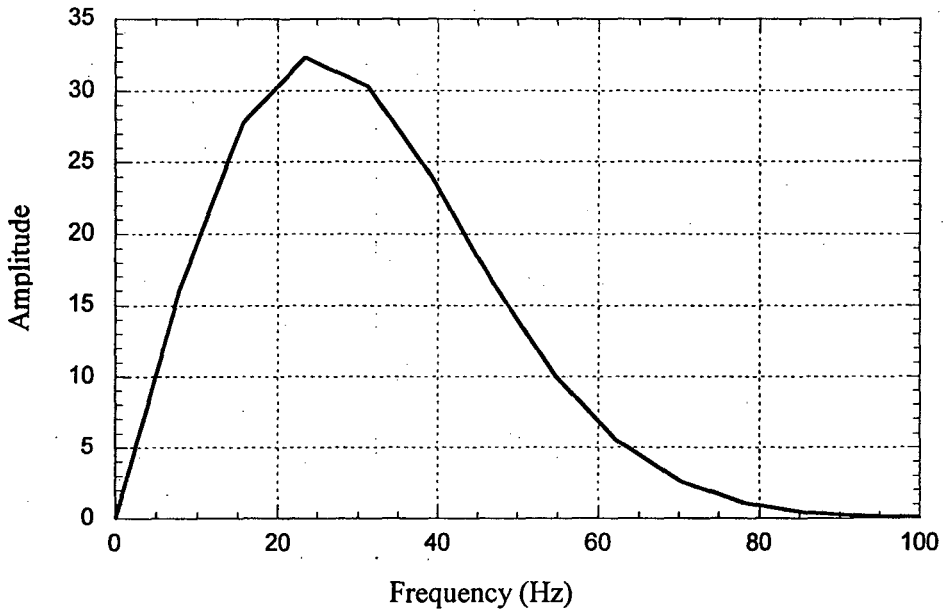

Figure A.4. The spectra of the integrated Ricker wavelet.

APPENDIX B

ANALYTIC SOLUTION FOR 2-D ACOUSTIC AND ELASTIC MEDIA

(1) Analytical Solution in a 2-D Homogeneous, Isotropic Acoustic Medium

The pressure Green's function in a 3-D acoustic medium (Friedlander, 1958; Miklowitz, 1978) is

$$G(X',t) = \frac{1}{4\pi c^2} \frac{F(t - r/c)}{r(X,X')}, \tag{B-1}$$

where c is the velocity, r is distance from a point source at X to a receiver at X' (Figure B.1), $F(t-r/c)$ is a causal source function (zero for $t-r/c < 0$).

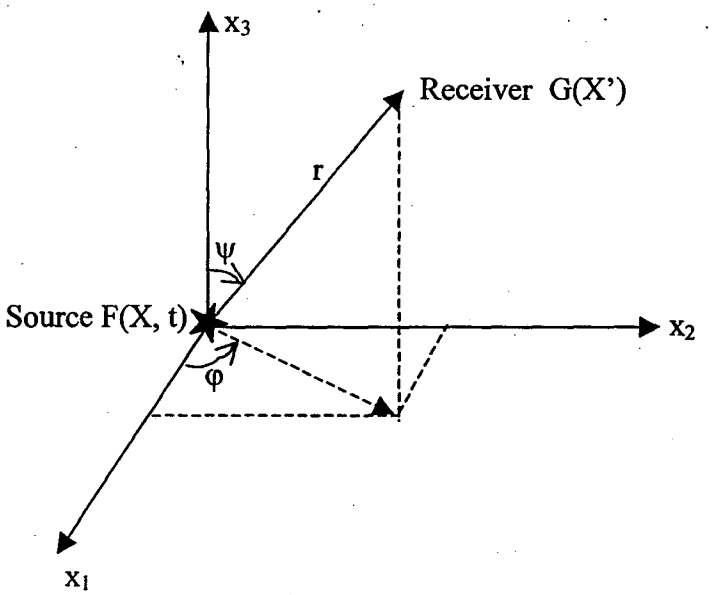

Figure B.1. The Green's function for a point source.

If the source is not a point source then the solution can written as

$$G(X',t) = \frac{1}{4\pi c^2} \oint_{\Omega} \frac{F(X, t - r/c)}{r(X, X')} dv, \qquad \text{(B-2)}$$

where $\Omega(X)$ is the volume in which the source is located, and $r(X,X')$ and $F(X,t)$ are functions of space. Figure B.2 shows the source area and receiver.

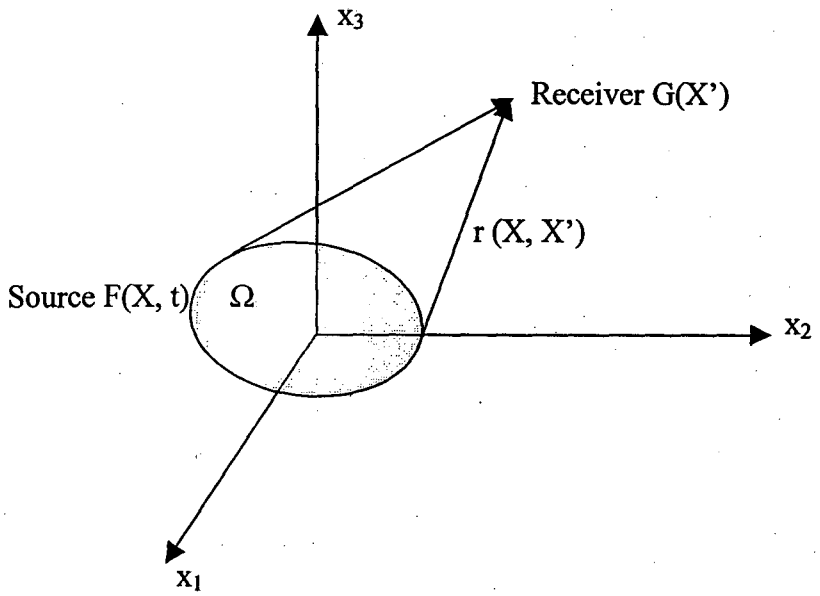

Figure B.2. Geometry for a distributed source.

A 2-D medium with a point source (Figure B.3) is equivalent to an infinite line source in a 3-D medium (Figure B.4).

The solution of a point source in a 2-D medium can be obtained by integration of the Green's function along an infinite line source in a 3-D medium.

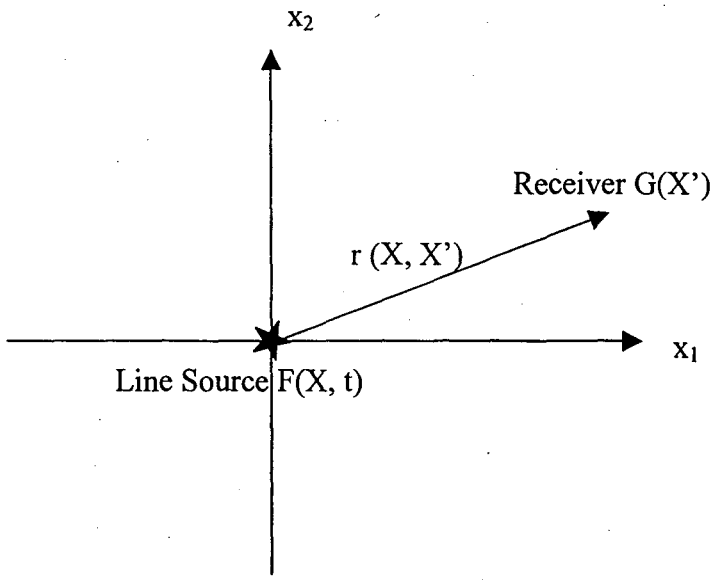

Figure B.3. A point source in a 2-D medium.

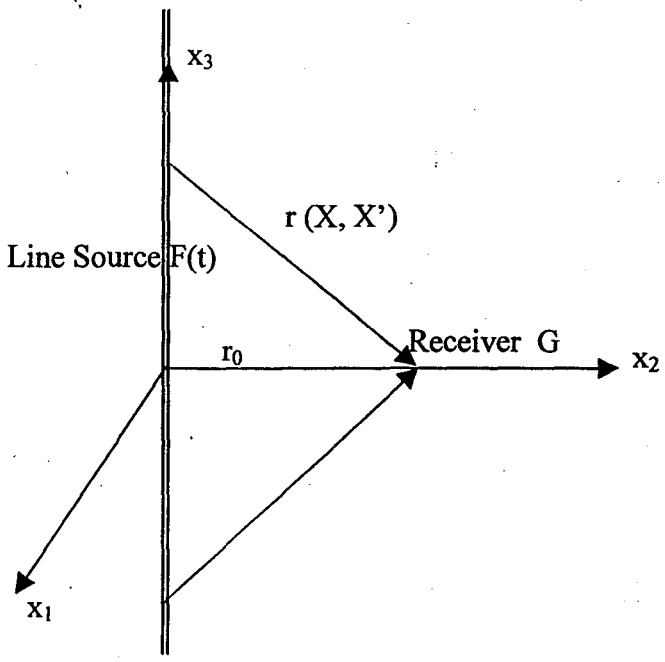

Figure B.4. An infinite line source in a 3-D medium.

$$G(X',t) = \frac{1}{4\pi c^2} \int_{-\infty}^{\infty} \frac{F(x_3, t - r/c)}{r(x_3, X')} dx_3, \tag{B-3}$$

where $r(x_3, X') = \sqrt{x_3^2 + r_0^2}$ as shown in Figure B.4. Since *F(t-r/c)* is zero when *t-r/c* < *0* ($r > ct$, or $x_3 > \sqrt{(ct)^2 - r_0^2}$). The integration can be rewritten as

$$G(X',t) = \frac{1}{4\pi c^2} \int_{-a}^{a} \frac{F(x_3, \frac{ct - \sqrt{r_0^2 + x_3^2}}{c})}{\sqrt{r_0^2 + x_3^2}} dx_3, \tag{B-4}$$

where $a = \sqrt{(ct)^2 - r_0^2}$.

Figure B.3 shows the geometry for an example of a homogeneous medium with velocity of 2000 m/s. A receiver is located 500 m away from a 2-D point source (a 3-D line source). The source uses a unit intensity integrated Ricker wavelet (equation A-1) with a central frequency f_c = 25 Hz (T =1.6/25 = 6.4 s). The waveform is calculated by Simpson numerical integration.

Figure B.6 shows the waveform computed from equation (B-4), and Figure B.7 shows the corresponding spectra. Compared to the source wavelet in Figure A.1, the waveform has a tail and the amplitude of the negative part of the wavelet is much smaller than that for the positive part. In addition, the central frequency is about 17 Hz which is lower than the 25 Hz of the source wavelet.

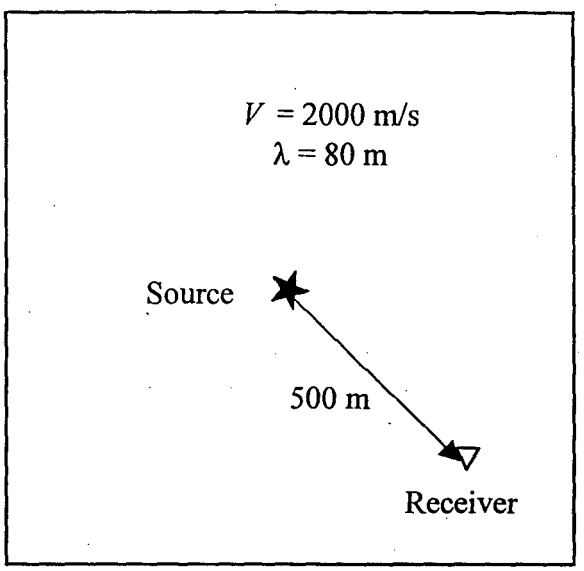

Figure B.5. Geometry for the calculation of the analytic Green's function solution in a 2-D homogeneous medium.

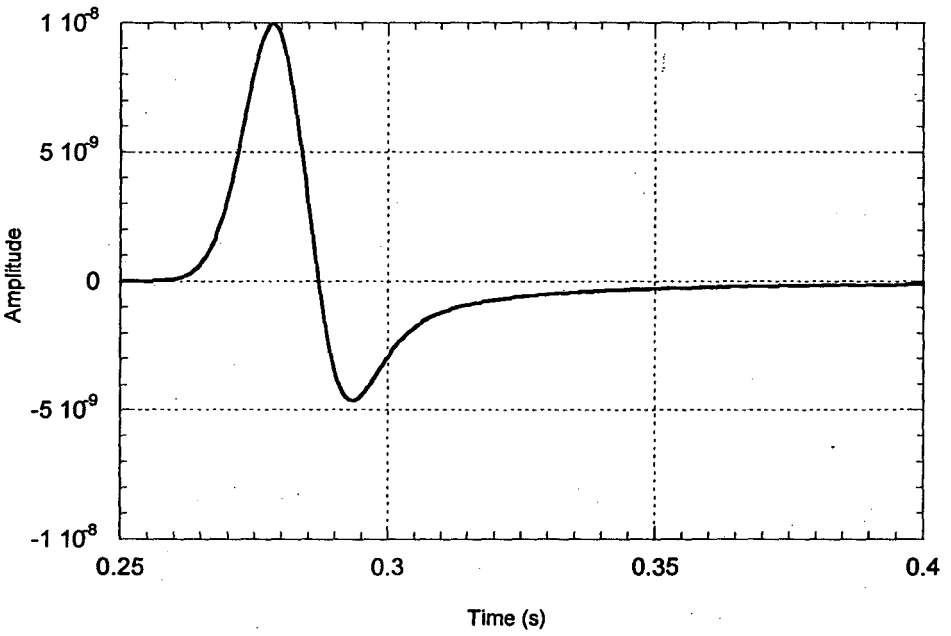

Figure B.6. Waveform for a receiver 500 m away from the source.

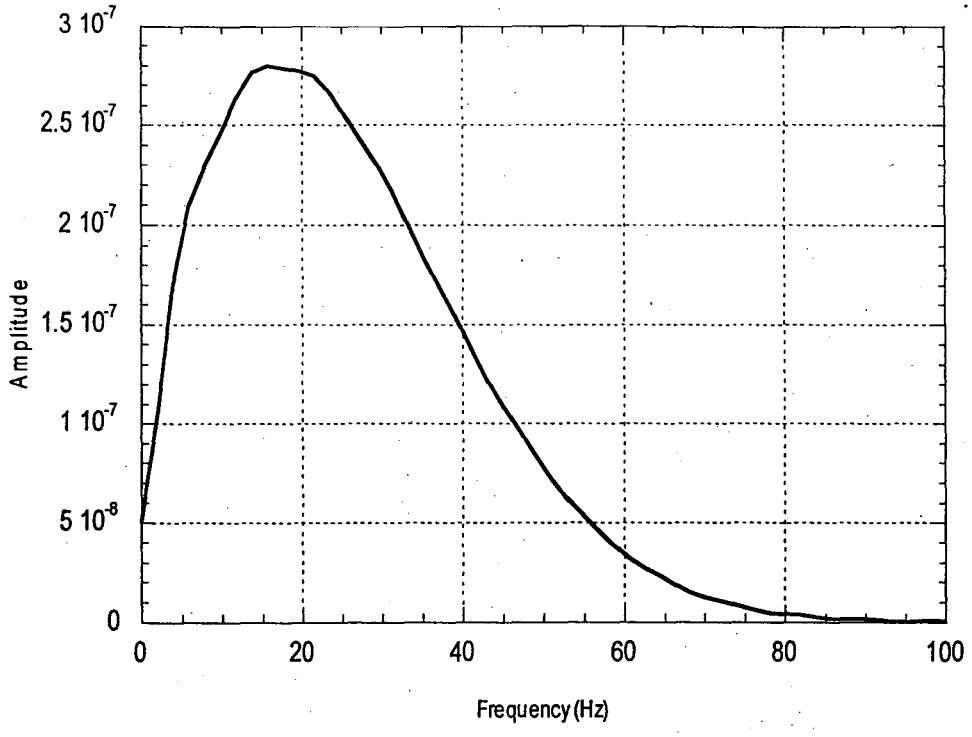

Figure B.7. Spectrum of the waveform for a receiver 500 m away from the source.

(2) Analytic Solution in a 2-D Homogeneous, Isotropic Elastic Medium

The Green's function in a 3-D elastic medium under a body force $F(t)$ in x_j-direction (Aki and Richards, 1980; Miklowitz, 1978) is

$$u_i(X',t) = \frac{1}{4\pi\rho}(3\gamma_i\gamma_j - \delta_{ij})\frac{1}{r^3}\int_{r/\alpha}^{r/\beta} \tau F(t-\tau)d\tau + \frac{1}{4\pi\rho\alpha^2}\gamma_i\gamma_j\frac{1}{r}F(t-\frac{r}{\alpha}) - \frac{1}{4\pi\rho\beta^2}(\gamma_i\gamma_j - \delta_{ij})\frac{1}{r}F(t-\frac{r}{\beta}), \quad \text{(B-5)}$$

where α, β are P-wave, S-wave velocities, respectively, ρ is density of the medium, δ_{ij} is the Dirac delta function, γ_i and γ_j are direction cosines,

$$\gamma_i = \frac{x_i}{r} = \frac{\partial r}{\partial x_i}, \qquad \gamma_j = \frac{x_j}{r} = \frac{\partial r}{\partial x_j}. \tag{B-6}$$

In equation (B-1), the first term is called the near-field term since its amplitude decreases very abruptly (r^{-3}) with increasing distance r and it only can be seen near the source. The second and third terms decrease quite slowly (r^{-1}) and travel with P-wave and S-wave velocities, respectively. These terms are the far-field P-wave and S-wave.

Similar to the acoustic case, the solution for 2-D problem can be obtained by integration of the Green's function in equation (B-5) along the infinite source in one direction. Here an example of a 2-D point source with an integrated Ricker wavelet is performed by integration. The source acts in the x_2-direction and the receiver is placed on the x_2-axis (Figure B.8). The displacement in the x_2-direction can be integrated as

$$\begin{aligned} u_2(X',t) = {} & \frac{1}{4\pi\rho}\int_{-a}^{a}\left[(3\frac{r_0}{r}\frac{r_0}{r}-1)\frac{1}{r^3}\int_{r/\alpha}^{r/\beta}\tau F(t-\tau)d\tau\right]dx_3 \\ & + \frac{1}{4\pi\rho\alpha^2}\int_{-a}^{a}\frac{r_0}{r}\frac{r_0}{r}\frac{1}{r}F(t-\frac{r}{\alpha})dx_3 \\ & - \frac{1}{4\pi\rho\beta^2}\int_{-b}^{b}(\frac{r_0}{r}\frac{r_0}{r}-1)\frac{1}{r}F(t-\frac{r}{\beta})dx_3, \end{aligned} \tag{B-7}$$

where $a = \sqrt{(\alpha t)^2 - r_0^2}$, $b = \sqrt{(\beta t)^2 - r_0^2}$ and $r = \sqrt{x_3^2 + r_0^2}$.

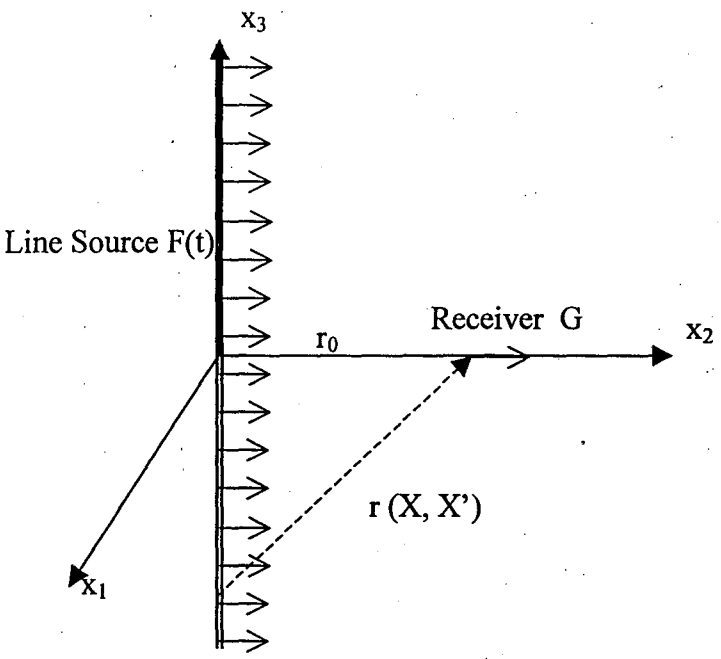

Figure B.8. An infinite line source in a 3-D medium.

Figure B.9 shows the waveforms from a receiver and the different components which are contributing from the terms in equation (B-5). The receiver is 400 m away from the 2-D point source (a 3-D line source) with a unit intensity Ricker-integral source a unit intensity integrated Ricker wavelet (equation A-1) in the homogeneous medium with α=2191 m/s, β=1265 m/s and ρ = 2000 kg/m^3. The waveform is calculated by Simpson numerical integration. Figure B.7 shows their spectra.

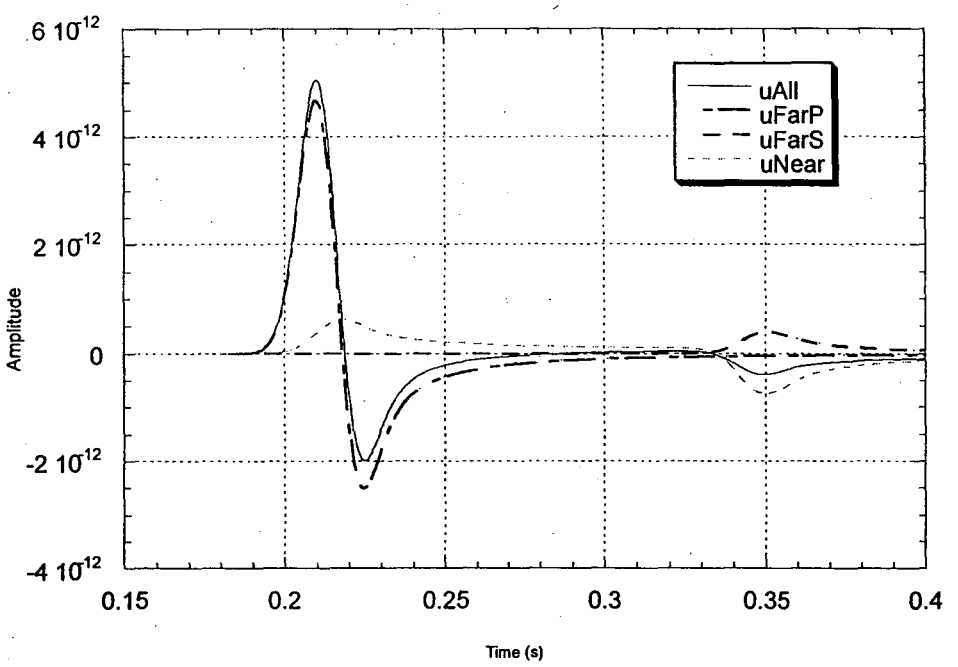

Figure B.9. Waveform from a receiver 400 m away from a point source.

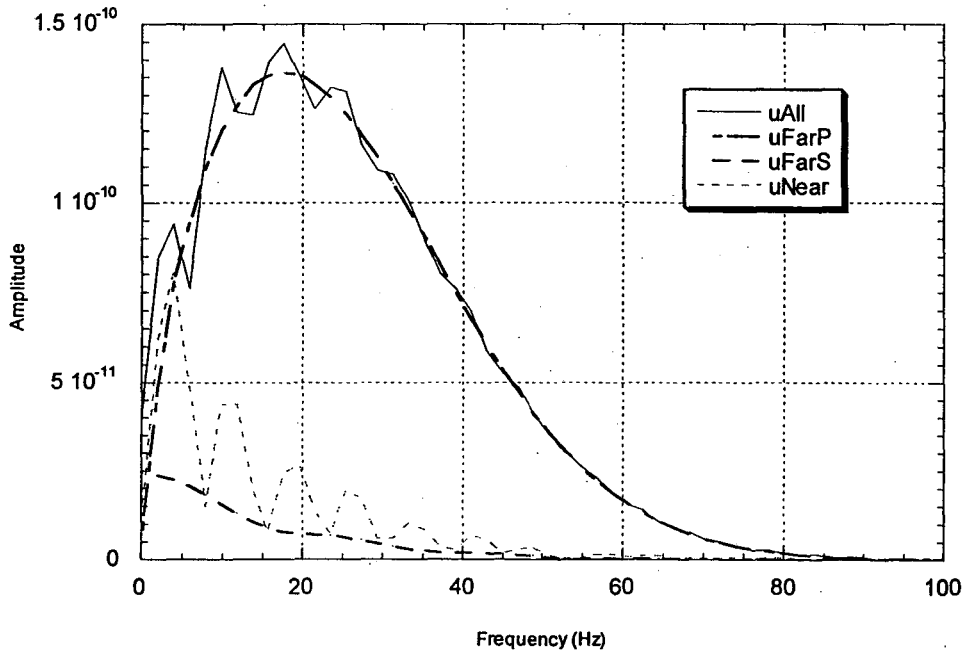

Figure B.10. Spectra of the waveform for a receiver 400 m away from a point source.

APPENDIX C

STABILITY CONDITION SOLUTION

(1) The Stability Condition by the Von Neumman Approach

The finite difference scheme from the equation (2.6.12) in the Section 2.6 is

$$u(x_m,t_{n+1}) = 2u(x_m,t_n) - u(x_m,t_{n-1}) + C_0^2\Delta t^2 \frac{\partial^2 u(x_m,t_n)}{\partial x^2}. \tag{C-1}$$

Using the definition of equation (2.6.2), $\tau = C_0^2\Delta t^2 \dfrac{\partial^2 u(x_m,t_n)}{\partial x^2}\Big/ u(x_m,t_n)$, the eigenvalues of stability condition can be rewritten from the equation (2.6.12) in Section 2.6 as

$$\begin{aligned} \lambda_1 &= 0.5[(2+\tau) + \sqrt{\tau(4+\tau)}], \\ \lambda_2 &= 0.5[(2+\tau) - \sqrt{\tau(4+\tau)}]. \end{aligned} \tag{C-2}$$

According to the Von Neumman condition, if $|\lambda_i| \le 1$, the finite difference scheme of (C-1) is stable. We need to find τ to satisfy the Von Neumman condition.

(i) If $\tau > 0$, therefore, $\tau + 4 > 4, \sqrt{\tau(4+\tau)} > 0$ and $2 + \tau > 2$. Then

$$\lambda_1 = 0.5[(2+\tau) + \sqrt{\tau(4+\tau)}] > 0.5[2+0] > 1. \tag{C-3}$$

Therefore, the FD scheme (C-1) is not stable.

(ii) If $\tau < -4$, then $\tau + 4 < 0, \sqrt{\tau(4+\tau)} > 0$, $-\sqrt{\tau(4+\tau)} < 0$, $2 + \tau < -2$ and

$$\lambda_2 = 0.5[(2+\tau) - \sqrt{\tau(4+\tau)}] < 0.5[-2-0] < -1. \tag{C-4}$$

Therefore, the FD scheme (C-1) is not stable.

(iii) If $0 \geq \tau \geq -4$, then $\tau + 4 \leq 0, \sqrt{\tau(4+\tau)} \leq 0$ and $\sqrt{-\tau(4+\tau)} \geq 0$. The equation (C-2) can be rewritten as

$$\lambda_i = 0.5[(2+\tau) \pm i\sqrt{-\tau(4+\tau)}], \tag{C-5}$$

where $i = \sqrt{-1}$ and the magnitude of λ_i is

$$\begin{aligned} |\lambda_i| &= 0.5[(2+\tau)^2 + \sqrt{-\tau(4+\tau)}^2]^{1/2} \\ &= 0.5[(4 + 4\tau + \tau^2 - 4\tau - \tau^2)]^{1/2} \\ &= 1. \end{aligned} \tag{C-6}$$

Therefore, the FD scheme (C-1) is stable. The stability condition is

$$0 \geq \tau \geq -4. \tag{C-7}$$

(2) The Stability Condition by Another Approach

Assume a solution of equation (2.6.1) have a form

$$u(x_m, t_n) = u_0 e^{i(kx-\omega t)} = u_0 e^{i(km\Delta x - \omega n\Delta t)}, \tag{C-8}$$

where $x = m\Delta x$, $t = n\Delta t$ and the wavenumber k is in the band of the numerical mesh.

A second order difference of the time portion of equation (2.6.1) can be discretized as

$$\frac{\partial^2 u(x_m,t_n)}{\partial t^2}=\frac{1}{\Delta t^2}[u(x_m,t_{n+1})-2u(x_m,t_n)+u(x_m,t_{n-1})]. \qquad \text{(C-9)}$$

Substituting the harmonic solution of equation (C-7) into above equation produces

$$\begin{aligned}\frac{\partial^2 u(x_m,t_n)}{\partial t^2}&=\frac{u_0 e^{i(kx-wt)}}{\Delta t^2}[e^{-iw\Delta t}-2+e^{iw\Delta t}]\\&=\frac{2}{\Delta t^2}[\cos(\omega\Delta t)-1]u(x_m,t_n)\\&=-\frac{4\sin^2(\omega\Delta t/2)}{\Delta t^2}u(x_m,t_n).\end{aligned} \qquad \text{(C-10)}$$

Substituting the above equation into equation (2.6.1) gives

$$-\frac{4\sin^2(\omega\Delta t/2)}{\Delta t^2}u(x_m,t_n)=C_0{}^2\frac{\partial^2 u(x_m,t_n)}{\partial x^2}. \qquad \text{(C-11)}$$

Using the definition of τ in equation (2.6.3), gives

$$-\frac{\tau}{4}=\sin^2(\omega\Delta t/2). \qquad \text{(C-12)}$$

For equation (C-12) to hold for real ω, the time step must satisfy the relation

$$0\le-\frac{\tau}{4}\le 1,$$

or

$$0\ge\tau\ge-4. \qquad \text{(C-13)}$$

This stability condition is the same as the condition in equation (C-7).

APPENDIX D

PSEUDOSPECTRAL FORMULA FOR AN ELASTIC MEDIA

For equation (3.5.1), the Fourier PS method needs two passes of the Fourier transform to calculate the spatial derivatives in two directions. The Fourier transforms of $u[x(l),z(m),t(n)]$ and $w[x(l),z(m),t(n)]$ are:

$$\hat{u}[k_x(l),k_z(m),t(n)=\sum_{j=0}^{M-1}\sum_{i=0}^{L-1}u[x(i),z(j),t(n)]e^{-ik_x(l)x(i)-ik_z(m)z(j)}, \tag{D.1}$$

$$\hat{w}[k_x(l),k_z(m),t(n)=\sum_{j=0}^{M-1}\sum_{i=0}^{L-1}w[x(i),z(j),t(n)]e^{-ik_x(l)x(i)-ik_z(m)z(j)}, \tag{D.2}$$

where the wavenumbers $k_x(l)=2\pi l/(N\cdot\Delta x)$, $k_z(m)=2\pi m/(M\cdot\Delta z)$ and $\Delta x=x_m-x_{m-1}$, $\Delta z=z_m-z_{m-1}$. At the same time, $u[x(l),z(m),t(n)]$ and $w[x(l),z(m),t(n)]$ can be expressed as the inverse Fourier transforms

$$u[k_x(l),k_z(m),t(n)=\frac{1}{LM}\sum_{j=0}^{M-1}\sum_{i=0}^{L-1}\hat{u}[x(i),z(j),t(n)]e^{ik_x(l)x(i)+ik_z(m)z(j)}, \tag{D.3}$$

$$w[k_x(l),k_z(m),t(n)=\frac{1}{LM}\sum_{j=0}^{M-1}\sum_{i=0}^{L-1}\hat{w}[x(i),z(j),t(n)]e^{ik_x(l)x(i)+ik_z(m)z(j)}. \tag{D.4}$$

Then the first order spatial derivatives can be obtained from the above equation

$$f=\frac{\partial u[x(i),z(j),t(n)]}{\partial z}=\frac{1}{LM}\sum_{m=0}^{M-1}\sum_{l=0}^{L-1}-ik_z(m)\cdot\hat{u}[k_x(l),k_z(m),t(n)]e^{ik_x(l)x(i)+ik_z(m)z(j)}, \tag{D.5}$$

$$g=\frac{\partial w[x(i),z(j),t(n)]}{\partial z}=\frac{1}{LM}\sum_{m=0}^{M-1}\sum_{l=0}^{L-1}-ik_z(m)\cdot\hat{w}[k_x(l),k_z(m),t(n)]e^{ik_x(l)x(i)+ik_z(m)z(j)}, \tag{D.6}$$

$$h=\frac{\partial u[x(i),z(j),t(n)]}{\partial x}=\frac{1}{LM}\sum_{m=0}^{M-1}\sum_{l=0}^{L-1}-ik_x(l)\cdot\hat{u}[k_x(l),k_z(m),t(n)]e^{ik_x(l)x(i)+ik_z(m)z(j)}, \quad (D.7)$$

$$k=\frac{\partial w[x(i),z(j),t(n)]}{\partial x}=\frac{1}{LM}\sum_{m=0}^{M-1}\sum_{l=0}^{L-1}-ik_x(l)\cdot\hat{w}[k_x(l),k_z(m),t(n)]e^{ik_x(l)x(i)+ik_z(m)z(j)}, \quad (D.8)$$

Define

$$a[x(l),z(m)]=\lambda[x(l),z(m)]\{h[x(l),z(m)]+g[x(l),z(m)]+2\mu[x(l),z(m)]h[x(l),z(m)]\}, \quad (D.9)$$

$$b[x(l),z(m)]=\mu[x(l),z(m)]\{k[x(l),z(m)]+f[x(l),z(m)]\}, \quad (D.10)$$

$$c[x(l),z(m)]=\lambda[x(l),z(m)]\{h[x(l),z(m)]+g[x(l),z(m)]+2\mu[x(l),z(m)]g[x(l),z(m)]\}. \quad (D.11)$$

Then, using the Fourier transform again for the derivatives in equation 3.5.1, the final PS solution for a heterogeneous medium is

$$\begin{aligned}u(x_l,y_m,z_n,t_{i+1})&=2u(x_l,y_m,z_n,t_i)-u(x_l,y_m,z_n,t_{i-1})\\&+\frac{\Delta t^2}{\rho}\{\frac{1}{LM}\sum_{m=0}^{M-1}\sum_{l=0}^{L-1}-ik_x(l)\cdot\hat{a}[k_x(l),k_z(m),t(n)]e^{ik_x(l)x(i)+ik_z(m)z(j)}\\&+\frac{1}{LM}\sum_{m=0}^{M-1}\sum_{l=0}^{L-1}-ik_z(m)\cdot\hat{b}[k_x(l),k_z(m),t(n)]e^{ik_x(l)x(i)+ik_z(m)z(j)}\},\end{aligned} \quad (D.12)$$

and

$$\begin{aligned}w(x_l,y_m,z_n,t_{i+1})&=2w(x_l,y_m,z_n,t_i)-w(x_l,y_m,z_n,t_{i-1})\\&+\frac{\Delta t^2}{\rho}\{\frac{1}{LM}\sum_{m=0}^{M-1}\sum_{l=0}^{L-1}-ik_z(m)\cdot\hat{c}[k_x(l),k_z(m),t(n)]e^{ik_x(l)x(i)+ik_z(m)z(j)}\\&+\frac{1}{LM}\sum_{m=0}^{M-1}\sum_{l=0}^{L-1}-ik_x(l)\cdot\hat{b}[k_x(l),k_z(m),t(n)]e^{ik_x(l)x(i)+ik_z(m)z(j)}\}.\end{aligned} \quad (D.13)$$

APPENDIX E

COMPARISON BETWEEN THE ODD FD-PS AND THE FD METHODS IN THE CHANNEL MODELING

Figure E.1 shows a snapshot and a waveform along the center of channel by the mixed ODD PS-FD4 method at a time 0.4 ms for the horizontal component of the wavefield. And Figure E.2 shows the results by the conventional FD4 method with the same parameters. The waveform by the FD4 method in Figure E.2(b) has high frequency noise compared to the clean waveform obtained with the ODD PS-FD4 method in Figure E.1(b). For comparison of the results, Figure E.3 plots the relative errors of the FD4 method (differences from the results between the ODD PS-FD4 method and the FD4 method). The snapshot in Figure E.3(a) shows that the errors by the FD4 method mainly come from the S wave and the wave in the low velocity channel which have short wavelengths. The same errors shown in the waveform in Figure E.3(b) are the high frequency components which are caused by the numerical dispersion produced by the lower accurate FD4 method.

This comparison demonstrates the flexibility and efficiency of coupling of the different numerical methods using the ODD technique. Therefore, the mixed ODD PS-FD4 method was used for all the numerical simulations for the channel wave modeling.

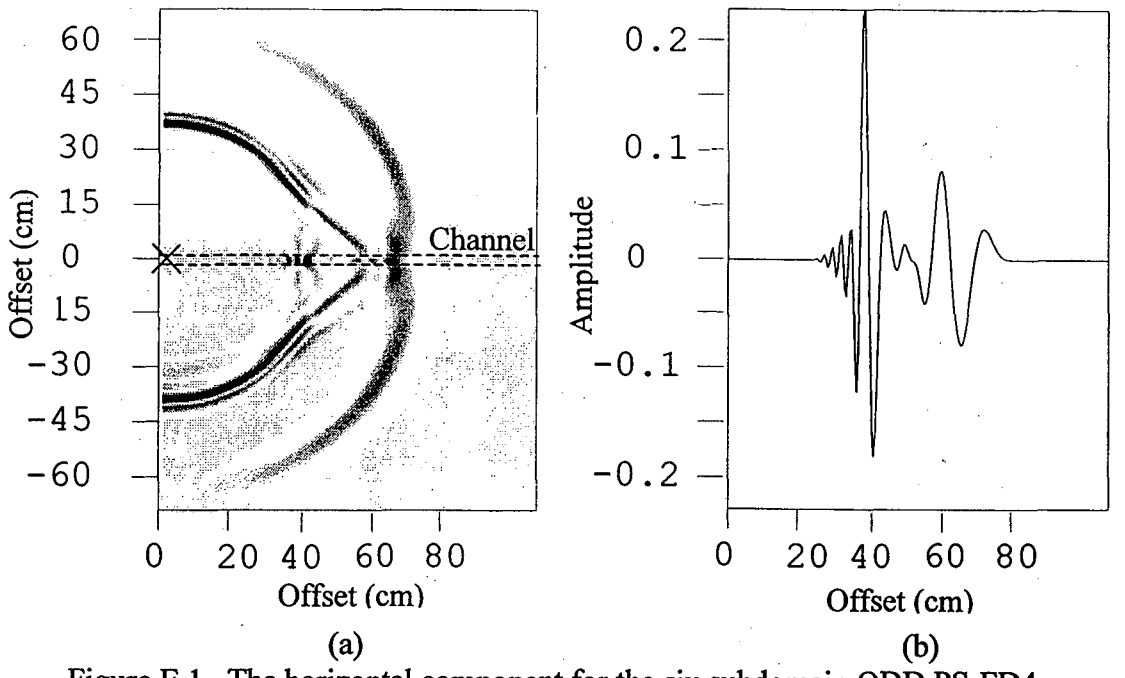

Figure E.1. The horizontal component for the six subdomain ODD PS-FD4: (a) snapshot, and (b) waveform along the center of channel.

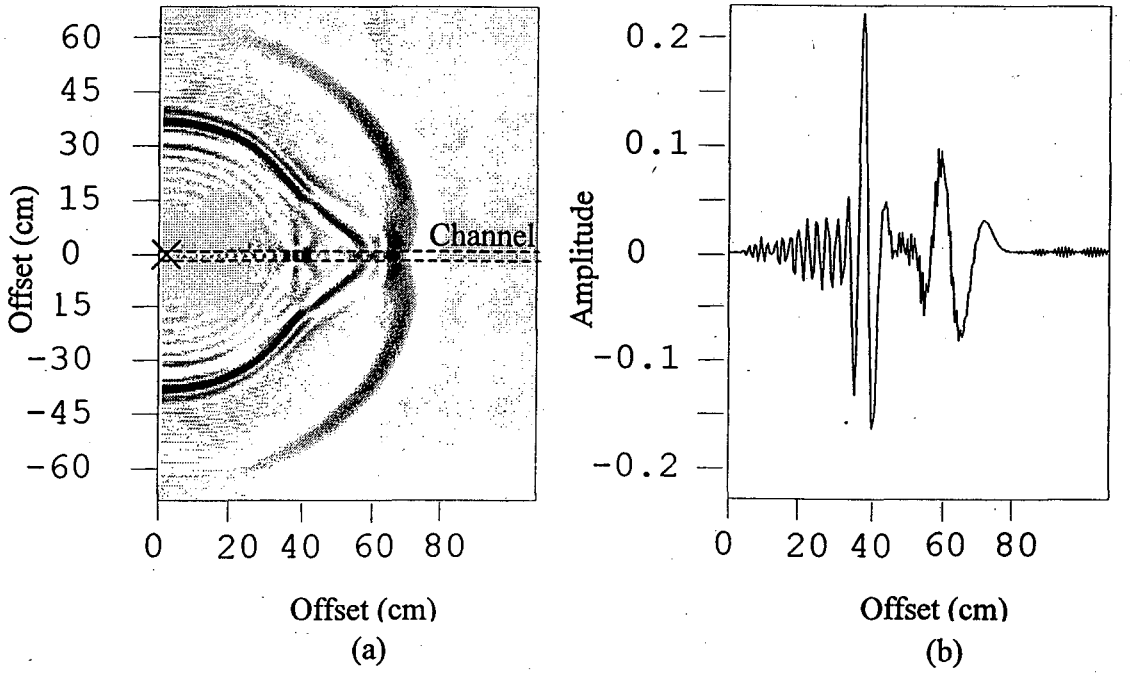

Figure E.2. The horizontal component for the conventional FD method: (a) snapshot, and (b) waveform along the center of channel.

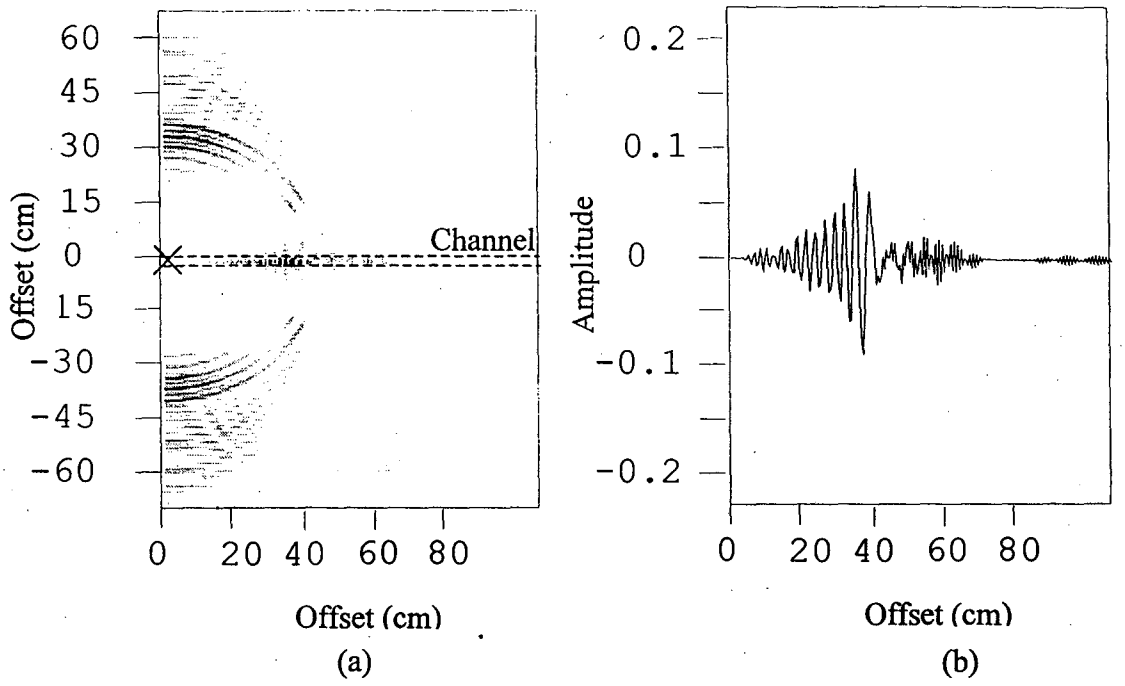

Figure E.3. The difference between the results of the ODD PS-FD4 and FD4 methods: (a) snapshot, and (b) waveform along the center of channel.

Ernest Orlando Lawrence Berkeley National Laboratory
One Cyclotron Road | Berkeley, California 94720

Prepared for the U.S. Department of Energy under Contract No. DE-AC03-76SF00098